SPRINGER BRIEFS IN APPLIED SCIENCES AND TECHNOLOGY · MANUFACTURING AND SURFACE ENGINEERING

Konstantinos Salonitis

Grind Hardening Process

Springer

SpringerBriefs in Applied Sciences and Technology

Manufacturing and Surface Engineering

Series editor

Joao Paulo Davim, Aveiro, Portugal

More information about this series at http://www.springer.com/series/10623

Konstantinos Salonitis

Grind Hardening Process

Springer

Konstantinos Salonitis
Manufacturing Department
School of Aerospace,
Transport and Manufacturing
Cranfield University
Cranfield, UK

ISSN 2191-530X ISSN 2191-5318 (electronic)
SpringerBriefs in Applied Sciences and Technology
ISBN 978-3-319-19371-7 ISBN 978-3-319-19372-4 (eBook)
DOI 10.1007/978-3-319-19372-4

Library of Congress Control Number: 2015939989

Springer Cham Heidelberg New York Dordrecht London

Printed on acid-free paper

Springer International Publishing AG Switzerland is part of Springer Science+Business Media (www.springer.com)

To my wife Ioanna
and my daughter Eftychia

Preface

Grinding is one of the most important processes in the manufacturing discipline. One of the key goals for successful grinding is controlling the heat transfer in order to ensure that the workpiece material does not undergo any metallurgical changes. However, this problem can also be considered as an opportunity. By controlling the amount of heat that is conducted in the workpiece material, it can result in its surface heat treatment. Grind-hardening process thus is a novel, non-conventional, machining process that can be used for the simultaneous surface hardening and grinding of metallic components.

Grind-hardening process can potentially substitute conventional heat treatment methods by integrating this process in the grinding phase. The key benefit of doing so is the elimination of the need for transportation of the work in progress and the minimization of additional set-ups. The process can be used for selective surface hardening of cylindrical and flat components such as shafts, rail-guides, etc.

The main objective of this book is to present the *Grind-Hardening Process* and the main studies published since it was introduced in the 1990s. Modelling of the various aspects of the process, such as the process forces, temperature profile developed, hardness profiles, residual stresses, etc., are presented in detail. The book is directed to the research community interested in the mathematical modelling and optimization of such a manufacturing process. It is intended to be employed mainly at the postgraduate level.

In the present book, the *Grind-Hardening Process* is introduced and analysed. Chapter 1 compares grind-hardening process to alternative surface modification processes. The state of the art of the grind-hardening process is reviewed and discussed in Chap. 2. The modelling of the process is presented in Chap. 3. In Chap. 4, the energy efficiency issues of the process and its environmental impact is analysed. Finally in Chap. 5, concluding remarks on the grind-hardening process are presented.

Cranfield, UK — Konstantinos Salonitis

Contents

Chapter 1
Hybrid Processes for Surface Modification and the Grind-Hardening Process

Abstract This chapter reviews the various available surface-hardening processes. The principles of surface modification are briefly described before presenting the most known surface hardening processes such as induction, high frequency, laser beam and flame hardening processes. Grind hardening as an alternative surface hardening process is presented.

1.1 Introduction

The production of high precision steel parts usually includes a hardening process for altering the surface structure. Conventional heat treatment methods are characterized by high energy consumption and the utilization of polluting treatment salts. Furthermore, the heat treatment process is usually performed in wage hardeners that are outside the production plant and thus, the workpieces have to be transported to and from, increasing as a result both the energy consumption and the environmental impact. Additionally, the necessary cleaning of the workpieces, before and after the heat treatment process, requires a copious amount of water.

Grind hardening is a hybrid manufacturing process that can be used for the simultaneous surface hardening and grinding of metallic components by eliminating all the above steps since both the grinding and grind-hardening processes are performed on the same grinding machine with the same set-up (Fig. 1.1). Hybrid processes have been defined as processes that "are based on the simultaneous and controlled interaction of process mechanisms and/or energy sources/tools having a significant effect on the process performance" [1]. Lauwers et al. classified hybrid processes into two large groups; those that are based on a combination of more than one energy sources in order to deliver a synergetic effect in the processing zone and those that combine two or more different processes for delivering simultaneously the effect of such processes. Based on Lauwers et al. classification, grind hardening can be grouped under the latter group of processes.

K. Salonitis, *Grind Hardening Process*, SpringerBriefs in Manufacturing and Surface Engineering, DOI 10.1007/978-3-319-19372-4_1

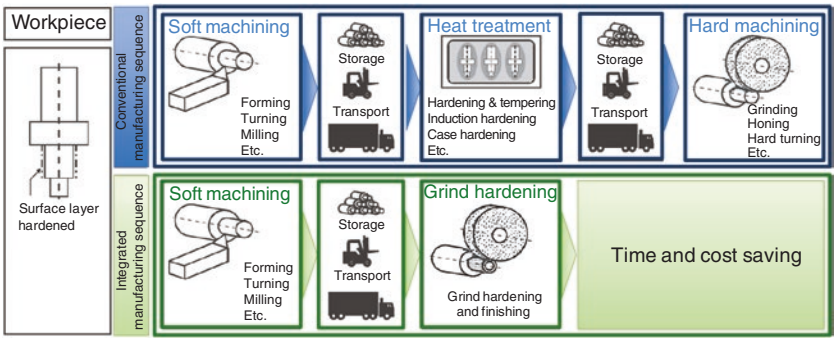

Fig. 1.1 Comparison of a conventional production chain and a production chain including grind hardening

The process of grind hardening relies on controlling the generated heat for heating locally the processed workpiece in order to increase its surface hardness. The metallurgic change required for hardening is achieved by heating the surface above austenitization temperature and through the subsequent quenching martensitic transformation is induced on the workpiece surface.

1.2 Principles of Surface Modification

As already mentioned, conventionally the workpiece surface can be modified through heat treatment methods. "Heat treatment" term refers to the controlled heating and cooling of metals to alter their physical and mechanical properties without changing the geometry characteristics [2]. The most common way to harden steel is by using martensite surface hardness methods. Martensite surface hardening is basically austenization initiated in the surface layer, followed by quenching in a suitable medium in conditions enabling as much of the austenite as possible to transform into martensite and, if necessary, bainite. Directly after hardening, the workpiece is generally subjected to low temperature tempering that reduces the brittleness of the hardened microstructure with minimum losses in hardness.

The steel before any heat treatment process is composed of a mixture of ferrite and carbides, presenting a lamellar microstructure known as pearlite. When the steel is heated or cooled, allotropic changes take place when there is a change in crystal lattice structure.

The ferrite-pearlite structure has a face-centred cubic and when it is heated, it reaches a temperature at which the carbides in the lamellar pearlite begin to dissolve into iron. As the temperature is raised, more of the carbides are dissolved until the steel consists completely of a solid solution of carbon in iron called

austenite having face-centred cubic lattice structure. The temperature at which pearlite begins to transform into austenite is identified as the lower critical temperature, the temperature at which the steel becomes composed completely of austenite is called the upper critical temperature, and the temperature range between is the critical range or transformation range for the particular alloy.

In order to heat uniformly all the sections of the steel processed, the part is maintained at the upper critical temperature long enough to ensure that all of the part is at the same temperature. This operation, called *equalizing*, is not applicable to selective hardening methods but only for through hardening operations.

Quenching refers to the rate of cooling. The microstructure obtained from the process is directly dependent on quenching and thus any lamellar crystal structure (pearlite, bainite or martensite) may form. The primary purpose of quenching steel is to produce martensite. Therefore, it is essential to employ fast enough cooling rates to prevent the steel from dwelling in the higher temperature ranges where pearlite and/or bainite will form. The precise hardness of martensite is dependent on the amount of carbon present in steel.

1.3 Surface Hardening Methods

Surface hardening methods are categorized into two major groups:

- Thermal diffusion processes (selective hardening processes)
- Thermo-chemical diffusion processes

Thermo-chemical diffusion processes are characterized as diffusing an element, such as carbon, nitrogen, sulphur, boron and oxygen, into the surface of the steel by application of the appropriate amount of heat, time and the steel surface catalytic reaction. Such processes are outside the scope of the present paper.

Thermal diffusion processes are those that modify the surface phases of steel containing sufficient carbon to allow transformation from austenite to martensite when the appropriate amount of heat is applied to the immediate surface. These techniques are also familiar as *selective hardening processes* (or *localized heat treatment processes)* because they can selectively harden steel in specific regions by applying heat and quench only to those regions. In the following paragraphs, these processes will be briefly presented as comparison to the grind-hardening ones.

1.3.1 Induction Hardening

Induction hardening involves passing a high-frequency alternating current through a suitably shaped coil (Fig. 1.2) to induce rapid heating of the component surface situated appropriately within its electromagnetic field. Heating of the component is imposed due to hysteresis phenomena and the eddy currents in the material.

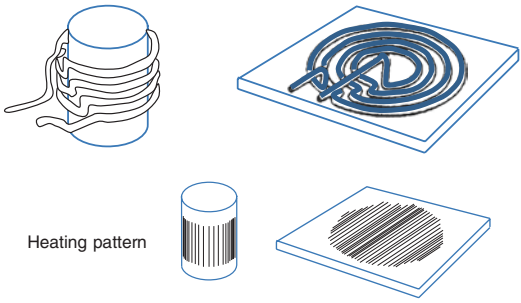

Fig. 1.2 Typical inductor coils and the heating pattern they produced on the surface of a material

The eddy currents dissipate energy and give rise to heating. The only requirement of a material in order to respond to induction hardening is electrical conductivity.

The basic components of an induction heating system are:

1. an induction coil (usually copper tubing through which suit cooling water passes and takes a variety of shapes to suit the part to be heated) (Fig. 1.2),
2. an alternating—current (AC) power supply and
3. the workpiece itself.

A variety of manipulation procedures can be employed to suit the geometry of the component including "single-shot hardening" in which the entire area to be hardened is heated in one operation then quenched, and "progressive hardening", which involves relative movement between the heating coil, quench head and the workpiece.

Induction hardening can be applied to a wide range of steels and cast irons. Normally medium-carbon steels (0.35–0.5 % carbon), with or without alloying additions, are used to ensure a satisfactory hardening response.

The depths of the hardened layer can be varied based the needs or specifications. The depth is a function of the frequency of the AC current, with lower frequency producing a deeper case. Typically, the hardness penetration depth ranges from 0.5 to 5 mm and the hardness that can be achieved is 50–60 HRc.

Induction hardening process includes water quench after the heating process.

1.3.2 High Frequency Resistance Hardening

For induction hardening a closed loop of current is required. For *high frequency resistance hardening* (400 kHz) this is not required, and thus any stripe of any reasonable shape can be heated between two points. The hardening apparatus consists of water cooled proximity conductor that is placed close to the surface to be heated and connected to the contacts (Fig. 1.3). The source of 400 kHz power for heating is typically 50–300 kW, depending on the area to be heated.

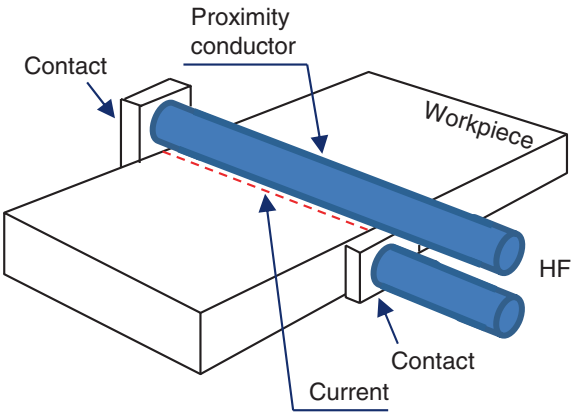

Fig. 1.3 Basic principle of high-frequency resistance hardening

In hardening steel, the metal is heated to about 870 °C. The high power densities generated by this process heat very rapidly and thus result in hardening through self-quenching by the cold steel surrounding the hot stripe. The achievable hardness reaches 62 HRc. The depth of the hardened layers varies from 0.64 to 0.89 mm for the steels, depending on the time of heating and the power level.

1.3.3 Flame Hardening

Flame hardening involves the direct impingement of a high temperature flame or a high-velocity composition-product gas from suitably designed and positioned burners onto the surface area to induce austenitizing. The martensite is usually imposed by a water quenching. Depth of hardening is controlled by the design of the flame head, time of heating and hardenability of the material.

The ideal material for flame hardening is medium carbon steels with 0.40–0.50 % carbon, but steels with up to 1.50 % carbon content can be flame-hardened. Case depths up to 12.70 mm are possible, typically hardness depths range from 0.25 to 6 mm and the hardness that can be achieved is 50–60 HRc. The heating media can be oxygen acetylene, propane or any other combination of fuel gases that will allow reasonable heating rate.

There are four general flame hardening methods (Fig. 1.4):

- *Spot method*. In this method the torch and the metal part are both held stationary.
- *Straight-line progressive method*. With the straight-line progressive method, the torch travels along the surface, treating a strip that is about the same width as the torch tip.

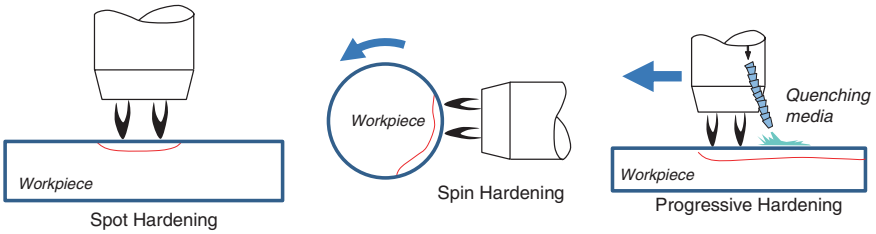

Fig. 1.4 Three basic methods of flame hardening

- *Spiral band progressive method*. For this technique a cylindrical part is mounted between lathe centres, and a torch with an adjustable holder is mounted on the lathe carriage. As the part rotates, the torch moves parallel to the surface of the part. This travel is synchronized with the parts rotary motion to produce a continuous band of hardness. Heating and quenching occur at the same time.
- *Circular band spinning method*. The circular band spinning method provides the best results for hardening cylindrical parts of small or medium diameters. The part is mounted between lathe centres and turned at a high rate of speed past a stationary torch. Enough torches are placed side by side to heat the entire part. The part can be quenched by water flowing from the torch tips or in a separate operation.

1.3.4 Laser Beam Hardening

Lasers with sufficiently high power density (from 0.5 to 15 kW) are used for hardening steels. The heat is generated as the laser impinges on the surface of the workpiece at a rate much faster than heat conduction into the interior can dissipate it. This results in the heating of a thin surface layer in austenitizing temperature while the interior of the workpiece is still cool. The quenching of the heated surface is by self-quenching (i.e. the mass of the cool workpiece is used as a heat sink in the same manner as welding).

The materials that can undergo such process are hardenable cast irons and steels. A minimum carbon content of 0.30 % is a prerequisite for a steel to be laser hardened. The absorption of the laser radiation is quite low, and thus energy-absorbing coatings are used increasing the absorbing ratio up to 60 %. As referenced above, laser hardened parts do not generally require external quenching. In order though to take advantage of self-quenching, the part should be 5–8 times thicker than the case at the point where the laser beam impinges.

The depth of the hardened layer depends on the hardenability of the material, but this is rarely more than 2.5 mm. Typical hardness penetration depth is in the range from 0.1 to 2 mm. The hardness values achieved are in the range of HV 490–820.

The basic component of a laser hardening system is the laser source (CO_2 gas type up to 15 kW or solid state YAG up to 400 W). The main difference from the metal-cutting lasers is the utilization of optical integrators, required for shaping the collimated beam into square or rectangular beam with uniform power density in the focal plane of the device. The integrators consist of an array of square or rectangular molybdenum mirrors mounted on a spherical surface. A number of other optical aids are used for hardening of areas of complex geometry such as toric mirrors, conical copper mirrors and beam splitters.

1.3.5 Electron Beam Hardening

Electron Beam Hardening involves high-power (1–10 kW) electron beam (2–3 mm spot size), scanned over surface by electromagnetic deflection. The process uses a concentrated beam of high-velocity electrons as an energy source to selectively heat the desired surface areas of ferrous parts. An electron beam gun is used to accelerate the electrons and form them into a beam. The directed beam passes through a focus coil to control the beam density levels. A deflection coil is used to move the beam spot on the workpiece surface.

The process can be highly automated, but needs to be performed under vacuum conditions since the electron beams dissipate easily in air. High vacuum (1.3×10^{-3} Pa) is required for the production of the electron beam.

There are two different set-ups:

- the static (employs no relative motion between the workpiece and the heating pattern) and
- travelling methods of electron beam heating (uses workpiece motion to accomplish surface hardening of large areas).

The bombarding of the area with electrons results in rapid heating of the surface layers (in 0.5–3.0 s the austenitizing temperature is achieved). Similar to laser hardening no quenchant is required and martensite formation is attained through self-quenching. Self-quenching is controlled by the mass of the workpiece, the hardenability of the metal, initial temperature of the workpiece and the rate of heating.

The materials that can be electron beam hardened must contain sufficient carbon and alloying elements. Furthermore, the workpiece must be big enough to allow self-quenching process (a mass of up to eight times that of the volume to be hardened is required). Maximum hardness that can be achieved is 62 HRC and the hardening depth is 1–2 mm.

1.3.6 Electrolytic Hardening

Electrolytic surface hardening is a special hardening method employing electrolysis in an aqueous solution under particular conditions. Variables include the electrolyte, the voltage and the current. If a stable hydrogen film is formed and electric

discharges including electron and ion avalanche occur, the workpiece, acting as the cathode, will be heated violently to the austenitizing temperature due to generation of resistance heat.

On disconnecting the electrical circuit, the hydrogen film disappears and the workpiece surface will be self-quenched or be quenched immediately by the cold electrolyte in its vicinity, the result being that the workpiece hardens.

1.4 Hybrid Surface Modification Methods

Given the definition of hybrid processes and the classification proposed by Lauwers et al. [1], grind hardening is considered a hybrid process that is based on the combination of controlled process mechanisms (in that case grinding and hardening). Similar processes include forming and hardening (due to hot stamping) and cryogenic deep rolling.

1.4.1 Grind Hardening

As already indicated, grind hardening is based on controlling the grinding process generated heat for heating locally the processed workpiece in order to increase its surface hardness (Fig. 1.5). The metallurgic change required for hardening is achieved by heating the surface above austenitization temperature and through subsequent quenching, martensitic transformation is induced on the workpiece surface. The main advantage of such process is the elimination of waste such as waiting, transportation and set-up time by combining the two processes into one. Klocke et al. [3] adapted the TRIZ methodology for analysing the evolution from grinding to grind-hardening process. A key step in their analysis was the common cause and effect relationship shared by grinding and hardening processes (as shown in Fig. 1.6).

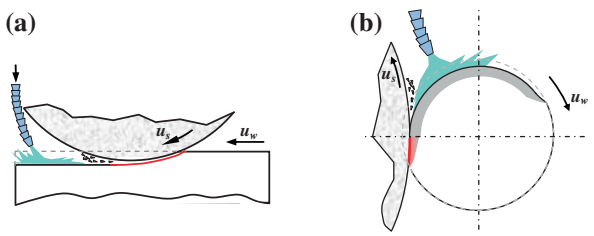

Fig. 1.5 Grind-hardening process principle: **a** surface and **b** cylindrical grind hardening

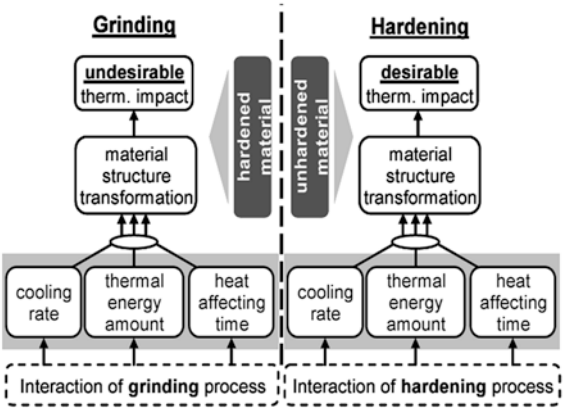

Fig. 1.6 Common cause and effect relationship shared by grinding and hardening processes proposed by Klocke et al. [3]

The grind-hardening process was introduced by Brinksmeier and Brockhoff [4]. Initially the process was investigated experimentally [5] in order basically to cover a number of different aspects such as the thermal analysis of the process [6], the cutting fluid significance [7], the grinding wheel specifications effect [8], the grinding forces [9] and recently the residual stresses [10]. The literature review has shown that the grind-hardening process is characterized by many physical quantities. In Chap. 2, a comprehensive and detailed state of the art of the grind-hardening studies will be presented.

1.4.2 Hot Stamping

Surface hardening by hot stamping can be achieved when the cooling rates after the forming process exceeds a critical level. In a few studies it has been reported, for example, in the hot stamping of 22MnB5 [11].

1.4.3 Cryogenic Deep Rolling and Hardening

Cryogenic deep rolling process has been proposed as an alternative hardening process [12]. The process is based on martensitic transformation that is mechanically induced, and has been proven its feasibility experimentally [13]. Key process parameters identified include the rolling ball diameter and the rolling pressure. Feed speed and circumferential speed are less important. In Fig. 1.7, a deep-rolling experimental set-up is shown.

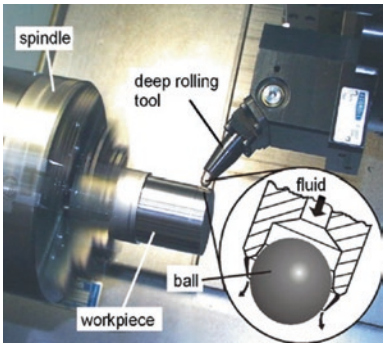

Fig. 1.7 Deep rolling experimental set-up [14]

	Fundamental research	Concept development	Prototype development	Series production test	Series production
Grinding hardening					
Hot stamping hardening					
Cryogenic deep rolling					
Hard machining					

Fig. 1.8 Technology maturity level (Based on Lauwers et al. [1])

1.4.4 Maturity of Hybrid Processes

Lauwers et al. [1] estimated the technological maturity level of various hybrid processes, indicating that all these process are still not up to the series production level (Fig. 1.8). The range is justified by the fact that for some materials the maturity (i.e. the control and repeatability of the process) is higher than for other materials. As indicated by Lauwers et al. [1] the development of such processes is driven by the industrial needs.

References

1. Lauwers B, Klocke F, Klink A, Tekkaya E, Neugebauer R, Mcintosh D (2014) Hybrid processes in manufacturing. CIRP Ann Manuf Technol 63(2):561–583
2. Wick C, Veilleux RF (1985) Tool and manufacturing engineers handbook, vol 3—materials, finishing and coating. Society of Manufacturing Materials, Michigan
3. Klocke F, Roderburg A, Zeppenfeld C (2011) Design methodology for hybrid production processes. Procedia Eng 9:417–430
4. Brinksmeier E, Brockhoff T (1996) Utilization of grinding heat as a new heat treatment process. CIRP Ann Manuf Technol 45(1):283–286
5. Brockhoff T (1999) Grind-hardening: a comprehensive View. CIRP Ann Manuf Technol 48(1):255–260

6. Salonitis K, Chryssolouris G (2007) Thermal analysis of grind-hardening process. Int J Manuf Technol Manage 12:72–92
7. Salonitis K, Chryssolouris G (2007) Cooling application in grind-hardening operations. Int J Adv Manuf Technol 33:285–297
8. Salonitis K, Chrondros T, Chryssolouris G (2008) Grinding wheel effect on grind-hardening process. Int J Adv Manuf Technol 38:48–58
9. Salonitis K, Stavropoulos P, Kolios A (2014) External grind-hardening forces modelling and experimentation. Int J Adv Manuf Technol 70:523–530
10. Salonitis K, Kolios A (2015) Experimental and numerical study of grind-hardening-induced residual stresses on AISI 1045 Steel. Int J Adv Manuf Technol. doi:10.1007/s00170-015-6912-x
11. Lechler J (2009) Beschreibung und Modellierung des Werkstoffverhaltens von presshaertbaren Bor-Manganstaehlen. Meisenbach Verlag
12. Meyer D, Brinksmeier E, Hoffmann F (2011) Surface hardening by cryogenic deep rolling. Procedia Eng 19:258–263
13. Meyer D (2012) Cryogenic deep rolling—an energy based approach for enhanced cold surface hardening. CIRP Ann Manuf Technol 61(1):543–546
14. Brinksmeier E, Garbrecht M, Meyer D (2008) Cold surface hardening. CIRP Ann Manuf Technol 57(1):541–544

Chapter 2
Grind-Hardening State-of-the-Art

Abstract Grind-hardening process has a history of almost 20 years. Since its introduction, numerous studies have been presented focusing on a number of aspects of the process such as the modelling of the process, the impact of the process parameters, the grinding wheel importance, etc. In the present chapter, the relevant literature to grind-hardening process is classified and summarized. More than 100 papers have been reviewed.

2.1 Introduction

In conventional grinding of hardened steels, the thermal impact on the surface layer can result in surface layer damages due to structural alterations by annealing or re-hardening. By annealing, the surface layer hardness can be reduced significantly, which causes a decrease of the wear resistance and rolling contact strength. Due to the extreme hard and brittle martensitic structure at the surface and an annealed zone lying beneath, re-hardened layers are characterized by very steep hardness gradients. Combined with surface stresses, this can cause crack initiation and crack propagation. In contrast to this, in grind hardening the heat dissipated in the contact zone between grinding wheel and workpiece is used for the material's surface layer austenitization. The critical cooling rate demanded for martensitic hardening of the austenitized surface layer is mainly achieved by self-quenching mechanism and supported by the ambient cooling lubricant. Due to the kinematical contact conditions in grinding, grind hardening is a short-time metallurgical process applying austenitization durations of splits of seconds.

Grind-hardening process is a relatively new one that was introduced by Brinksmeier and Brockhoff [1] in mid 1990s. However, the possibility of using the heat generated during grinding for changing the material's structure had been already studied by Eda et al. [2], Shaw and Vyas [3], and Zhang and Mahdi [4]. Since the introduction of the process, the interest in the process has been increased internationally as can be seen in Fig. 2.1 by the rising numbers of publications. Since 1995, 112 relevant publications were collected through searching scientific paper databases

K. Salonitis, *Grind Hardening Process*, SpringerBriefs in Manufacturing and Surface Engineering, DOI 10.1007/978-3-319-19372-4_2

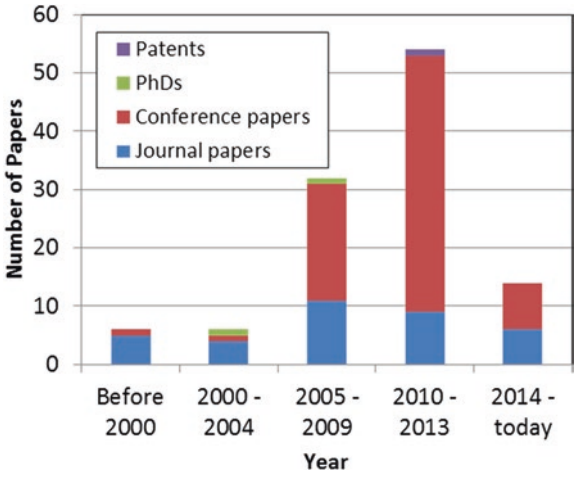

Fig. 2.1 Results of the literature research

(such as Scopus, Web of Science, Google Scholar etc.) and scientific publishers' archives. 30 % of these papers have been published in scientific journals whereas the rest were presented in scientific conferences after review. Two PhD theses and a patent on the grind-hardening process were also found. The present chapter highlights the state of the art with regards the grind-hardening process since its introduction in 1995. In a recent study, Klocke et al. [104] introduced a systematic design method that suggests that grind-hardening process was developed in order to overcome and enhance the limits of today's production technologies.

2.2 Grind-Hardening Process Overview

In industry, a number of different heat treatment methods for the production of the required surface layer properties are used, as was discussed in Chap. 1. The problem is that these processes cannot simply be integrated into the production line thus causing economical disadvantages. Furthermore, the manufacturing of high-quality steel parts involves usually grinding processes. Grind hardening (Fig. 2.2) is a process combining the grinding and heat treatment processes into one. It utilizes the friction-generated heat flow, in order to achieve high surface hardness. The surface hardness of the workpiece is increased by the dissipation of the heat into the workpiece. The heat dissipation increases the surface temperature of the workpiece in the austenitic range. Due to high heat flow rates and rapid advancement of the grinding wheel, the workpiece area left behind the grinding wheel is subjected to rapid quenching, mainly due to heat absorption from inner cold areas of the workpiece. This self-quenching process induces martensitic transformation to the workpiece material, resulting in hardness improvement.

The main process parameters are the workpiece speed, the depth of cut, the cutting speed, the workpiece material and the grinding-wheel type; while the result

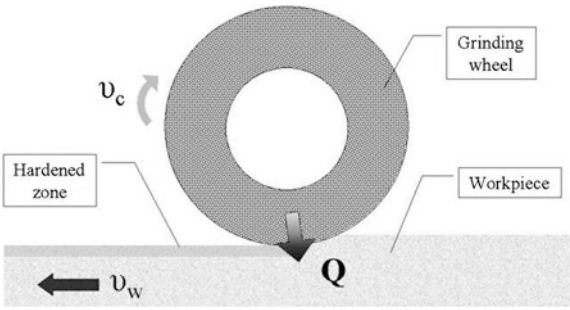

Fig. 2.2 Grind-hardening process outline

can be described from the hardness penetration depth (HPD) and the surface hardness. Hardness quantitatively represents the degree to which a metal will resist cutting, abrasion, penetration, bending and stretching. HPD on the other hand is the depth beneath the workpiece surface where the hardness has decreased to 80 % of the nominal hardness value on the surface.

A first concern in grind hardening is the proper selection of process parameters, so as to produce enough heat at the contact zone enabling the heat treatment of the workpiece. Moreover, the proper parameter selection must allow for suitable conditions for the quenching of the material in order to achieve maximum surface hardness.

The surface hardness and the HPD are mainly influenced by the material type and the temperature distribution in the workpiece. The surface hardness depends on the carbon content of the workpiece and the cooling rate. On the other hand, the HPD depends on the temperature field in the workpiece.

2.3 Fundamental Mechanisms in Grind Hardening

Heat treatment methods are utilized in order to alter the technological properties such as the strength, wear resistance, fatigue strength, hardness, impact strength and tendency for brittleness. Steels can be heat treated to produce a great variety of microstructures and thus obtain desired surface properties. The hardening mechanism is based on the phase transformation of austenite to martensite.

The steel before any heat treatment process has ferrite–pearlite structure (face-centred cubic). During grind hardening, heat flow from the contact zone dissipates in the steel, resulting in the increase of the surface temperature. There is a critical temperature at which the carbides in the lamellar pearlite begin to dissolve into iron. As the temperature is raised, more of the carbides are dissolved until the steel consists completely of a solid solution of carbon in iron called austenite (face-centred cubic lattice structure). These critical temperatures where the ferrite–pearlite transformations commences and finishes are depended on the carbon content of the steel and are derived from iron–carbon phase diagrams.

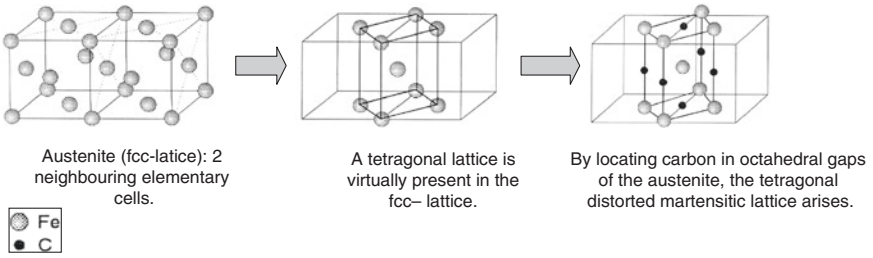

Fig. 2.3 Martensite formation

If the austenite-structured steel was left to cool in quasi-state mode, the austenite would be transformed back to ferrite–pearlite structure. Martensite is induced due to the rapid cooling or quenching in order to avoid the diffusion-dependent transformation that produces ferrite–pearlite. The exact cooling conditions that will result in martensite structure in any steel alloy are strongly dependent on carbon content, alloying and austenitic grain size.

The martensitic transformation is characterized by shearing of the austenite lattice (face-centred cube) to the martensite lattice (tetragonal deformed) without diffusion (Fig. 2.3), and therefore, the martensite has exactly the same composition as does its parent austenite, up to 2 % carbon, depending on the alloy composition. Since the diffusion is suppressed, the carbon atoms do not partition themselves between cementite and ferrite-pearlite but instead are trapped in the octahedral sites of the martensitic body-centred cubic structure.

The shear mechanism for the martensite formation is based on the simultaneous and cooperative movement of atoms in contrast to atom-by-atom movement across interfaces during diffusion-dependent transformation.

The critical cooling rate needed for martensite formation, for the case of grind hardening, is reached either by heat dissipation from the austenized surface layer to the cooler workpiece core or by using a coolant fluid. This immediate transformation due to self-quenching presents some advantages in comparison to through-hardening. Grind hardening along with laser hardening and induction hardening are categorized as short-time heat treatment processes due to the very short time required for heating and subsequently quenching. In contradiction to processes that require heating using furnaces and quenching in suitable mediums and are characterized as long-time processes. The heating rate for grind hardening was estimated to be 10^7–10^8 C/s and the heat affecting time is normally less than one second, whereas through heat treatment with all the process cycle times taken into consideration (heating, normalizing, quenching, tempering, etc.) may require up to 24 h processing.

Concerning their homogeneity, short-time austenized, hypoeutectoid steels differ just negligibly from long-time austenized steels, because the subsiding homogenization occurs very quickly (normalization). In short-time treatment of hypereutectoid steels containing higher carbon contents, the risk of overheating the material exists, that could lead to coarser martensite needles and more retained austenite within the hardened structure. In short-time heat treatment processes generally the

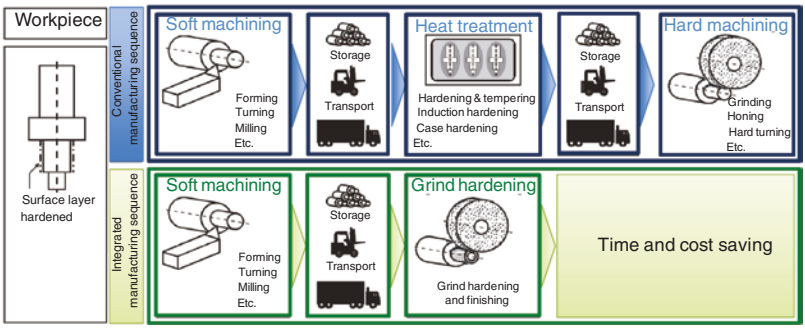

Fig. 2.4 Comparison of a conventional production chain and a production chain including grind hardening

austenizing time is decreased with increasing energy density in the surface layer to avoid melting of the material. As a result, the achievable hardness penetration depth decreases. The thermal aftereffect on martensite is suppressed due to rapid self-quenching, whereby an extremely fine-grained martensitic structure remains.

2.4 Alternative Process Chains

Grind-hardening process makes possible the integration of surface heat treatment not only into the production line, but moreover into the machining process [5]. The result of such integration will be the shortening of the production sequences and the subsequent reduction of the cost. The reduction of cost is justified by the substitution of a number of process steps (less machine set-ups) such as cleaning and transportation to the heat treatment department (Fig. 2.4). Conventional heat treatment methods are not categorized as "eco-friendly" processes due to the excess use of chemical additives, salts and oil quenchants. On the contrary, grind hardening is based on the efficient energy usage philosophy, utilizing the heat generated during grinding to harden the surface layer of the machined part.

2.5 Fundamental Investigations—Feasibility Studies

A number of aspects need to be considered for the controlling of the grind-hardening processes. Some of these aspects can be considered as system parameters and some as grinding process parameters. For example, the systems parameters include the grinding wheel, the grinding fluid, the workpiece material and geometry and the machine tool. On the other hand, the process parameters that need to be considered include the cutting speed, the depth of cut, the feed speed and the grinding fluid supply. Figure 2.5 summarizes the most influencing parameters on grind hardening.

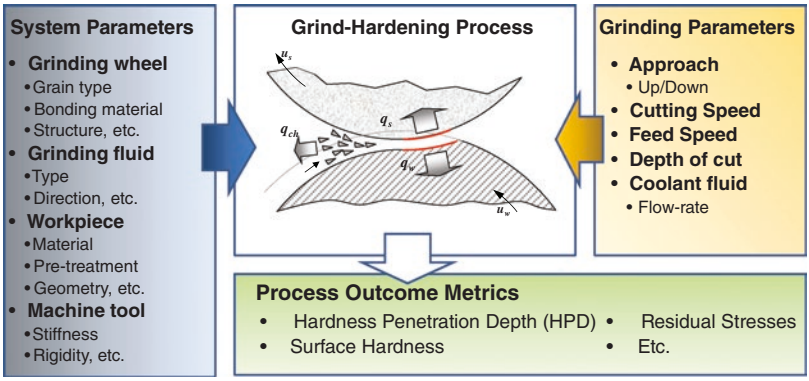

Fig. 2.5 Grind-hardening parameters and the process outcome metrics

2.5.1 Workpiece Material

Fundamental investigations on the process indicate that the hardening result is dependent on the chemical composition and the microstructure of the material, the grinding wheel specification and the process parameters. Conventional heat treatment interrelations are evidenced for grind hardening as well. Generally, martensitic hardenable steels can be ground-hardened. The most applicable metals for grind hardening are the heat-treatable and ball-bearing steels (Table 2.1). The hardening result is determined by the carbon content and the content of alloying elements. The maximum surface hardness that can be obtained is approximately 60 HRC. The comprehensive literature review has shown that research has been conducted on all possible materials (Table 2.2). However, most of the researchers have focused on AISI 52100, AISI 1045, AISI 1065, AISI 4140 and AISI 5140.

AISI 5120 was possibly the first material to be investigated for grind-hardening process [1]. AISI 52100 is a high-carbon, chromium containing low alloy steel and is considered a typical bearing steel alloy. The maximum hardness that can be achieved is usually close to 800 HV with a hardness penetration depth exceeding 300 μm [1, 6]. In a number of studies, though hardness penetration depths close to 1 mm when using lower feed speeds have been reported (indicative sources: [6–8]). In most cases the resulting residual stress profile exhibits compressive stresses close to the surface and can be controlled by careful consideration of the grinding parameters [9].

AISI 1045 is a medium-tensile steel used for a range of different applications such as gears, axles and rolls that require local hardening. It has low through-hardening capability, but can be hardened locally up to hardness levels of 54–60 HRc (400–550 HV). Usually, this hardening takes place through flame or induction hardening. As can be seen in Table 2.2, a number of investigations on grind hardening of this alloy that have been published were reported successful operations. Zurita et al. [10] reported quite lower achievable hardness (up to

Table 2.1 Chemical composition of relevant hardenable steels

Alloy steel designation	Nominal composition (wt%)						
	C	Mn	Si	Cr	Ni	Mo	Fe
AISI 1020	0.17–0.23	0.30–0.60	–	–	–	–	Balance
AISI 1045	0.42–0.50	0.50–0.80	0.17–0.37	≤0.25	≤0.3	–	Balance
AISI 1060	0.55–0.66	0.60–0.90	–	–	–	–	Balance
AISI 1065	0.60–0.70	0.60–0.90	–	–	–	–	Balance
AISI 1066	0.60–0.71	0.80–1.10	–	–	–	–	Balance
AISI 4140	0.38–0.43	0.75–1.00	0.10–0.35	0.80–1.10	≤0.25	0.15–0.25	Balance
AISI 4340	0.37–0.43	0.60–0.80	0.15–0.30	0.70–0.90	1.65–2.00	0.20–0.30	Balance
AISI 5140	0.37–0.44	0.50–0.80	0.17–0.37	0.80–1.10	≤0.030	–	Balance
AISI 52100	0.95–1.05	0.25–0.45	0.15–0.35	1.30–1.65	–	–	Balance
AISI D2	1.5	0.45	0.25	12	–	1	Balance

Table 2.2 Grind hardening studies presented classified per material

Alloy steel designation	Equivalent designation used in the studies	Relevant studies
AISI 1020		[35]
AISI 1045	C45E4, #45	[10–14, 26, 36–48]
AISI 1060		[49]
AISI 1065	65Mn	[15, 16, 50–55]
AISI 1066		[56]
AISI 4140	42CrMo4	[1, 5, 17, 48, 57–60]
AISI 4340		[61]
AISI 5140	40 Cr, 41Cr4, 48MnV	[18–22, 45, 47, 62–72]
AISI 52100	100Cr6	[1, 4–9, 27, 29–33, 48, 73–78]
AISI D2	SKD-11	[23–27]

250 HV); however, Nguyent et al. [11, 12] reported hardness up to 700 HV under dry grind hardening conditions and almost 1,000 HV when assisting the cooling with liquid nitrogen. The typical hardness penetration depth achieved is approximately 0.5 mm (in almost all studies reviewed). The residual stresses profile can be controlled in order to achieve compressive stresses close to the surface of the workpiece [11, 13, 14].

AISI 1065 is a high-carbon steel. Grind hardening of such workpiece materials can result in (close to surface) hardness in the range of 810–870 HV [15, 16]. The achievable hardness penetration can reach up to 2.0 mm as has been reported by Liu et al. [15]. No studies were reported on the residual stresses profile.

AISI 4140 was also among the first workpiece materials to be investigated for grind-hardening process [1, 5]. The maximum achievable hardness is close to 800 HV [1, 5] and the hardness penetration depth that can be achieved is up to 1.0 mm [5]. Fricker et al. [17] presented experimental results of hardness penetration depth values close to 2.0 mm. Compressive residual stresses can be achieved in the white etching areas and the following area of etchable martensite.

Grind hardening of AISI 5140 has been extensively investigated as can be seen in Table 2.2. Hardness can be increased up to 750 HV, with a hardness penetration depth of 1.6 mm [18–20]. Compressive residual stresses can be achieved at the surface of the workpiece material [21, 22].

AISI D2 is a high-carbon, high-chromium tool steel. It can be heat-treated and the hardness can be increased in the range 55-62 HRC. Typically, it is used for manufacturing dies, punches and rolls. Successful grind hardening of such material has been investigated in few studies [23–25]. Finally, one study per AISI 1060, 1066 and 4340 workpiece materials has been presented, and thus no strong conclusions can still be drawn for these alloys.

One of the prerequisites for hardening is sufficient carbon and alloy content. The materials that can be hardened with grind-hardening process usually have at least 0.3 % carbon content. Nevertheless, few papers have been published where successfully grind-hardening alloys of less than 0.3 % carbon content (such as AISI 1020 [26]) is reported.

Furthermore, the initial microstructure (pre-treatment) of the material is critical for the hardening result. In grind hardening, steels in annealed or tempered initial state are hardened. Due to finer dispersion of carbon, tempered initial states lead to reduced diffusion ways and advantageous conditions during austenitization. Deeper hardness penetration depths can be achieved for a tempered material than for an annealed material as pointed out by Brockoff [5] for the case of AISI 52100. Furthermore, the transition from the maximum hardness down to the hardness of the bulk material appears much steeper as for the tempered steel. The tempered material transforms to austenite at lower temperatures, which is equivalent to greater depths beneath the surface in grind hardening. This, furthermore, enables the faster homogenization compared to the austenite formed from the annealed structure.

2.5.2 Workpiece Geometry

Grind-hardening process can be used for selectively heat-treating the surface of both cylindrical and prismatic parts. Most of the papers reviewed focus on the surface grind-hardening process. The key challenge for using this process in complex geometries is the tempering of the already heat-treated surface when the grinding wheel has to pass more than once from the same vicinity. For this reason, the grinding wheel to be used ideally should be wide enough to process all the area. This can be achieved for the case of narrow prismatic parts, as shown by Salonitis et al. [27] for the case of a V-shaped guide.

For the case of cylindrical parts, overlapping is unavoidable as can be seen in Fig. 2.6. This results in tempering of the material, since when the grinding wheel "returns" to the entering point, the already quenched area is reheated in the martensitic range of temperatures. A number of different techniques have been investigated to overcome this problem, such as adaptive control of the grinding wheel rotation speed, modification of the workpiece material (altering the depth of cut) to name few. A recent patent [28] has been granted that attempts to control the overlapping through tangential plunging of the grinding wheel in the workpiece material.

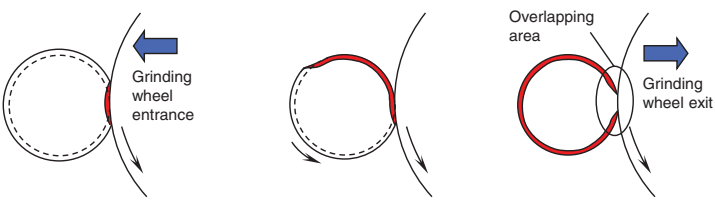

Fig. 2.6 Cylindrical grind-hardening challenge: overlapping area

Table 2.3 Grind hardening studies classified per grinding wheel (listed only the papers where the grinding wheel type is explicitly stated)

Grinding wheel types	References
Corundum	[1, 5–8, 10–15, 19–21, 26, 27, 29–33, 35, 40, 43, 45, 47, 49, 50, 52, 54, 56, 58, 61, 63, 69, 73–75]
CBN	[17, 57, 76, 79, 91]

2.5.3 Grinding Wheel

In grind hardening, the grinding wheel specification influences the heat dissipation and thus the hardening result decisively. In the papers reviewed, 38 reported to have used corundum (aluminium oxide) grinding wheels, and only 4 CBN wheels (Table 2.3). The preference to corundum wheels is due to their lower heat conductivity, allowing thus for more heat to directed in the workpiece material.

Most of the researchers are using fine-grained, resin-bonded corundum wheels of high bond hardness and closed structure. Salonitis et al. documented the effect of the corundum grinding wheel specifications (grain size, hardness and structure) on process forces [29] and hardness penetration depth [30]. Utilization of softer wheels was shown to result in reduced process forces since grain and bonding fracture occurs more easily, and consequently, fewer grains interact with the grinding wheel. Additionally, the hardness penetration depth is increased; this may be attributed to the fact that softer grinding wheels can be more easily deformed and thus, more grains are likely to interact with the workpiece material. The structure number of a grinding wheel represents its porosity; denser grinding wheels were shown to induce higher process forces. The grain size had the smallest effect on the process forces. Grinding wheels with finer grits resulted in higher process forces since more grains are involved in the process, and therefore, more chips are formed, while the cutting forces are increased. However, the hardness penetration depth is reduced since more grains are involved in the process, removing thus more material and thus more heat is removed from the grinding area.

Compared to resin bonded, the use of vitrified bonded wheels can result in heavy loading of the grinding wheel leading to high forces, increased wheel wear and unstable process [5].

CBN and corundum present great differences in terms of the thermal conductivity of the abrasives. Aluminium oxide grains direct the heat towards the workpiece material, whereas the CBN abrasive is able to remove a significant proportion of heat from the grinding zone by heat transfer through the abrasive segments into the steel hub of the wheel [17, 31]. However, CBN can be used for grind hardening, although it has been shown experimentally [17] that there is an upper limit on the workpiece surface speed that can be used.

2.5.4 Process Parameters

Grind hardening process occurs within a small window of process parameters combinations. A number of studies have been published that are focused in defining this process window. Indicatively, Fricker et al. [17] presented a process map (Fig. 2.7) for the case of dry CBN grind hardening of AISI 4140. Salonitis [7, 32] presented process maps for the case of both dry and wet grind hardening of AISI 52100 with corundum wheel (Fig. 2.8). The available maps can be used for selecting the process parameters based on the design requirements (such as hardness penetration depth) and the limitations set by the grinding machine. Salonitis et al. [27] used these process maps for selecting the process parameters for the grind hardening of a V-shaped guide. The process for deriving these process maps is described in detail in the Chap. 3 of the present book.

An interesting theoretical process limitation is the maximum achievable hardness penetration depth. Salonitis and Chryssolouris [33] estimated the maximum

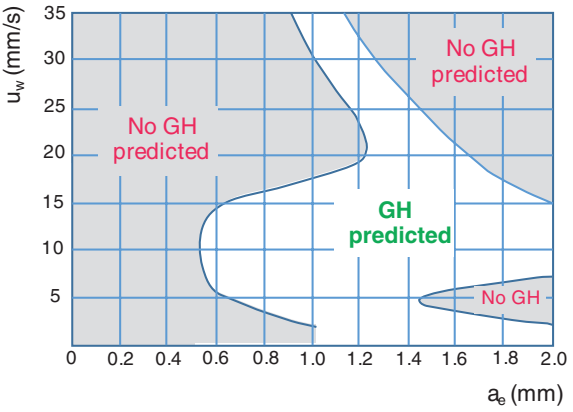

Fig. 2.7 Process map for the occurrence of grind hardening of AISI 4140 using a CBN grinding wheel (based on the results presented in [17])

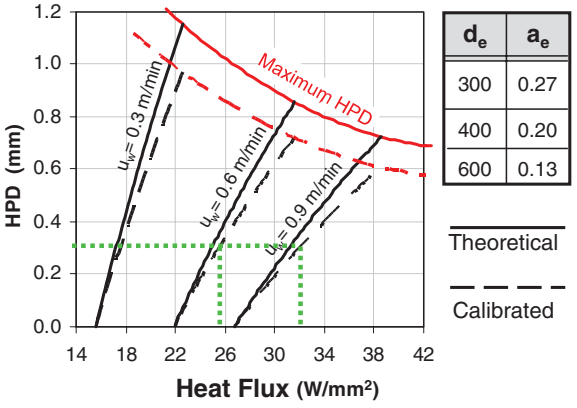

d_e	a_e
300	0.27
400	0.20
600	0.13

Fig. 2.8 Process map for selecting parameters combination for the grind-hardening of AISI 5120 using corundum grinding wheels [30]

depth based on the assumption that this will occur when the surface temperature reaches the melting temperature. This limit is depicted in the process maps developed as can be seen in Fig. 2.8.

It is thus obvious that the hardening result can be controlled by the process parameters with most important ones being the depth of cut and the feed speed. Furthermore, the cutting speed (grinding wheel speed) can be used for controlling the process.

- **Depth of cut**
  In surface grinding with constant feed speed, the depth of cut is proportional to the specific material removal rate as well to the equivalent chip thickness. For constant specific material removal rate, an increase of the depth of cut results in deeper HPD (Fig. 2.9). The maximum HPD is achieved in the transition area between the pendulum and creep feed grinding. A further increase of the depth of cut leads to decreasing HPD in the area of creep feed grinding.

To maximize the HPD in grind hardening, high depths of cut have to be applied. On the other hand, such a procedure will be limited by the spindle power of the machine tool and the required accuracy of the workpiece. Furthermore, too high energy inputs to the workpiece could lead to undesired alterations in the material like hardening cracks or tempered zones at the surface. For industrial applications, the depth of the cut needs to be optimized for each component considering its special demands and operational loadings.

- **Feed speed**
  The feed speed is directly affecting the heat entering the part. For very low feed speeds, the generated grinding power and thus the generated heat is too low for the austenitization. When increasing feed speed, the generated heat and the HPD increases (Fig. 2.9). A further increase of the feed speed results in shorter contact times leading to decreasing HPDs. Thus, maximum HPD can be achieved in for medium feed speeds.

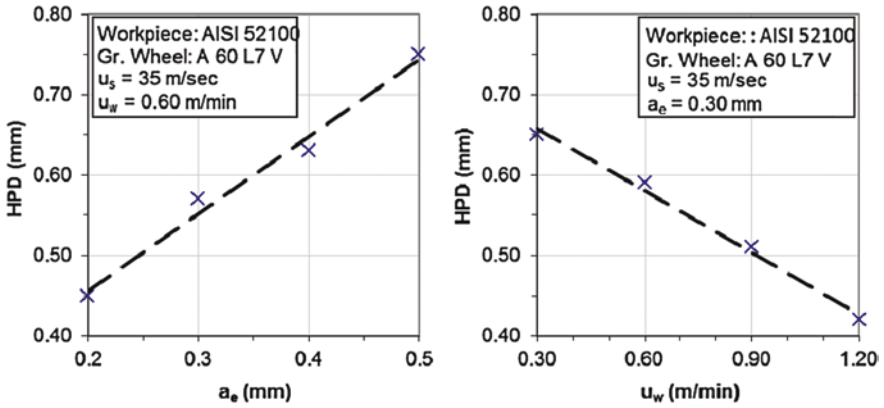

Fig. 2.9 Depth of cut and workpiece speed effect on hardness penetration depth (based on the experimental data presented in [33] for AISI 52100)

- **Cutting speed**
  The influence of the cutting speed is quite complex. The increased cutting speeds lead to partly decreasing cutting powers, while in some ranges the opposite occurs.

In a number of studies the effect of the process parameters on the surface quality of the processed workpiece has been presented as well. Indicatively, the impact on burr formation has been discussed [94, 106, 107]. Chamfer is also of interest with regards the impact it has to the achievable hardness distribution [107, 108].

2.6 Simulation of the Grind-Hardening Process

Modeling and simulation of grinding processes has been thoroughly reviewed [34]. Grind-hardening process modelling, being an abrasive process, was based on the models presented for relevant grinding processes. 50 papers out of the 112 reviewed presented models for predicting one or more aspects of the grind-hardening process. Most of the models presented for the estimation of temperature distribution within the workpiece material and the subsequent estimation of hardness penetration depth and/or residual stresses are based on finite element method. However, estimation of the heat generated between the grinding wheel and the workpiece material is in most cases either calculated empirically or using analytical models.

In the following Table 2.4, the classification of the papers based on the type of analysis (FEA or analytical), modelling dimensions, modelled attribute response

Table 2.4 Grind hardening simulation-modelling studies

	Modelled attribute					
Modelling method	Process forces	Temperature	Phase transformation	Surface hardness	HPD	Residual stresses
FEA—2D	–	[4, 6, 7, 9, 12–14, 21, 22, 27, 30–33, 35, 38, 39, 64–66, 69, 74, 76, 78, 80–87, 111]	[4, 9, 12, 65, 76, 82, 110]	[35, 57, 74, 76, 82, 85]	[6, 7, 27, 30–33, 35, 66, 74, 99, 100]	[4, 9, 13, 14, 21, 22, 76, 82, 85]
FEA—3D	–	[8, 27, 32, 37, 40, 41, 43, 47, 67, 68, 75, 78, 88, 89]	[8, 32, 40, 43, 75, 78]	[32, 40, 43, 78]	[27, 32, 40, 67, 68]	[89]
Analytical	[8, 29, 30, 32, 42, 69, 73]	[17, 36, 96–98]	[17, 20, 32, 78]	–	–	–
Empirical	[6, 31]	[102]	[7, 32, 33, 105, 112]	[7, 32, 33, 109]	[90, 95]	–

(temperature, forces, HPD, residual stresses, etc.). In the following chapter that focusses on the grind-hardening process modelling, these models are reviewed in more detail.

Further to the modelling and simulation of the process mechanics, a number of studies have been focused also on the environmental impact of the grind-hardening and the benefits gained by combining heat treatments with grinding. Chapter 4 will present in detail the state of the art, however for the sake of completeness, a brief overview will be given here as well. The benefits with regards the resource efficiency have been highlighted by Reinhart et al. [103]. Salonitis et al. in a number of studies focused on the environmental impact assessment using both life cycle assessment [93] and energy audits [77, 101]. Few other studies on the ecological merits of grind-hardening have been presented as well [92].

2.7 Challenges for Future

Although, grind hardening is a highly innovative process, industrial introduction is restricted by a number of factors. One of the main open issues of today's state of the art of grind-hardening technology is the formation of overlapping areas. Overlapping areas which can also occur in induction hardening are generated in cylindrical grinding after one revolution of the workpiece when an area which was already grind hardened is again thermally influenced by the grinding process. Particularly, in cylindrical grind hardening, improper junction of the hardened surface layer is generated in overlapping areas. In the overlapping area, the hardened surface layer material is annealed, resulting in reduced hardness and decreased hardness penetration depth. Thus grind-hardening technology today is limited to applications where overlapping areas are not generated like surface grinding applications or where the occurrence of overlapping areas can be accepted; for example, in the area of bearing fits or runways for packing rings. An important task of the proposed research project is the further development of such strategies and application in grinding tests.

A general limiting factor of grind hardening is the HPD, which is technologically restricted to about 2.5 mm due to high grinding forces and physical properties of the material. Furthermore, grind-hardening technology is restricted by the wear of the grinding wheel resulting in relative low G-ratios (grinding ratio) and decreased cost savings.

During the last years, the research on grind hardening has been focused on various aspects of the process such as the use of liquid nitrogen for the quenching of the part. The modelling of the process using hybrid analytical and finite element analysis methods was first introduced by Salonitis in a number of studies [7, 13, 14, 27, 30, 32, 33] and similar attempts have been presented recently by Zhang et al. and Kolkwitz et al. However, a number of issues have not yet been modelled such as residual stresses formation and geometry deformation.

References

1. Brinksmeier E, Brockhoff T (1996) Utilization of grinding heat as a new heat treatment process. CIRP Ann Manuf Technol 45:283–286
2. Eda H, Ohmura E, Yamauchi S (1993) Computer visual simulation on structural changes of steel in grinding process and experimental verification. CIRP Ann Manuf Technol 42(1):389–392
3. Shaw MC, Vyas A (1994) Heat-affected zones in grinding steel. CIRP Ann Manuf Technol 43(1):279–282
4. Zhang L, Mahdi M (1995) Applied mechanics in grinding—IV. The mechanism of grinding induced phase transformation. Int J Mach Tools Manuf 35(10):1397–1409
5. Brockhoff T (1999) Grind-hardening: a comprehensive view. CIRP Ann Manuf Technol 48(1):255–260
6. Chryssolouris G, Tsirbas K, Salonitis K (2005) An analytical, numerical, and experimental approach to grind hardening. J Manuf Process 7(1):1–9
7. Salonitis K, Chryssolouris G (2007) Cooling in grind-hardening operations. Int J Adv Manuf Technol 33(3-4):285–297
8. Foeckerer T, Kolkowitz B, Heinzel C, Zaeh MF (2012) Experimental and numerical analysis of transient behavior during grind-hardening of AISI 52100. Prod Eng Res Devel 6(6):559–568
9. Shah SM, Nelias D, Zain-ul-abdein M, Coret M (2012) Numerical simulation of grinding induced phase transformation and residual stresses in AISI-52100 steel. Finite Elem Anal Des 61:1–11
10. Zurita O, Acosta A, Moreno D (2003) Superficial hardening in the plane grinding of AISI 1045 steel. J Mater Eng Perform 12(3):298–303
11. Nguyen T, Zarudi I, Zhang LC (2007) Grinding-hardening with liquid nitrogen. Int J Mach Tools Manuf 47:97–106
12. Nguyen T, Zhang LC (2010) Grinding–hardening using dry air and liquid nitrogen. Int J Mach Tools Manuf 50:901–910
13. Salonitis K (2014) On surface grind hardening induced residual stresses. Procedia CIRP 13:264–269
14. Salonitis K, Kolios A (2015) Experimental and numerical study of grind hardening induced residual stresses on AISI 1045 Steel. Int J Adv Manuf Technol. doi:10.1007/s00170-015-6912-x
15. Liu JD, Wang GC, Wang Z, Fan ST (2006) Experimental research on grind-hardening of 65Mn steel. Mater Sci Forum 505–507:787–792
16. Liu LF, Zhuang JZ, Huang SW, Xu ZL (2010) Influence of original structure on the grind-hardened layer structure and its property of 65Mn steel. Key Eng Mater 455:580–584
17. Fricker DC, Pearce TRA, Harison JL (2004) Predicting the occurrence of grind hardening in cubic boron nitride grinding of crankshaft steel. Proc Inst Mech Eng Part B: J Eng Manuf 218:1339–1355
18. Xiao B, Park YC, Su HH, Ding WF, Fu YC, Xu JH (2006) The influence of grinding parameters on the superficial hardening effect of 48MnV microalloyed steel. Key Eng Mater 315–316:15–19
19. Han Z, Zhang N, Gao D, Yang G (2007) Research into grinding hardening of microalloyed non-quenched and tempered steel. J China Univ Mining Technol 17(2):238–241
20. Xiao B, Su HH, Li SS, Xu HJ (2007) Research on grind-hardening temperature and cooling rate of 48MnV microalloyed steel. Key Eng Mater 359–360:148–152
21. Zhang L, Ge P, Bi W, Zhang Q (2011) Experiment and simulation on residual stress of surface hardened layer in grind-hardening. Solid State Phenom 175:166–170
22. Li SS, Xiao B, Su HH, Gong SL (2012) Simulation on grind-hardening residual stress field of 48MnV steel. Key Eng Mater 499:301–306

23. Ming WW, Liu G, Chen M (2007) Experimental study on the hardened surface layer of grinding SKD-11 hardened steel. Key Eng Mater 359–360:224–228
24. Ming WW, Liu G, Chen M (2007) Study on surface grind-hardening of SKD-11 hardened steel. Int J Manuf Tech Manag 12(1/2/3):236
25. Ming WW, An QL, Chen M (2008) Study on the effect of grinding parameters to the white layer formation in grinding SKD-11 hardened steel. Adv Mater Res 53–54:279–284
26. Yang G, Han Z, Du C (2009) External grind-hardening experiments and its grinding force. J Shanghai Univ (English Ed) 13(2):169–173
27. Salonitis K, Stavropoulos P, Stournaras A, Chryssolouris G (2007) Finite element modeling of grind hardening process. In: Proceedings of the 10th CIRP international workshop on modeling of machining operations, Calabria, Italy, pp 117–123
28. Niemeyer B, Foeckerer T, Chaphalkar N, Hyatt GA (2013) Grind hardening method and apparatus. US Patent with Pub. No.: US 2013/0273811 A1
29. Salonitis K, Stavropoulos P, Kolios A (2014) External grind-hardening forces modelling and experimentation. Int J Adv Manuf Technol 70(1–4):523–530
30. Salonitis K, Chondros T, Chryssolouris G (2008) Grinding wheel effect in the grind-hardening process. Int J Adv Manuf Technol 38:48–53
31. Tsirbas K (2002) Theoretical and experimental investigation of grind-hardening process. Ph.D. dissertation, Patras University (in Greek http://nemertes.lis.upatras.gr/jspui/bitstream/10889/301/1/76.pdf)
32. Salonitis K (2006) A methodology for the prediction of the hardness distribution and the hardness penetration depth caused by grind-hardening process. Ph.D. dissertation, Patras University (in Greek http://nemertes.lis.upatras.gr/jspui/bitstream/10889/1430/1/Nimertis_Salonitis%28a%29.pdf)
33. Salonitis K, Chryssolouris G (2007) Thermal analysis of grind-hardening process. Int J Manuf Technol Manage 12(1/2/3):72–92
34. Toenshoff HK, Peters J, Inasaki I, Paul T (1992) Modelling and simulation of grinding processes. CIRP Ann Manuf Technol 41(2):677–688
35. Zhang J, Ge P, Jen T-G, Zhang L (2009) Experimental and numerical studies of AISI1020 steel in grind-hardening. Int J Heat Mass Transf 52:787–795
36. Efremov VD, Zheludkevich MS, German ML (2000) Computer thermal model for hardening grinding. J Eng Phys Thermophys 73(2):428–435
37. Nguyen T, Zhang LC (2009) Temperature fields in workpieces during grinding-hardening with dry air and liquid nitrogen as the cooling media. Adv Mater Res 76–78:3–8
38. Nguyen T, Zhang LC, Le SD (2011) Heat transfer in grinding-hardening of a cylindrical component. Adv Mater Res 325:35–41
39. Nguyen T, Zhang LC (2011) Prediction of the hardened layer in traverse cylindrical grinding-hardening. Mater Sci Forum 697–698:13–18
40. Nguyen T, Zhang LC (2011) Realisation of grinding-hardening in workpieces of curved surfaces: Part 1: Plunge cylindrical grinding. Int J Mach Tools Manuf 51:309–319
41. Li J, Liu S, Du C (2013) Experimental research and computer simulation of face grind-hardening technology. Strojniški vestnik - J Mech Eng 59(2):81–88
42. Han ZT, Yang G, Luo HB (2013) Grinding-hardening experiments and grinding force analysis in infeed external grinding for 45 steel. Adv Mater Res 753–755:281–286
43. Hyatt GA, Mori M, Foeckerer T, Zaeh MF, Niemeyer N, Duscha M (2013) Integration of heat treatment into the process chain of a mill turn center by enabling external cylindrical grind-hardening. Prod Eng Res Devel 7(6):571–584
44. Yuan W, Liu JD, Xu ZL (2013) Orthogonal experimental study on the grinding-hardened layer's depth and its uniformity of 45 steel. Adv Mater Res 668:898–901
45. Yang G, Han ZT, Du CL (2014) Comparative study on the external grind-hardening experiments of 40Cr steel and 45 steel. Adv Mater Res 971–973:26–29
46. Alonso U, Ortega N, Sanchez JA, Pombo I, Plaza S, Izquierdo B (2014) In-process prediction of the hardened layer in cylindrical traverse grind-hardening. Int J Adv Manuf Technol 71(1–4):101–108

47. Songyong L, Gang Y, Jiaqiang Z, Xiaohui L (2014) Numerical and experimental studies on grind-hardening cylindrical surface. Int J Adv Manuf Technol (published online)
48. Alonso U, Ortega N, Sanchez JA, Pombo I, Izquierdo B, Plaza S (2015) Hardness control of grind-hardening and finishing grinding by means of area-based specific energy. Int J Mach Tools Manuf 88:24–33
49. Liu J, Yuan W, Huang S, Xu Z (2012) Experimental study on grinding-hardening of 1060 steel. Energy Procedia 16:103–108
50. Liu LF, Zhuang JZ, Liu C (2011) Influence of depth of cut on grind-hardened layer and its uniformity. Appl Mech Mater 109:345–349
51. Liu JD, Zhuang JZ, Huang SW (2011) Influence of the grinding pass on microstructure and its uniformity of the grind-hardened layer. Adv Mater Res 211–212:36–39
52. Zhuang JZ, Liu LF, Zhang YZ (2011) Study on depth and its uniformity of 65Mn steel grind-hardened layer. Key Eng Mater 487:94–98
53. Liu J, Zhuang J, Xiong J (2011) Study on grinding force of grind-hardening based on orthogonal experimental method. In: The proceedings of the second international conference on mechanic automation and control engineering (MACE), pp 1676–1678
54. Liu J, Xiong J, Yuan W (2012) Experiment study on grinding force of 65Mn steel in grinding-hardening machining. In: Future control and automation, pp 239–246
55. Liu JD, Yuan W, Xiong JK, Huang SW (2012) Quality and control of grinding-hardening in workpieces. Key Eng Mater 522:87–91
56. Liu JD, Wang GC, Wang BL, Chen KM (2007) Study on the formation of grind-hardening of steel AISI 1066. Eng Mater 329:57–62
57. Hou YL, Li CH, Ding YC (2009) An investigation into integrate the surface hardening with the grinding precision finishing. Key Eng Mater 407–408:560–564
58. Ma Z, Liu KM, Zhang LY (2011) Study on the structure of grind-hardened layer and parameter of hardening depth of 42CrMo steel. Adv Mater Res 189–193:969–973
59. Liu KM, Zhang LY, Ma Z, Liu B (2012) Research on the properties of grind-hardening and abrasion of 42CrMo steel in agricultural diesel engine crankshaft. Adv Mater Res 619:567–571
60. Zhang LY, Sun FH, Jiang YH (2012) Research on the structure and wear properties of grind-hardened 42CrMo. Adv Mater Res 619:561–566
61. De Lima A, Gambaro LS, Vieira M, Baptista EA (2011) The use of cylindrical grinding to produce a martensitic structure on the surface of 4340 steel. J Braz Soc Mech Sci Eng 33(1):34–40
62. Liu JD, Wang GC, Li QF, Pei HJ, Jia ZH, Wang Z (2006) Research of surface hardening based on transverse feed grinding. Mater Sci Forum 532–533:584–587
63. Wang GC, Liu JD, Pei HJ, Jia ZH, Ma LJ (2006) Study on forming mechanism of surface hardening in two-pass grinding 40Cr steel. Key Eng Mater 304–305:588–592
64. Zhang L, Ge PQ, Zhang JH, Zhu ZJ, Luan ZY (2007) Experimental and simulation studies on temperature field of 40Cr steel surface layer in grind-hardening. Int J Abras Technol 1(2):187–197
65. Wang GC, Pei HJ, Zhang JY, Zhang CY, Li QF (2008) Formation and control of 40Cr grind-hardening. Key Eng Mater 373–374:758–761
66. Li SS, Xiao B, Qin SX, Song ZH, Su HH, Gong H (2008) Investigation on simulation for grind-hardening temperature field of non-quenched and tempered steel. Key Eng Mater 375–376:520–524
67. Zhang R, Ge P, Zhang L, Li B, Zhao C (2010) Numerical simulation of temperature field for rack grind-hardening. Adv Mater Res 135:200–204
68. Zhang L, Gao Y, Bi W (2010) Simulation and prediction studies on harden penetration depth of AISI 5140 alloy steel in surface grinding. Appl Mech Mater 29–32:1898–1901
69. Zhang Z, Ge P, Zhang L, Tian M (2010) Study on grind-hardening temperature field based on infrared temperature measurement and numerical simulation. Key Eng Mater 443:394–399

70. Liu J, Yuan W (2012) Experimental study on wear test of grind-hardened layer. Adv Mater Res 562–564:115–118
71. Han ZT, Yang G, Luo HB (2014) Research on grind-hardening process through integration of physical experiments and dynamic simulation. Adv Mater Res 941–944:1570–1573
72. Yang G, Han ZT, Du CL (2014) Study on external grind-hardening experiments and the analysis of hardening effects for 40Cr steel. Appl Mech Mater 597:223–227
73. Chryssolouris G, Salonitis K (2004) Theoretical Investigation of the grinding wheel effect on grind hardening process. In: Proceedings of the IFAC-MIM'04 conference on manufacturing, modelling, management and control, Athens, Greece
74. Zah MF, Brinksmeier E, Hainzel C, Huntemann J-W, Fockerer T (2009) Experimental and numerical identification of process parameters of grind-hardening and resulting part distortions. Prod Eng Res Devel 3(3):271–279
75. Kolkwitz B, Foeckerer T, Heinzel C, Zaeh MF, Brinksmeier E (2011) Experimental and numerical analysis of the surface integrity resulting from outer-diameter grind-hardening. Procedia Engineering 19:222–227
76. Duscha M, Eser A, Klocke F, Broeckmann C, Wegner H, Bezold A (2011) Modeling and simulation of phase transformation during grinding. Adv Mater Res 223:743–753
77. Salonitis K (2012) Efficient grinding processes: an energy efficiency point of view. In: Proceedings of the 10th international conference on manufacturing research (ICMR 09), Birmingham, pp 541–546
78. Foeckerer T, Zaeh MF, Zhang OB (2013) A three-dimensional analytical model to predict the thermo-metallurgical effects within the surface layer during grinding and grind-hardening. Int J Heat Mass Transf 56(1–2):223–237
79. Luo SY, Wu SQ, Hsu FJ (2011) Analysis of the vitrified CBN wheels for the performance of grinding hardened steel. Adv Mater Res 264–265:937–942
80. Zhang L, Ge PQ, Zhang JH, Zhang Q (2007) Study on hardness depth variation of different grinding zone in grind-hardening. Adv Mater Res 24–25:333–336
81. Wang GC, Pan ZF, Jin Y, Zhang CL, Hua J, Liu D (2009) Finite element prediction of grind-hardening layer thickness. Key Eng Mater 416:253–258
82. Ge PQ, Zhang Q, Zhang L, Zhang JH (2009) Prediction of the residual stress in grind-hardening with thermal-mechanical-phase transformation stress coupled analysis. Mater Sci Forum 626–627:345–350
83. Nguyen T, Zhang LC (2010) Understanding the temperature field in plunge cylindrical grinding for grinding-hardening. Key Eng Mater 443:388–393
84. Zhang Y, Ge PQ, Zhang L (2011) Numerical analysis of surface temperature in grind-hardening based on time variation heat flux. Mater Sci Forum 697–698:34–38
85. Zhang Y, Ge PQ, Zhang L, Jiang JL (2012) The numerical simulation for thermal deformation in grinding hardening thin workpiece. Key Eng Mater 501:500–504
86. Cheng W, Liang P (2013) Design of automatic control system of grinding zone temperature in grinding hardening. Key Eng Mater 589–590:723–728
87. Liu JD, Yuan W, Xu ZL, Yu DM (2013) Numerical simulation of grinding-hardened layer's depth in the reciprocating grinding of 45 steel. Appl Mech Mater 401–403:656–659
88. Wang GC, Hua CL, Zou JF, Pei HJ, Huang J (2014) Characteristic of residual stress distributions at workpiece surface in grind-hardening. Appl Mech Mater 494–495:624–627
89. Zhang Y, Ge P, Be W (2015) Plane grind-hardening distortion analysis and the effect to grind-hardening layer. Int J Adv Manuf Technol (published online)
90. Tsirbas K, Mourtzis D, Chryssolouris G (1999) Grind-hardening modeling with the use of neural networks. In: Proceedings of the 5th international conference on advanced manufacturing systems and technology, Udine, Italy, pp 289–300
91. Stöhr R, Heinzel C (2002) Grind-hardening with CBN. Grind Abras Mag 06–07(2002):22–30
92. Liu ZQ, Xing A, Wang ZH (2006) A comparison study of surface hardening by grinding versus machining. Key Eng Mater 304–305:156–160

93. Salonitis K, Tsoukantas G, Drakopoulos S, Stavropoulos P, Chryssolouris G (2006) Environmental impact assessment of grind-hardening process. In: Proceedings of the 13th CIRP international conference on life cycle engineering, Leuven, Belgium, pp 657–662
94. Wang GC, Liu JD, Li QF, Zhu YM, Pei HJ, Zhang JY (2007) Formation and control of burr in grind-hardening. Key Eng Mater 359–360:98–102
95. Pan ZF, Wang GC, Hua CL, Pei HJ (2009) Research and development of LM neural network prediction system for grind-hardening. Eng Mater 416:248–252
96. Zhang ZG, Ge PQ, Zhang L, Bi WB (2010) A study on critical heat flux in grind-hardening. Key Eng Mater 431–432:130–133
97. Zhang L, Bi WB, Zhang RB (2010) An approximate solution of energy partition in grind-hardening process. Adv Mater Res 135:298–302
98. Zhang JH, Zhang XJ, Yu GY, Gu ML, Ge PQ (2010) An investigation on the heat partitioning in grind-hardening. Adv Mater Res 97–101:2095–2098
99. Zhang L, Xu XH, Yan CF (2010) Analysis of grinding parameters on hardness layer depth. Appl Mech Mater 37–38:131–134
100. Liu JD, Zhuang JZ, Zhang XL, Xu ZL (2010) Influence of grinding parameters on the depth and uniformity of cylindrical grinding-hardened layer. Adv Mater Res 102–104:733–737
101. Salonitis K (2015) Energy efficiency assessment of grinding strategy. Int J Ene Sec Manag 9(1):20–37
102. Cheng W, Wang Gui Cheng, Liang P (2011) Automatic control technology of grinding zone temperature in grinding hardening. Adv Mater Res 381:48–51
103. Reinhart G, Reinhardt S, Föckerer T, Zäh MF (2011) Comparison of the Resource Efficiency of alternative process chains for surface hardening. In: Globalized solutions for sustainability in manufacturing, pp 311–316
104. Klocke F, Roderburg A, Zeppenfeld C (2011) Design methodology for hybrid production processes. Procedia Engineering 9:417–430
105. Xiu SC, Liu MH, Wei JH (2012) Analysis of microstructure of grinding strengthening layer in point grinding under small depth of cut conditions. Adv Mater Res 472–475:974–977
106. Liu JD, Yuan W, Xiong JK, Xu ZL, Huang SW (2012) Study on the two-side direction burr in grinding-hardening machine based on orthogonal experimental method. Appl Mech Mater 217–219:1869–1873
107. Liu JD, Yuan W, Xiong JK, Xu ZL (2013) Influence of chamfer size on the two-side direction burr formed in grinding-hardening machine. Adv Mater Res 645:392–395
108. Liu JD, Yuan W, Xiong JK, Xu ZL (2013) Influence of grinding parameters and chamfer size on the grinding-hardened layer's depth. Adv Mater Res 718–720:1569–1572
109. Liu JD, Yuan W, Chen M (2013) Influence of workpiece's size on the structure and performance of grinding-hardened layer. Key Eng Mater 579–580:56–60
110. Liu M, Nguyen T, Zhang LC, Qiong W, Le Sun D (2014) On the profile and microstructure variations of grinding-induced hardening layer in a cylindrical workpiece. Adv Mater Res 1017:3–8
111. Li H, Zou JF, Wang GC (2014) Prediction of thermal gradient in traverse cylindrical grind-hardening. Appl Mech Mater 590:280–283
112. Liu JD, Zhuang JZ, Xu ZL (2014) Study on the grind-hardening of the loader clevis pin. Key Eng Mater 621:140–145

Chapter 3
Grind-Hardening Process Modelling

Abstract Grind-hardening process is a complex hybrid process integrating heat treatment process with high material rate grinding. The modelling of the process thus is quite complex and a number of aspects need to be considered. The present chapter presents a holistic model able to predict the grinding forces, temperature distribution, metallurgical changes, surface hardness and residual stresses. The model is composed of a number of sub-models that are also verified experimentally.

3.1 Introduction

The grinding process is characterized by a series of stochastic engagement between the grinding wheel grits and the workpiece, that depend on a number of factors such as the grinding wheel microstructure, the process parameters and the geometry of the grinding wheel. These engagements result in the generation of the chips but also in heat within the grinding area. The modelling of the grinding process (and grind-hardening process as the mechanics and kinematics of the process are the same), requires the consideration of the topography of the grinding wheel. Topography models can be developed and feed info in chip formation models in order to derive estimations of the grinding exerted forces and the heat generated. It has been shown, mainly for the grinding process, that strong relationships exist between the topography of the grinding wheel, the process forces, the heat generation and the grinding wheel wear.

Based on the wheel topography models, the chip thickness and the surface roughness can be predicted. As already mentioned, besides the forces and the generated energy, the topography of the grinding wheel affects the grinding area temperature and the subsequent metallurgical transformations and the sub-surface integrity of the ground part. In the present chapter, an approach to modelling the various aspects of the grind-hardening process is presented. As it is expected, the model is composed of a number of sub-models, as can be seen in Fig. 3.1, that

K. Salonitis, *Grind Hardening Process*, SpringerBriefs in Manufacturing and Surface Engineering, DOI 10.1007/978-3-319-19372-4_3

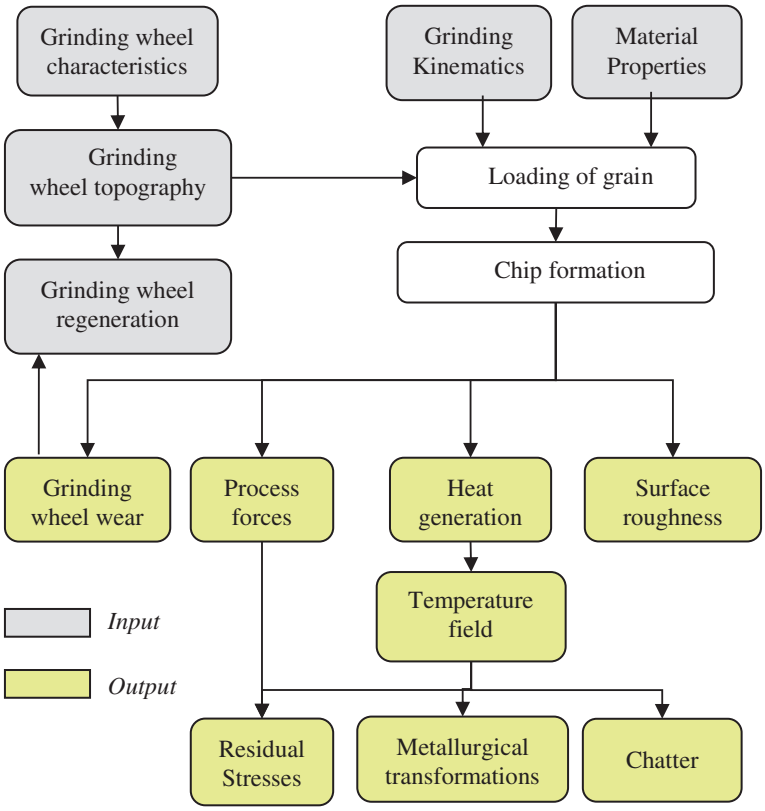

Fig. 3.1 Modelling grinding processes

are either solved analytically or with the use of finite element method. All the sub-models presented are validated with experimental results and provide insights on how the process behaves under different processing conditions.

3.2 Grinding Kinematics—Grinding Wheel Topography

Toenshoff et al. [1] indicated that the grinding process kinematics is a series of stochastic engagements that depend on a number of factors such as the microstructure of the grinding wheel, the process parameters and the geometric parameters. Through the analysis of grinding kinematics, a number of process characteristics can be determined that will be used later on for estimating the grinding forces and the process energy.

The grinding wheel topography modelling is very important in understanding the result of the interaction between the grinding wheel and the workpiece material.

The microstructure of the grinding wheel is characterized by the number of static and active grains. Active grains are considered to be the ones that are in contact with the workpiece material and contribute to the formulation of chips and the heat generation due to friction. On the other hand, the static ones are all the grains in the contact surface, either they participate or not in the material removal process.

3.2.1 Static Grains

Static grains are the grains that are in the grinding wheel–workpiece interface. In the past, most of the relative research studies presented attempted to calculate the number of static grains using experimental results. A number of different experimental methods can be used such as photography, photogrammetry, profilometers, etc. for the calculation of the number of static grains. Toenshoff et al. [1] based on previous studies proposed a simple empirical model for the estimation of the number of static grains

$$n_s = c \cdot z^{e2} \tag{3.1}$$

where n_s is the number of static grains, c is the specific cutting edge density, z is the profile depth and $e2$ is an empirically determined exponent. It is evident that such an approach relies on experimental results.

A simplified method for estimating the number of static grains as a function of grinding wheel specifications and process parameters was presented by Salonitis et al. [2]. By considering a finite volume including all the grains in the contact area, as it can be seen in Fig. 3.2, the number of static grains intersected by the grinding arc area can be determined. This finite volume will have its three dimensions equal to contact length, grinding wheel width and grain height. The grains

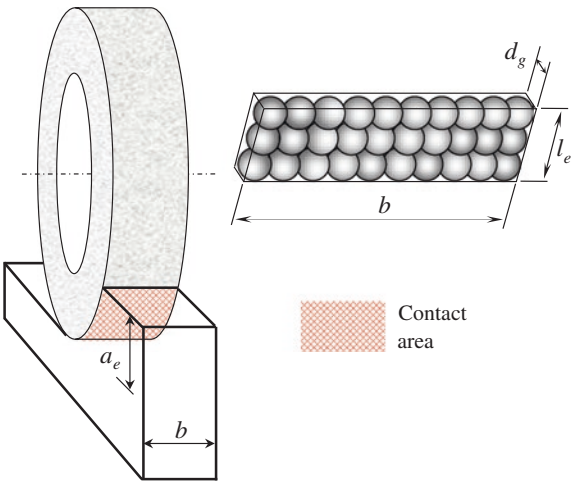

Fig. 3.2 Finite volume for the estimation of the number of the active grains

are considered spherical, thus the height of each grain will be equal to the average grain diameter. The volumetric concentration of grains in the finite volume can be determined from the following equation:

$$V_g = \frac{n_s \times V_{\text{grain}}}{V_{\text{tot}}} \tag{3.2}$$

where V_g is the volumetric concentration of abrasive grains in the grinding wheel, n_s the number of static grains, V_{grain} the average volume of each grain and V_{tot} the finite element volume.

Therefore the number of static grains can be estimated from the following equation:

$$n = 6 \cdot V_g \cdot \frac{l_c \cdot b}{\pi \cdot d_g^2} \tag{3.3}$$

where V_g is the volumetric concentration of abrasive grains in the wheel, l_c is the geometric length of contact zone ($l_c = \sqrt{d_e a_e}$), d_e is the equivalent diameter, a_e is the depth of cut, b is the grinding wheel width and d_g is the average diameter of the grains.

The volumetric concentration of abrasive grains is a function of the grinding wheel structure. The volumetric concentration of the abrasive grains, the grain diameter and the porosity of the grinding wheel are characteristics defined while it is being manufactured and its specifications are depicted qualitatively in its specifications (Fig. 3.3). Malkin [3] proposed an empirical relationship for the volumetric concentration and the grinding wheel structure number (S):

$$V_g = \frac{2(32 - S)}{100} \tag{3.4}$$

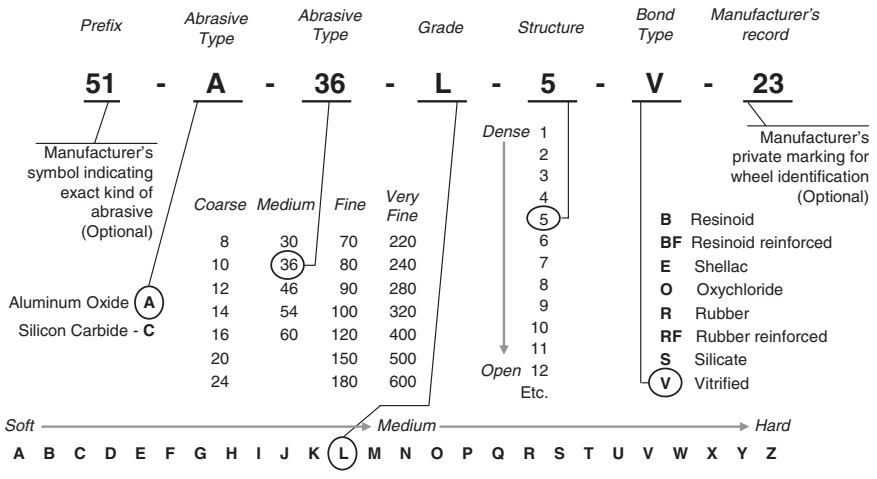

Fig. 3.3 Grinding wheel specification

The average grain diameter is correlated with the grain size number M from the grinding wheel marked with the following equation:

$$d_g = 15.2 \cdot M^{-1} \tag{3.5}$$

The above equation approximates the grit dimension d_g as 60 % of the average spacing between adjacent wires in a sieve, whose mesh number equals the grit number M.

3.2.2 Active Grains

During the grinding process, only a small number of grains are contacting and interacting with the workpiece material. This fraction of static grains is characterized as "active" or "kinematic" grains, and can be determined from the following equation.

$$n_a = \Phi_a \cdot n \tag{3.6}$$

where Φ_a is the fraction of static grains that are active.

The fraction of static grains that are active depends on a number of factors, such as the elasticity and the deformation of the grinding wheel, as well as of the workpiece during the grinding process, etc. The volumetric concentration of the bonding material on the grinding wheel can be considered as a metric of this fraction, since this parameter greatly affects the elasticity of the grinding wheel.

Since a grinding wheel is composed of grains, bonding material and air (as internal pores), the volumetric concentration of bonding (V_b) can be estimated from the following equation:

$$V_b = 1 - \left(V_g + V_p\right) \tag{3.7}$$

The volumetric concentration of grains (V_g) can be estimated from Eq. (3.4). The volumetric concentration of the pores (V_p) is a function of the "hardness" number of the grinding wheel, and the following equation can be used [3].

$$V_p = \frac{1}{100}\left(45 + \frac{S - 2n}{1.5}\right) \tag{3.8}$$

where n is an integer ($n = 1, 2, 3, 4, \ldots$) corresponding to the hardness letter (E, F, G, H, …), respectively. The above equation is valid for grinding wheels having $V_g \leq 60$ %.

For extracting the relationship between the fraction of the active grains and the volumetric concentration, the experimental data stated in [4, 5] were used. Based on a reference fraction of active grains and the experimental dependence of the number of active grains on the volumetric concentration of bonding material V_b (Fig. 3.4) a normalized factor was introduced.

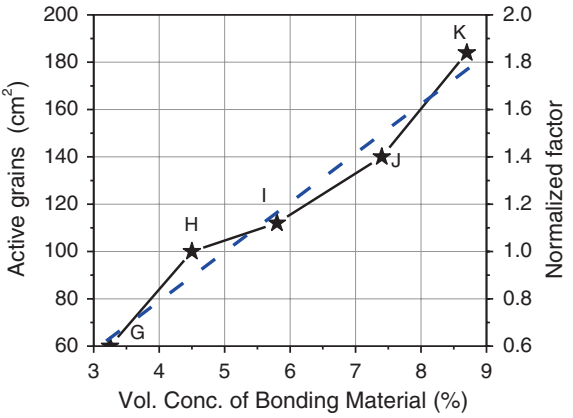

Fig. 3.4 Variation of the number of active grains per unit area with the volumetric concentration of bonding material (based on experimental data from [4])

$$(\text{normalized factor}) = 20.535 \cdot V_b - 0.217 \tag{3.9}$$

The fraction active grains can therefore be determined by the following equation:

$$\Phi_a = \Phi_{\text{ref}} \times (\text{normalized factor}) \tag{3.10}$$

For the definition of the reference fraction the results of Hou and Komanduri [5] have been used. Based on the statistical distribution of abrasive grains to the surface of a grinding wheel and the loading conditions, they have shown that although the number of grains passing through the grinding zone may be a million or more per second, the actual contacting grains are only a small fraction of those (~3–4 %) and the actual cutting grains are even less (~0.15 %). This result was obtained for a conventional alumina wheel A46H8V, and thus, the proposed model for estimating the fraction of grains that are active was calibrated for bonding material H, and fraction 3.8 %. For assessing this reference value, in the same paper, in the case of a high material removal rate grinding process, the fraction of the active grains was estimated to be 18 % (for grinding A24R6B). The proposed model, for such wheel specifications, estimates the fraction to be 19.5 %.

The approach presented is based on both existing experimental results and a simplified representation of the grinding wheel structure. Additionally, a number of empirical models for describing the topography of the grinding wheels have been presented in the past. Toenshoff et al. [1] combined these models and presented a generic equation:

$$N_{\text{kin}} = c_{gw} \cdot \left(\frac{1}{q}\right)^{e1} \cdot a_e^{e1/2} \cdot \left(\frac{1}{d_{eq}}\right)^{e1/2} \tag{3.11}$$

where N_{kin} is the number of active grains, c_{gw} is a constant for the grinding wheel effect, $e1$ is an experimentally determined exponent, q is the speed ratio, a_e is the depth of cut and d_{eq} is the equivalent diameter of the grinding wheel.

3.3 Process Forces Semi-empirical Modelling

The grinding forces can be analyzed into a tangential (F_t) and a normal component (F_n). Alternatively, grinding forces can also be described by their horizontal (F_h) and vertical (F_v) components as can be seen in Fig. 3.5. Since the diameter of the grinding wheel is much larger than the depth of cut, the horizontal component can be assumed to be identical to the tangential one.

The total grinding force can be represented as the sum of the grinding force exerted for the chip formation, for the plastic deformation (plowing) of the workpiece and for the sliding of the grinding grains on the workpiece surface.

$$F_t = F_{t,sl} + F_{t,ch} + F_{t,pl} \tag{3.12}$$

where $F_{t,sl}$, $F_{t,ch}$ and $F_{t,pl}$ are the tangential force for sliding, for chip formation and for plowing, respectively. The cutting forces include the forces exerted for chip formation and plowing:

$$F_c = F_{t,ch} + F_{t,pl} \tag{3.13}$$

3.3.1 Sliding Forces

Malkin [3], based on experimental results, has correlated the sliding forces with the friction coefficient between the workpiece material and the grinding wheel, the average contact pressure and the area of contact:

$$F_{t,sl} = \mu \cdot p_m \cdot A_a \tag{3.14}$$

where μ is the friction coefficient between the workpiece material and the abrasive grains, p_m is the average contact pressure of the abrasive grains on the workpiece and A_a is the actual area of contact between the abrasive grains and the workpiece.

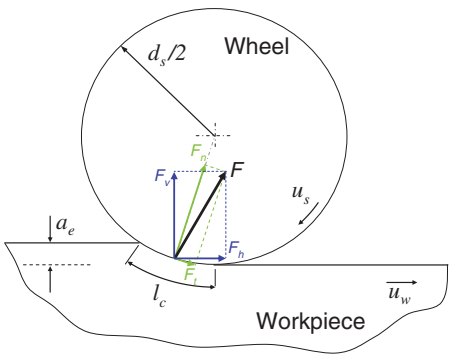

Fig. 3.5 Relationship between grinding force components

3.3.1.1 Average Contact Pressure

Malkin [3] has conducted a number of experiments with various grinding wheels and different process parameters and has proved that the average contact pressure depends solely on the cutting curvature difference.

The average contact pressure p_m is usually experimentally defined. Assuming that there is a linear relationship between curvature difference Δ and average contact pressure p_m (Fig. 3.6):

$$p_m = k_1 \Delta + k_2 \tag{3.15}$$

The cutting curvature difference Δ characterizes the degree of non-conformity between the wheel radius and the cutting path radius. Its value is strongly dependent both on the peripheral speed of the grinding wheel and the workpiece speed. When the peripheral grinding wheel speed u_c is significantly larger than the workpiece speed u_w, as for the case of the grind-hardening process, the curvature difference can be expressed as [3]:

$$\Delta = \frac{4\upsilon_w}{d_e \upsilon_c} \tag{3.16}$$

Thus the average contact pressure can be estimated by:

$$p_m = k_1 \frac{4u_w}{d_e u_s} + k_2 \tag{3.17}$$

where d_e is the equivalent diameter, and k_1 and k_2 are linear coefficients that are experimentally defined and can be considered to be a function of processing environment (grinding machine, coolant type, etc.).

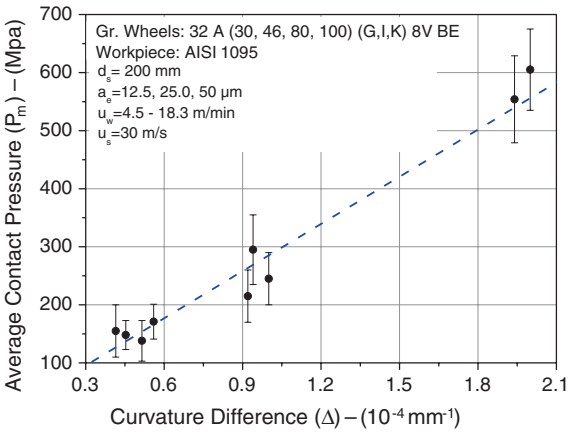

Fig. 3.6 Average contact pressure as a function of curvature difference (based on experimental results presented by Kannapan and Malkin [6])

3.3.1.2 Actual Area of Contact

The actual area of contact between the grains and the workpiece depends on the process parameters and on the grinding wheel composition. The specification of a grinding wheel describes comprehensively its composition as can be seen in Fig. 3.3.

It is assumed that the heat is generated only between the grains and the workpiece material. Therefore, the actual area of contact is the product of the number of active grains n_a adjacent to the workpiece surface and the average wear flat area A_g per grain.

$$A_a = n_a \cdot A_g \tag{3.18}$$

The average wear flat area is considered to be equal to that of a circle having diameter l_{wf} equal to the two-thirds of the average grain diameter (Fig. 3.7):

$$A_g = \frac{1}{4}\pi l_{wf}^2 = \frac{\pi d_g^2}{9} \tag{3.19}$$

3.3.1.3 Friction Coefficient

Friction coefficient is usually related to the grinding force ratio (λ) that links the normal component of the grinding forces with the tangential ones. The force ratio depends on grinding parameters, grinding wheel condition, work material, etc. For a sharp wheel, it is relatively low, as tangential force component is higher compared to normal force and for dull wheel it is opposite. The ratio of the sliding components of the forces is equal to friction coefficient (μ) between wear flat and work. Similarly, the ratio of the cutting components (φ) depends on tip angle of grain [3]. Therefore, the grinding force ratio can be expressed using the following equation [7]:

$$\lambda = \varphi \frac{F_{n,c}}{F_n} + \mu \frac{F_{n,s}}{F_n} \tag{3.20}$$

Grinding force ratio depends on both φ and μ, however, when the chip formation is more dominant than sliding; φ will be governing the force ratio. Similarly, if

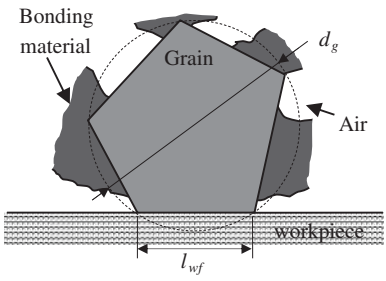

Fig. 3.7 Grain–material interaction

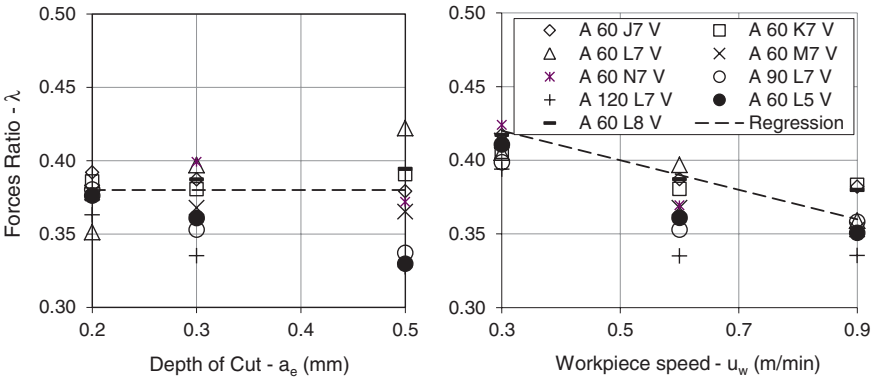

Fig. 3.8 Forces ratio dependence on depth of cut and workpiece speed (based on [2])

sliding is more dominant then μ will have more dominance grinding force ratio [8]. Therefore, for the case of grind hardening it is safe to assume that the force ratio equals the friction coefficient.

Salonitis et al. [2] derived both theoretically and experimentally that force exerted due to chip forming and plowing is negligible (less than 3 % of the total forces) in comparison to the sliding force, supporting further the validity of the assumption to use the force ratio for assessing the friction coefficient. Their experimental work on grind hardening using different alumina grinding wheels indicates that there is a strong dependence of force ratio to the workpiece speed, whereas the depth of cut change impact is not so significant (Fig. 3.8).

3.3.1.4 Sliding Forces

Combining the above-mentioned equations, the tangential grinding forces due to the grits sliding on the workpiece can be estimated using the following closed equation:

$$F_{t,sl} = \frac{3}{100 \times 15.2^2} \mu \cdot \Phi_a \cdot b \cdot l_{wf}^2 \cdot M^2 (32 - S) \sqrt{d_e \cdot a_e} \left[k_1 \frac{4u_w}{d_e \cdot u_s} + k_2 \right] \quad (3.21)$$

3.3.2 Cutting Forces

The cutting forces can be determined from the specific energy which is defined as the energy expended per unit volume of material removed. The specific energy is given by the following equation:

$$u_c = \frac{F_{t,c} \cdot u_s}{b \cdot a_e \cdot u_w} \quad (3.22)$$

where u_c is the specific cutting energy and $F_{t,c}$ is the sum of chip formation and plowing forces.

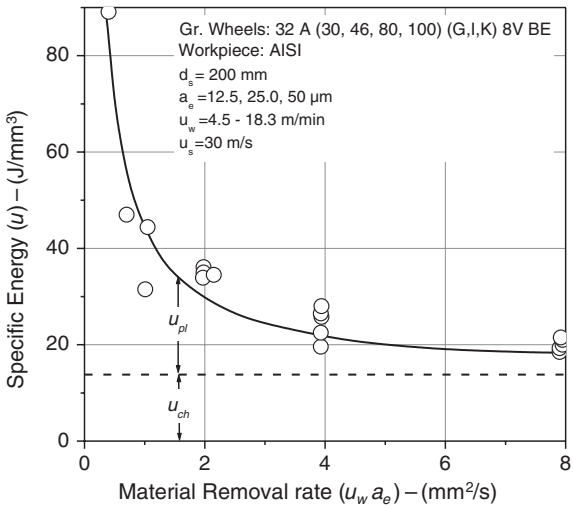

Fig. 3.9 Specific energy as a function of material removal rate (based on [3])

The cutting energy is the sum of the chip formation and the plowing energy. It has been shown [3] that the cutting energy asymptotically approaches the chip formation energy as the metal removal rate is increased (Fig. 3.9). Furthermore, it has been proven experimentally that the chip formation energy has a constant value that does not depend on the process parameters, the grinding wheel specifications or the workpiece material. Almost all the relevant studies have indicated an indicative value of specific cutting energy being equal to 13.8 J/mm^3.

Based on the experimental results presented in [3], the following equation can be drawn:

$$u_c = u_{ch} + u_{pl} = u_{ch} + \frac{28.1}{u_w a_e} \tag{3.23}$$

From Eqs. (3.22) and (3.23), the cutting forces can be estimated using the following closed format equation:

$$F_{t,c} = F_{t,ch} + F_{t,pl} = b \cdot a_e \left(\frac{u_s}{u_w}\right)^{-1} \left[u_{ch} + \frac{28.1}{u_w a_e}\right] \tag{3.24}$$

3.3.3 Model Implementation and Validation

Salonitis et al. [2] validated the model for the grind hardening of AISI 52100 for a number of different alumina grinding wheels. They concluded that cutting forces account typically for less than 3 % of the total forces (Fig. 3.10). Thus the tangential component of the process forces (Eq. 3.12) can be considered equal to the sliding component (Eq. 3.19) neglecting the cutting forces.

The process parameters and the grinding wheel specifications have an important impact on the grinding forces, indicatively in Fig. 3.11a their effect as predicted

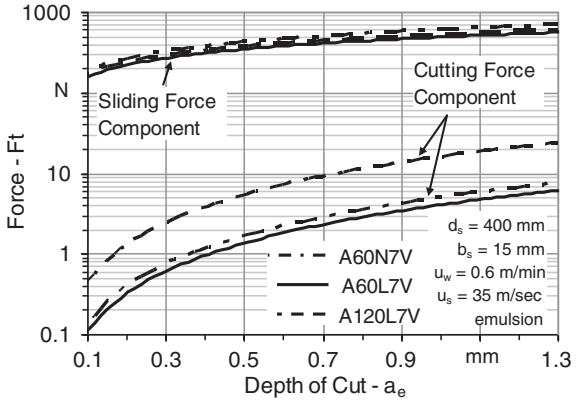

Fig. 3.10 Sliding and cutting forces versus depth of cut [2]

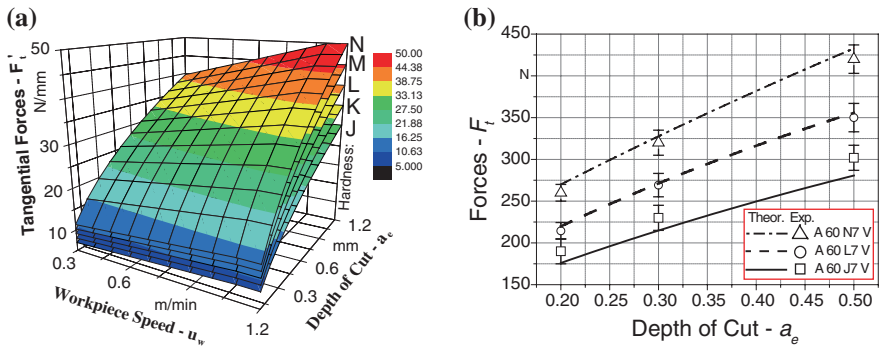

Fig. 3.11 **a** Tangential forces prediction as function of process parameters and grinding wheel structure and **b** experimental verification [2]

is shown in the model. Salonitis et al. [2], experimentally proved the models prediction and shown that the depth of cut has a significant effect on the process forces (Fig. 3.11b). The key specification characteristic was determined to be the grinding wheel hardness.

3.4 Modelling Heat Generation and Partition

As it has been noted, grind-hardening process relies on the selection of a proper set of parameters that can result in high heat generation rates in the grinding area. The heat generated should be adequate for the workpiece material to undergo heat

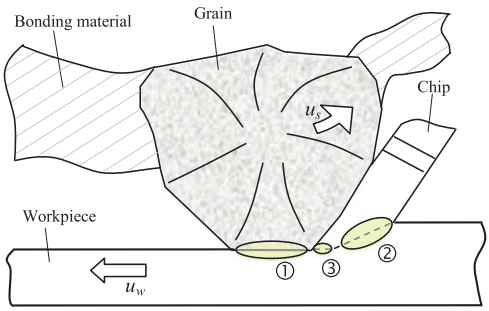

Fig. 3.12 Heat generation mechanisms during grinding

① Heat generation due to friction
② Heat generation due to plastic deformation
③ Heat generatio due to plowing

treatment and increase finally its surface hardness. In common grinding processes, the primary goal is the reduction of the generated heat and even more important the reduction of the heat entering the workpiece material as to avoid damaging the lattice structure of the material. It is evident that in grind hardening, we have the opposite goal: generating high heat flux rates and disseminate locally in the workpiece material.

During the grind-hardening process the heat generation mechanisms, as shown in Fig. 3.12, are:

- the friction among abrasive grains and workpiece material (wear flat),
- the plastic deformation in shear planes during material removal and
- the plastic deformation of workpiece material without material removal (plowing)

The dominant heat generation mechanism is that of the friction among abrasive grains and workpiece material while the other two have significantly less contribution. Lavine [9, 10] studied the heat generation due to plastic deformation in shear planes and revealed that no significant error is expected if neglected in the case of dull wheels, such as the ones used for grind-hardening applications. Malkin [3] on the other hand, proved that for grinding operations with very high removal rates, as is the case of grind hardening, the magnitude of the plowing energy is negligible in comparison with that of the heat generated by friction and the heat consumed for chip formation.

The actual amount of heat generated during the process equals to the grinding wheel spindle power:

$$P = F_t \cdot (u_s \pm u_w) \tag{3.25}$$

where P is the grinding wheel spindle power, F_t is the tangential component of the cutting forces, u_w is the workpiece speed and u_s is the grinding wheel speed. The plus sign is considered for up-grinding processes whereas the minus sign for

down-grinding processes. Since during grind hardening, the grinding wheel speed is much higher than that of the workpiece, the above equation can be simplified to:

$$P = F_t \cdot u_s \tag{3.26}$$

3.4.1 Heat Partition

The heat generated is transferred to the workpiece, grinding wheel, chips, coolant and surrounding environment. The heat transferred to the surrounding environment, due to irradiation, is considered negligible when compared to the heat dissipated to other heat sinks involved in the heat balance. Furthermore, the heat transferred through the coolant fluid can also be considered negligible as the coolant fluid cannot easily enter the grinding zone given that the grinding wheel rotates towards the fluid flow (Fig. 3.13) [11]. Additionally, even if some amount of coolant fluid enters the grinding zone, it will boil immediately since the temperature of the workpiece surface in this region exceeds 900 °C [12], and therefore, the maximum heat that could be convected by this fluid is the heat required to boil the fluid [13].

It can be argued therefore that the heat generated, due to grinding wheel—workpiece interaction, is dissipated to the workpiece, grinding wheel and the chips (Fig. 3.14). This heat balance can be expressed in terms of heat fluxes as:

$$q_t = q_w + q_s + q_{ch} \tag{3.27}$$

where q_t is the heat generation flux and q_w, q_s and q_{ch} are the amounts of heat convected by the workpiece, the grinding wheel and the chips, respectively.

The heat generation flux can be calculated from the power consumed during the process.

$$q_t = \frac{P}{b \cdot l_c} \tag{3.28}$$

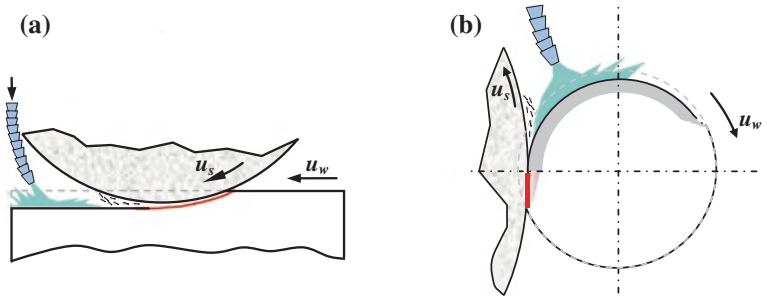

Fig. 3.13 Coolant fluid application during grind-hardening process for **a** prismatic and **b** cylindrical workpieces

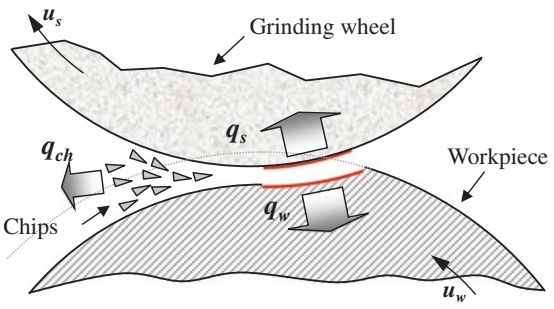

Fig. 3.14 Grinding heat transfer to workpiece (q_w), to chips (q_{ch}) and to grinding wheel (q_s)

where b is the grinding wheel width and l_c is the geometrical contact length between the workpiece and the grinding wheel:

$$l_c = \sqrt{a_e \cdot d_e} \tag{3.29}$$

where d_e is the equivalent diameter and a_e is the depth of cut. However, the geometric contact length is an underestimation of the real contact length. The shape of the contact area is deformed, due to the elastic and plastic behaviour of the wheel and the workpiece system. Experimentally, it has been shown that the actual contact length can be 50–200 % greater than the geometrical contact length [14, 15]. For the purposes of the present work though, the geometrical contact length will be used, since no analytical expressions of the actual contact length have been derived for the case of high material removal rate grinding processes such as the grind hardening.

The amount of heat transferred by the various "sinks" (grinding wheel, workpiece, chips, coolant, etc.) is of great interest for the process modelling. In the literature, a number of theoretical models have been presented, that can be classified in two major categories (Fig. 3.15):

- "grain" models, in which the analysis takes place at the interaction plane between the grinding wheel grit and the workpiece material (most of these models are based on Lavine et al. [16] work, indicative studies include the work by Rowe et al. [13, 17–20], Guo and Malkin [21–24], and
- "grinding zone" models, in which the analysis takes place at the interface between the grinding wheel and the workpiece (typical examples of such models include the works by Jin et al. [25], Toenshoff et al. [26], Rowe et al. [17, 20, 27].

For the grind-hardening process modelling, a grinding zone model is adapted due to higher simplicity and experimental verification of the results in a number of publications [11, 28, 29].

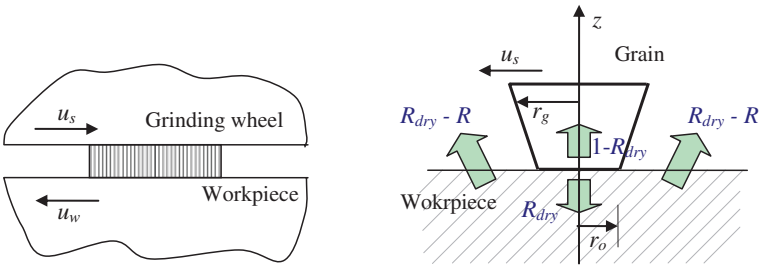

Fig. 3.15 Heat partition models formulation

3.4.2 Heat Dissipation by the Chips

As aforementioned, heat is dissipated with process chips. In case of shallow grinding, this amount of heat can be neglected; however, for high material removal rates [30], as is grind hardening, this heat dissipation should be taken into consideration. The heat flux convected by the chips can be expressed as a function of specific energy distributed over the grinding zone:

$$q_{ch} = e_{ch} \cdot \frac{a_e \cdot u_w}{l_c} \tag{3.30}$$

where e_{ch} is the specific energy convected by chips, a_e is the depth of cut, u_w is the workpiece speed and l_c is the geometric contact length

The chip temperature may easily reach the melting point as argued by Malkin [3]. Therefore, the maximum specific energy convected by the chips can be assumed to equal the required energy for raising the temperature of the chip to the melting point:

$$e_{ch} = \rho_{w,T=Tmp} \cdot c_{w,T=Tmp} \cdot T_{mp} \tag{3.31}$$

where T_{mp} is the melting point.

The ratio of the heat flux partition to chips can be therefore estimated by the heat flux convected by the chips and the total heat flux generated.

$$R_{ch} = \frac{q_{ch}}{q_t} \tag{3.32}$$

3.4.3 Heat Dissipation by the Grinding Wheel

The partition of the heat between the workpiece and the grinding wheel has been thoroughly investigated. Malkin [3], Lavine [9], Rowe [13, 20, 30, 31] and Jin et al. [25] are few of the researchers that studied this subject. The partition ratio R_{ws} is defined as the fraction of the heat shared by the workpiece and the grinding wheel entering the workpiece.

$$R_{ws} = \frac{q_w}{q_w + q_s} \tag{3.33}$$

The partition ratio in earlier grinding studies was approached based on heat transfer models that compared the grinding process to that of machining and the grains were thought of as machine tools. Most of these models were based on Hahn's [32] preliminary modelling work that partitioned the heat between the grain and the workpiece. However, in machining, the majority of the heat is generated at the shear plane and the heat enters the tool through the tool–chip interface. Since in grinding, most of the heat is generated by friction at the grain–workpiece interface, and the contact area is much larger, the simplified heat partitioning model developed by Rowe et al. [20], which assumes that the grinding wheel and the workpiece can be thought of as two sliders, seems to better simulate the heat transfer during grinding. The aforementioned partition model is utilized for the present study:

$$R_{ws} = \left(1 + \frac{\beta_s}{\beta_w} \cdot \sqrt{\frac{u_s}{u_w}}\right)^{-1} \tag{3.34}$$

where factor β_w is the coefficient of heat diffusion of the workpiece and factor β_s is the average heat coefficient of the grinding wheel defined, respectively, as:

$$\beta_w = \sqrt{k_w \cdot \rho_w \cdot c_w} \tag{3.35}$$

$$\beta_s = \sqrt{\bar{k}_s \cdot \bar{\rho}_s \cdot \bar{c}_s} \tag{3.36}$$

where k, ρ and c are the average values of thermal conductivity, density and specific heat of the workpiece or the respective effective values of the grinding wheel for a temperature equal to that of the contact zone.

A number of attempts have been reported having focused on determining the effective properties of the grinding wheel. Rowe et al. [20] attempted to measure experimentally the coefficient of the heat diffusion. Kim et al. [33] simulated the grinding wheel, in the grinding zone, as a thermal composite consisting of abrasive grains and fluid between them. They used the "law of mixtures" for determining the effective properties. The thermal composite body is considered to be consisted of grains and air between them, since no cooling fluid enters the grinding zone during the grind-hardening process [28]. Using the "law of mixtures", the effective thermal properties can be determined by equation:

$$\bar{i}_s = \varphi \cdot i_g + (1 - \varphi) i_a \tag{3.37}$$

where i_s is the effective value of the property of the thermal composite (density, thermal conductivity and specific heat), i_g and i_a are the properties of the grain and the air, respectively. Finally, φ is the surface density of the thermal composite.

The surface density is a means of estimating the concentration of active grains on the surface of the grinding wheel. The volumetric concentration of grains on the grinding wheel that can be estimated by using the empirical relations

presented, is quite higher than that on the surface, since no differentiation exists between the active and static grains and thus, cannot be used for estimating the effective thermal properties. The surface density of the grinding wheel can be determined as the fraction of the real contact area to the total surface area:

$$\varphi = \frac{A_a}{l_c \cdot b} \tag{3.38}$$

where A_a is the real contact area determined from the total number of active grains and the wear flat area, l_c is the length of the arc contact and b is the width of the grinding wheel.

3.4.4 Heat Entering the Workpiece

Once the heat partition ratio among the grinding wheel and the workpiece and the heat flux dissipated by the grinding chips have been determined, the heat flux entering the workpiece can be derived by combining Eqs. 3.27 and 3.33 as:

$$q_w = R_{ws} \cdot (q_t - q_{ch}) \tag{3.39}$$

The heat partition to the workpiece and the grinding wheel can therefore be estimated from the following equations

$$R_w = \frac{q_w}{q_t} \tag{3.40}$$

$$R_s = \frac{q_s}{q_t} \tag{3.41}$$

3.4.5 Model Implementation and Validation

The model proposed for the heat partition has been validated for the case of dry grind hardening of AISI 52100 and AISI 1045. In grind hardening the grinding wheel speed is many times higher than the workpiece speed. The speed ratio (u_s/u_w) is usually in the range of 1,000–8,000. Thus for the case of grind hardening with a corundum grinding wheel of a workpiece made of AISI 52100, the heat that enters the workpiece lies between 48 and 63 %. Similar findings are noted for AISI 1045 as well. As a comparison, for conventional finish grinding process (with depth of cut between 0.005 and 0.050 mm and a speed ratio less than 40), the heat partition ratio is between 75 and 90 %. The use of CBN wheels could reduce significantly the heat partition ratios (30–50 %), since CNC grits present higher thermal conductivity and thus absorb more heat.

Using the heat partition model described, the heat partition to the chip, the workpiece and the grinding wheel as a function of workpiece speed and depth of cut was calculated and presented in Fig. 3.16. The heat that enters the workpiece

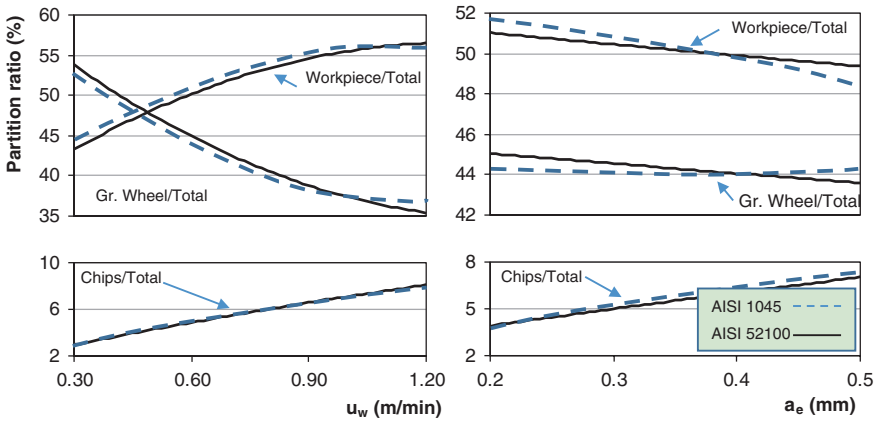

Fig. 3.16 Heat partition ratio **a** $u_w = 0.60$ m/min, **b** $a_e = 0.3$ mm ($u_s = 35$ m/s, grinding wheel: A 60 L7V)

is in the range of 40–60 % of the total generated heat. The portion of heat entering the workpiece increases with the increase of the workpiece speed. Increasing the depth of cut, results in the slight reduction of portion of the heat that enters the workpiece.

It can be thus concluded that most of the heat generated is shared between the workpiece material and grinding wheel, with only a small portion rejected with the grinding chips (with a maximum portion of 10 %). Comparing to other high material removal rates, during high efficiency deep grinding (HEDG) most of the heat is dissipated through chips [34] whereas for the case of creep feed grinding, up to 80 % of the heat is dissipated by the cutting fluid and only 3–4.5 % is conducted within the workpiece material [33].

3.5 Modelling of Temperature Distribution

Having determined the amount of heat entering the workpiece, the next step is to calculate the temperature distribution within the workpiece material. A number of theoretical models have been presented for the estimation of the temperature field in grinding [13, 16, 22, 23, 35–39], that are based on the "moving heat source" model developed by Carslaw and Jaeger [40].

The driving equations are different based on whether the modelling of the process is on prismatic or cylindrical workpiece geometries. Furthermore, the use or not of a coolant fluid affects the boundary conditions. A common characteristic of both models presented hereafter is that since the heat source width is quite larger than the heat penetration depth, they are modelled in two dimensions with infinite length.

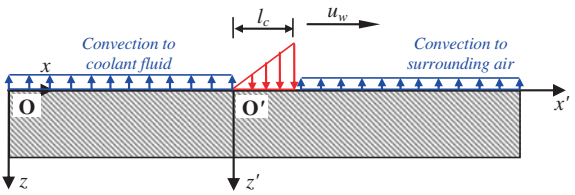

Fig. 3.17 A theoretical temperature model of grind hardening for prismatic workpieces

3.5.1 Modelling of Prismatic Workpiece Geometries

The basic theoretical model for estimating the temperature distribution in prismatic workpieces is shown in Fig. 3.17. A workpiece of finite dimensions is considered. The heat source moves along the positive direction of the x-axis on the workpiece surface with a constant velocity u_w. The coordinate system x′Oz′ is fixed at the start of the heat source and moves along with it. The global coordinate system xOz is fixed to the workpiece and coincides with the moving coordinate system at the instant $t = 0$.

For modelling purposes, the grinding process is assumed to be quasi-stationery and therefore, the temperature field is the solution to the following differential equation:

$$\frac{\partial^2 T}{\partial x^2} + \frac{\partial^2 T}{\partial z^2} + \frac{u_w}{a_w}\frac{\partial T}{\partial x} = 0 \tag{3.42}$$

where T is the temperature rise relative to the ambient temperature T_o and a_w is the thermal diffusivity of the workpiece material. The boundary conditions the solution should follow are defined by the heat source and the heat convection to the air and the coolant fluid (if used). The initial condition for solving the differential equation is:

$$T(x, z)|_{t=0} = T_o \tag{3.43}$$

The heat source distribution affects the calculated temperature filed. A number of different distribution models have been presented in the literature as can be seen in Fig. 3.18.

For the case of grind hardening, the heat source distribution is assumed to present triangular distribution over the contact length, with its peak being at the direction of movement. It has been proven experimentally that the heat generation rate is proportional to the rate of material removal [30]. Since the material removal rate varies linearly across the contact zone with its maximum value at the direction of movement, it is safe to assume that the heat flux distribution will present its peak at the leading edge of the contact zone. The above argument can be also justified by the chip geometry according to Jin and Cai [41]. Temperature predictions, using a triangular heat source distribution, have also been found to be more consistent with temperature measurements in the

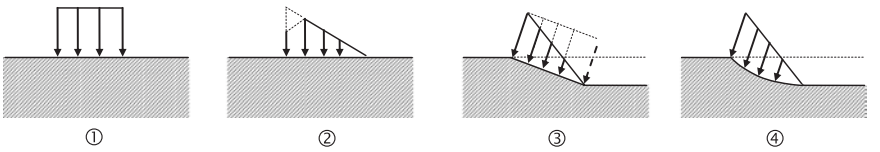

Fig. 3.18 Heat source distribution models: *1* Top hat, *2* Triangular, *3* Inclined and *4* Triangular on an arc contact length

workpiece sub-surface during a grinding pass [20]. Therefore, the heat source is expressed by the following equation:

$$q(x') = \begin{cases} \frac{q_w}{l_c} x', & 0 \le x' \le l_c,\ z = 0 \\ 0, & x' \le 0 \text{ and } x' \ge l_c,\ z = 0 \end{cases} \tag{3.44}$$

3.5.1.1 Dry Grind Hardening

Grind hardening, at least initially, was performed without the use of a coolant fluid. In that case the heat is transferred to the surrounding through convention everywhere besides the area where the heat source lies. The boundary conditions in that case can be described through the following equations:

$$\begin{cases} k_w \frac{\partial T}{\partial z}\Big|_{z=0} = \begin{cases} q(x'), & 0 \le x' \le l_c \\ -h_a\big(T(x') - T_o\big), & x' \le 0 \text{ or } x' \ge l_c \end{cases} \\ T \to T_o,\ \frac{\partial T}{\partial x}, \frac{\partial T}{\partial z} \to 0, \quad \text{when } z, x \to \infty \end{cases} \tag{3.45}$$

where h_a is the heat transfer coefficient to the surrounding air.

3.5.1.2 Wet Grind Hardening

In order to better understand the need and usage of the coolant fluid during grind hardening, the process will be compared with that of the creep feed grinding, which presents many similarities. Both processes are characterized by very slow workpiece speeds and extremely large cut depths. However, the friction heat generated due to these process characteristics can either be catastrophical in the case of creep feed grinding or beneficial in the case of grind hardening. In the case of creep feed grinding, the heat generated is removed with the aid of a copious supply of cutting fluid delivered, at high pressure, to the grinding zone. On the other hand, in the case of grind hardening, the heat generated is dissipated inside the workpiece so as to raise the surface temperature and induce metallurgical transformations. When bulky materials are grind hardened, the quenching of the workpiece is achieved by the dissipation of the heat inside the workpiece. However, for utilizing the process with thick or small diameter cylindrical parts, the cooling rate achieved is not so significant as to allow the martensitic transformation.

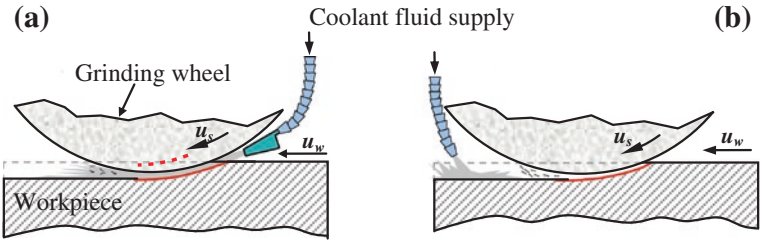

Fig. 3.19 Cutting fluid supply in the case of **a** creep feed grinding and **b** grind hardening

Therefore, the application of a coolant fluid directly after the contact area is mandatory for achieving the quenching of the part. The application of the coolant fluid also reduces the grinding wheel temperature thus, prolonging its life. Figure 3.19 compares the application of the coolant fluid for creep feed and grind-hardening operations in the case of surface workpieces.

Following the process mechanics presented in Fig. 3.19b, the boundary conditions can be derived. The heat is convected to air in front of the grinding area and to the coolant fluid behind the grinding area. Therefore, the boundary conditions of the differential Eq. 3.42 are:

$$\begin{cases} k_w \frac{\partial T}{\partial z} = \begin{cases} q(x'), & 0 \le x' \le l_c,\ z = 0 \\ -h_a T(x'), & x' \ge l_c,\ z = 0 \\ -h_f T(x'), & x' \le 0,\ z = 0 \end{cases} \\ T \to T_o,\ \frac{\partial T}{\partial x}, \frac{\partial T}{\partial z} \to 0, \quad \text{when } z, x \to \infty \end{cases} \tag{3.46}$$

where h_a and h_f are the heat transfer coefficient to the surrounding air and to the coolant fluid, respectively.

3.5.1.3 Final Cooling Stage

The grinding wheel–workpiece interaction finishes when the grinding wheel exits the workpiece. The quenching of the workpiece surface is further enhanced by a final cooling phase. Coolant fluid is amply supplied to the workpiece until its temperature drops to that of the environment. During this phase, the boundary conditions (Eqs. 3.45 or 3.46 depending on whether coolant fluid is used) are replaced by the following equation:

$$-k_w \left.\frac{\partial T}{\partial z}\right|_{z=0} = h_{f,\text{final}} \cdot \left(T(x) - T_f\right) \text{ for } t \ge l_p / u_w \tag{3.47}$$

where $h_{f,\text{final}}$ is the average heat transfer coefficient to the coolant fluid, and T_f is the cutting fluid temperature and l_p the length of the workpiece.

3.5.1.4 Temperature Distribution Calculation

The solution of the differential Eq. 3.42 with the boundary conditions provides the temperature distribution within the workpiece material. The above equations can be solved either numerically or they can be numerically approached by using FEA.

3.5.2 Modelling of Cylindrical Workpiece Geometries

The basic theoretical model for estimating the temperature distribution in cylindrical workpieces is shown in Fig. 3.20. A cylindrical workpiece with a radius r_w is considered. The heat source is assumed to be moving on the circumference of the cylinder with a constant velocity equal to that of the workpiece u_w. The polar coordinate system is fixed at the centre of the workpiece.

The differential equation that is governing the heat conduction problem is the energy equation expressed in polar coordinates:

$$\rho_w \cdot c_w \cdot \frac{\partial T}{\partial t} = k_w \cdot \left(\frac{\partial^2 T}{\partial r^2} + \frac{1}{r} \cdot \frac{\partial T}{\partial r} + \frac{1}{r^2} \cdot \frac{\partial^2 T}{\partial \theta^2} \right) \tag{3.48}$$

where ρ_w, c_w and k_w are density, specific heat and heat conductivity of the workpiece material, respectively, and r and θ is the cylindrical coordinates with $r \geq 0$ and $\theta \in [0, 2\pi)$.

The boundary conditions are defined by the heat source and the heat convection by the coolant fluid (if used) and the surrounding air. The initial condition for solving the differential equation is:

$$T(r, \theta)|_{t=0} = T_o \tag{3.49}$$

where T_o is the workpiece's initial temperature.

The heat source distribution is assumed to present triangular distribution over the contact length with its peak towards the direction of moving, as has been assumed for the case of prismatic geometries as well. It is assumed that for time

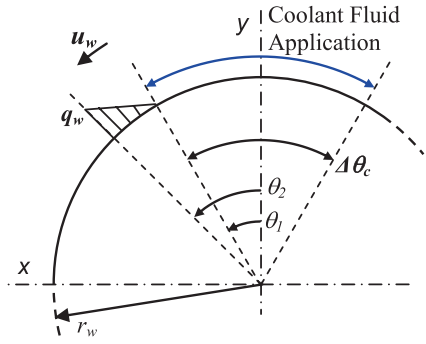

Fig. 3.20 Workpiece modelling (for simplicity only one quarter of the workpiece is presented)

$t = 0$ the heat source coincides with axis y, therefore, θ_1 determines the heat source position at an arbitrary time t. Furthermore, θ_1 and θ_2 determine the length of the heat source, as shown in Fig. 3.20, which is equal to grinding wheel–workpiece contact length. Finally, $\Delta\theta_{\text{contact}}$ determines the workpiece surface to which the coolant fluid is applied for quenching assistance.

$$\theta_1 = \omega_w \cdot t = \frac{u_w}{r_w} \cdot t \tag{3.50}$$

$$\theta_2 = \theta_1 + \Delta\theta_{\text{contact}} = \theta_1 + \frac{l_c}{r_w} \tag{3.51}$$

where ω_w is the workpiece rotational speed and l_c is the contact length between the workpiece and the grinding wheel.

The heat source triangular distribution expressed in polar coordinates is given by the following equation.

$$q(\theta) = \frac{q_w \cdot r_w}{l_c} \cdot \cos\left(\frac{\pi}{2} \cdot \frac{\theta_2 - \theta}{\theta_2 - \theta_1}\right) \tag{3.52}$$

3.5.2.1 Dry Grind Hardening

Under dry conditions (without the use of coolant fluid), the heat is transferred to the surrounding air through conduction from the workpiece surface besides the area where the heat source lies. The boundary conditions in that case can be described through the following equations:

$$-k_w(T) \cdot \left.\frac{\partial T}{\partial r}\right|_{r=r_w} = -q_w(\theta) \text{ for } \theta \in [\theta_1, \theta_2] \;\&\; t \leq 2\pi \times r_w/u_w \tag{3.53}$$

$$-k_w \left.\frac{\partial T}{\partial r}\right|_{r=r_w} = h_a(T) \cdot (T(r = r_w, \theta) - T_a) \text{ for } \theta \in [0, \theta_1) \cap (\theta_2, 2\pi) \;\&\; t \leq 2\pi \times r_w/u_w \tag{3.54}$$

where q_w is the heat source distribution, h_a is the respective coefficient between the workpiece material and the surrounding air and T_a is the surrounding air temperature. It is assumed that for time $t = 0$ the heat source coincides with axis y, therefore, θ_1 determines the heat source position at an arbitrary time t. Furthermore, θ_1 and θ_2 determine the length of the heat source, as shown in Fig. 3.20, which is equal to grinding wheel–workpiece contact length.

3.5.2.2 Wet Grind Hardening

As mentioned during the prismatic geometry model presentation, during grind hardening the coolant fluid is usually supplied directly after the contact zone

for assisting the quenching of the workpiece material. In conventional grinding processes, the coolant fluid is applied to the wedge, formed by the wheel and the workpiece through a nozzle. Another difference from conventional grinding is that during grind hardening, the coolant fluid does not enter the grinding zone since the grinding wheel rotates towards the fluid flow. Therefore, the contact zone is under dry conditions. For cylindrical grind hardening, only one quadrant of the workpiece is effectively cooled by the coolant fluid (Fig. 3.20). Thus, parameter $\Delta\theta_c$ is assumed to be equal to 90°. The boundary conditions in that case can be described through the following equations:

$$-k_w(T) \cdot \left.\frac{\partial T}{\partial r}\right|_{r=r_w} = -q_w(\theta) \text{ for } \theta \in [\theta_1, \theta_2] \;\&\; t \leq 2\pi \times r_w/u_w \tag{3.55}$$

$$-k_w(T) \cdot \left.\frac{\partial T}{\partial r}\right|_{r=r_w} = h_f(T) \cdot \left(T(r = r_w, \theta) - T_f\right) \text{ for } \theta \in [\theta_1 - \Delta\theta_c, \theta_2] \;\&\; t \leq 2\pi \times r_w/u_w \tag{3.56}$$

$$-k_w(T) \cdot \left.\frac{\partial T}{\partial r}\right|_{r=r_w} = h_a(T) \cdot (T(r = r_w, \theta) - T_a) \text{ for } \theta \in [0, \theta_1 - \Delta\theta_c) \cap (\theta_2, 2\pi) \;\&\; t \leq 2\pi \times r_w/u_w \tag{3.57}$$

where q_w is the heat source distribution, h_f is the heat transfer coefficient between the workpiece material and the coolant fluid, h_a is the respective coefficient between the workpiece material and the surrounding air, T_f is the cutting fluid temperature and T_a is the surrounding air temperature. It is assumed that for time $t = 0$, the heat source coincides with axis y, therefore, θ_1 determines the heat source position at an arbitrary time t. Furthermore, θ_1 and θ_2 determine the length of the heat source, as shown in Fig. 3.20, which is equal to grinding wheel–workpiece contact length. Finally, $\Delta\theta_c$ determines the workpiece surface to which the coolant fluid is applied for quenching assistance.

3.5.2.3 Final Cooling Stage

The grinding wheel–workpiece engagement ends once the workpiece has completed one full rotation. Afterwards, the workpiece rotates with full speed under a direct coolant flow rate until the workpiece temperature reaches environment temperature. During this phase, the boundary conditions (Eqs. 3.53–3.57) are replaced with the following equation.

$$-k_w(T) \cdot \left.\frac{\partial T}{\partial r}\right|_{r=r_w} = h_f \cdot \left(T(r = r_w, \theta) - T_f\right) \tag{3.58}$$

3.5.3 Modelling Using Finite Element Analysis

It is evident that the differential equations characterizing the grind-hardening process can be more easily solved using numerical methods or finite element methods.

In this case, the heat transfer problem (Eq. 3.42 or 3.48, depending on whether prismatic or cylindrical geometries are modelled) can be described by the following equation:

$$[C(T)]\{T\prime(t)\} + [K(T)]\{T(t)\} + \{v\} = \{Q(t)\} \tag{3.59}$$

where $[K]$ is the conductivity matrix, $[C]$ the specific heat matrix, $\{T\}$ the vector of nodal temperatures, $\{T'\}$ the vector of time derivative of $\{T\}$, $\{v\}$ is the velocity vector, which is equal to zero as no mass transport is assumed in the current problem, and $\{Q\}$ the nodal heat flow vector. Since the expected temperature is always below melting temperature, no phase change occurs and thus the enthalpy of the material does not need to be considered.

The procedure for developing and solving a finite element model for the case of grind hardening is shown in Fig. 3.21, and is identical either the geometry is considered prismatic or cylindrical. Since the heat source width is quite larger than the heat penetration depth, they are modelled in two dimensions with infinite length. The meshing of the geometry is determined by running the model a number of times, with the modelled geometry having in each run twice as many elements as in the previous run. The final meshing density can be determined when two succeeding runs presents less that 2 % difference. The elements distribution should be denser in the workpiece surface since the temperature is expected to be considerably higher in this area. Their size can be increased gradually towards the workpiece centre for the case of cylindrical geometries or as we move further away from the area of heat generation. Two typical examples of finite element models for a cylindrical and a prismatic workpieces shown in Fig. 3.22.

The heat source is considered presenting triangular heat distribution and its length being equal to the grinding wheel–workpiece geometrical contact length. The workpiece feed speed can be modelled through the movement of the heat source on the workpiece surface with a constant velocity equal to that of the workpiece feed. The heat transfer problem thus can be considered a quasistationary one. Therefore, for a finite time step, the heat source can be assumed to be static in a specific position on the workpiece surface and at the succeeding time step, the heat source will move over a length equal to the product of the workpiece speed with the time step duration. The time step duration affects the accuracy of the analysis results.

Another significant aspect of such modelling is the material properties to be considered for the workpiece material. Since the temperature exceeds in some cases 1,000 °C, it is important to consider temperature-dependent properties. The temperature dependence of the workpiece material results thus in a highly nonlinear heat transfer problem.

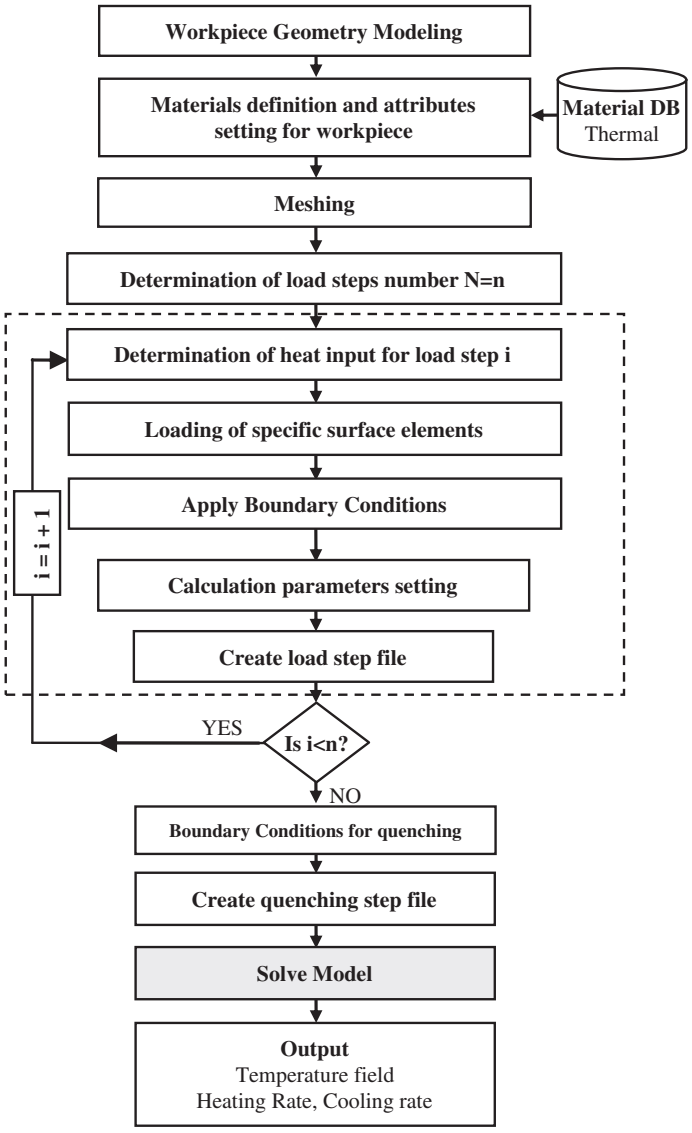

Fig. 3.21 FEA model generation and solving approach

3.5.4 Model Implementation and Validation

Following the finite element model development process outlined in Fig. 3.21, Salonitis et al. solved it for the simple case of a prismatic workpiece material [28] and cylindrical ones [11] (Figs. 3.23 and 3.24, respectively). In Fig. 3.25, the temperature as a function of heat flux and the distance below the grinding zone is shown.

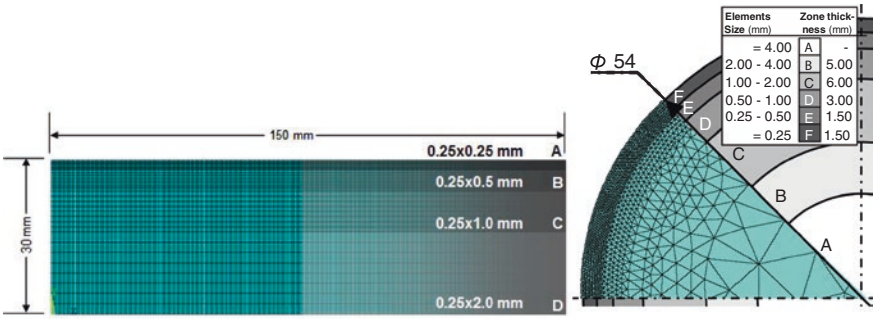

Fig. 3.22 FEA models: **a** prismatic [28] and **b** cylindrical geometry [11]

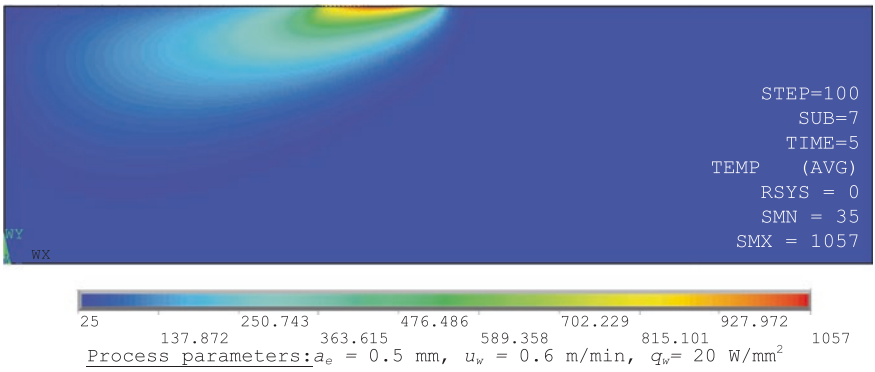

Fig. 3.23 Temperature distribution calculated using finite element models for a prismatic geometry

3.6 Modelling of Metallurgical Changes

3.6.1 Introduction Surface Heat Treatment Mechanisms

Heat treatment processes are used for the improvement of the workpiece performance under dynamic loads and friction. In their simplest form, the entire workpiece is heated above the austenitization temperature in a furnace, hold in that temperature for a specific period of time, and subsequently quenched with an appropriate medium (usually water or oil). This sequence of controlled heating and cooling alters the lattice structure within the material and as a result the surface hardness can be increased.

However, usually it is not required by the design of the component to be heat treated throughout its geometry, making thus the conventional heat treatment approaches inefficient. Instead, surface or even localized hardening is required and can be used for the production of high added value and precision components.

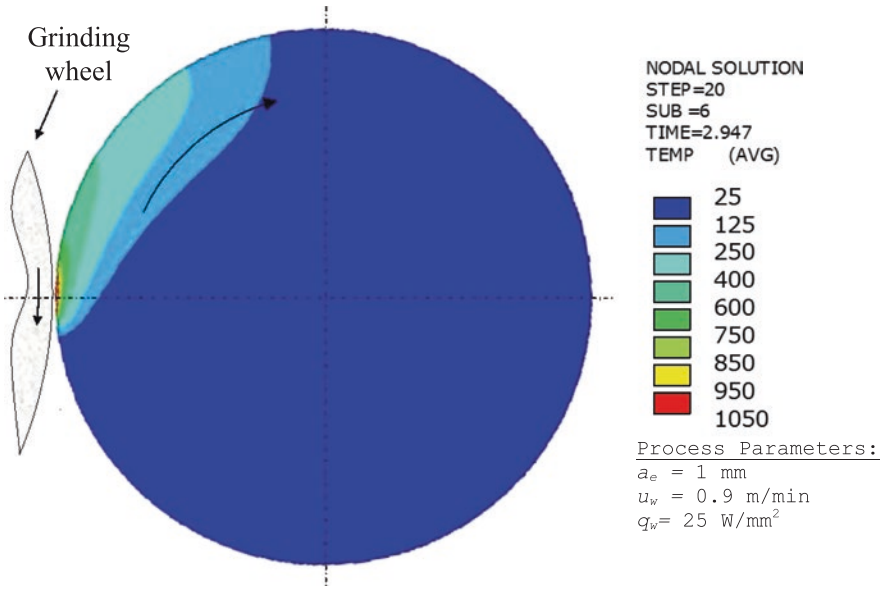

Fig. 3.24 Temperature distribution calculated using finite element models for a cylindrical geometry

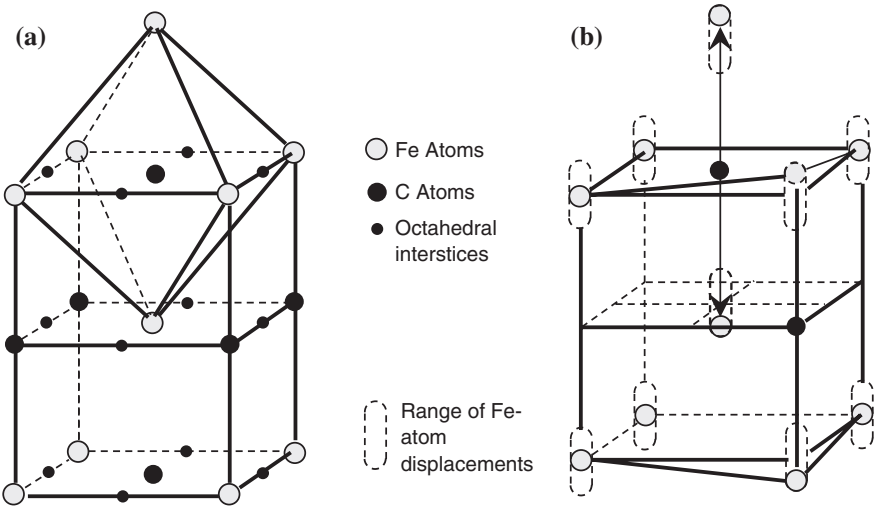

Fig. 3.25 **a** Body-centred tetragonal crystal structure of martensite in Fe-C alloys **b** iron atom displacements due to carbon atoms in martensite

Such localized surface hardening methods can prove beneficial for industry due to their advantages such as increased flexibility, reduced lead times, and reduced heat treatment deformation.

The usual methods for surface and/or local hardening can be classified into two big categories: ones with and ones without alteration of the chemical composition of the workpiece material. Indicatively, local hardening methods with simultaneous change of chemical composition are the carbonization and nitridization methods. The hardening of the component without the alteration of chemical composition is achieved through local and rapid heating of the workpiece surface with the subsequent self-quenching to the rest of the workpiece material mass. In such cases, the heating is achieved through conventional methods such as flame torches (flame hardening) or by utilizing more state-of-the-art methods such us induction coils, laser beams and electron beams. Grind hardening can be considered as one of these methods, since the heat generated in the grinding zone is the root cause for the local and rapid increase of the workpiece temperature that results in the formation of martensite.

The high hardness values observed in a steel material is due to the presence of martensite in its structure. Martensite is one of the phases that the steel can take and represents a specific lattice structure, where the carbon atoms are trapped in octahedral structure. The key reason that the martensite structure is characterized by high strength and hardness is due to the trapped carbon atoms [42] that result in displacements of iron atoms in the body-centred crystal structure (Fig. 3.25). Such deformation of the crystal structure prohibits the displacement of deformations, increasing thus the strength and hardness of steel.

Martensite's origin is austenite. When a steel material is heated above the austenitization temperature, carbon atoms have increased mobility and can freely move within the crystal structure. If the steel is cooled down with slow rates, the carbon atoms through diffusion have enough time to return to pre-austenitization phases such as ferrite and cementite. However, if the cooling is rapid, diffusion is prohibited and austenite is transformed to martensite. Since this martensitic transformation is diffusionless, the martensite has exactly the same composition as does its parent austenite. The carbon atoms do not partition themselves between cementite and ferrite but instead are trapped in the octahedral sites of a body-centred tetragonal unite cell (Fig. 3.25a).

The cooling rate of the austenite structure is critical and determines the lattice crystal structure that will be formatted during the quenching. As it has been described, depending on the cooling rate, the austenite structure can be transformed in various crystal structures such as ferrite, cementite, perlite, bainite and martensite. The effect of a specific cooling rate on the crystal structure is depicted in the CCT diagram (Fig. 3.26).

In Fig. 3.26, two diagrams are presented, the Isothermal Transformation (IT) with dashed lines and the Continuous Cooling Transformation (CCT) with continuous lines. These lines define the beginning and the end of specific transformations when the cooling curve of the workpiece material passes through these areas. The key difference between IT and CCT diagrams lies in the cooling

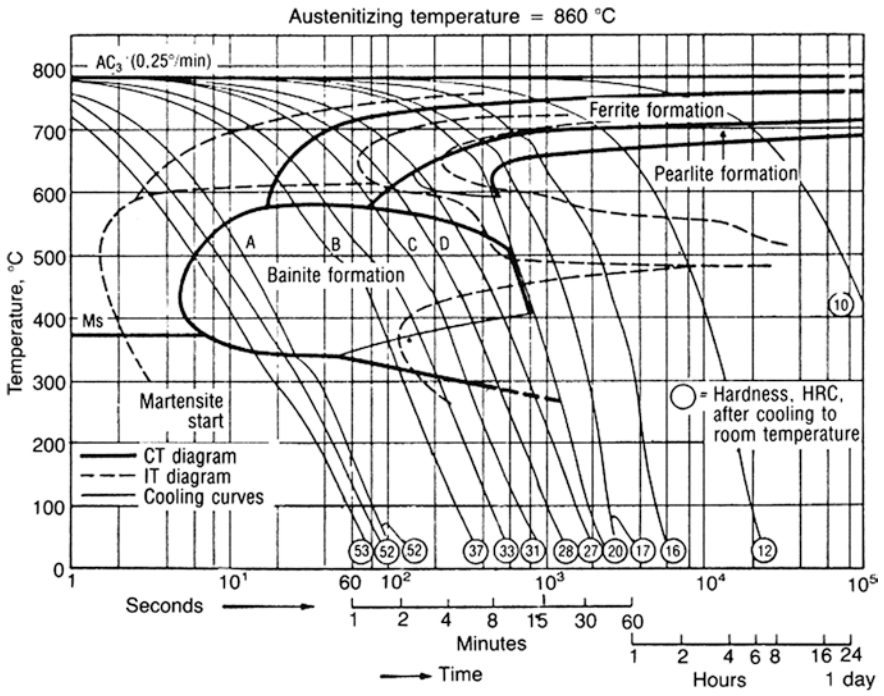

Fig. 3.26 IT and CCT diagrams for 42CrMo4

environment. IT diagrams describe the crystal transformations due to isothermal holding, whereas CCT diagrams represent the continuous cooling processes at various rates. Both IT and CCT diagrams are determined experimentally. Grind-hardening process is described by CCT diagrams, since the cooling rate is high. In order to achieve the highest possible hardness, thus 100 % transformation of the crystal structure to martensite, the cooling curve should not enter the bainite area. The temperature where the Martensitic transformation begins (*Ts*), depends on the steel composition.

However, grind hardening and all other surface hardening processes are characterized by very high heating rates and brief austenitizing periods. These characteristics have a significant effect both on the metallurgy transformations and the temperature at which these are realized (Fig. 3.27).

3.6.2 Austenitization Temperature

The austenitizing temperature depends on the heating rate, the peak temperature and the holding time of a specific material. In the case of 100Cr6, the correlation of these parameters was experimentally determined by Liedtke and Jonsson [43]

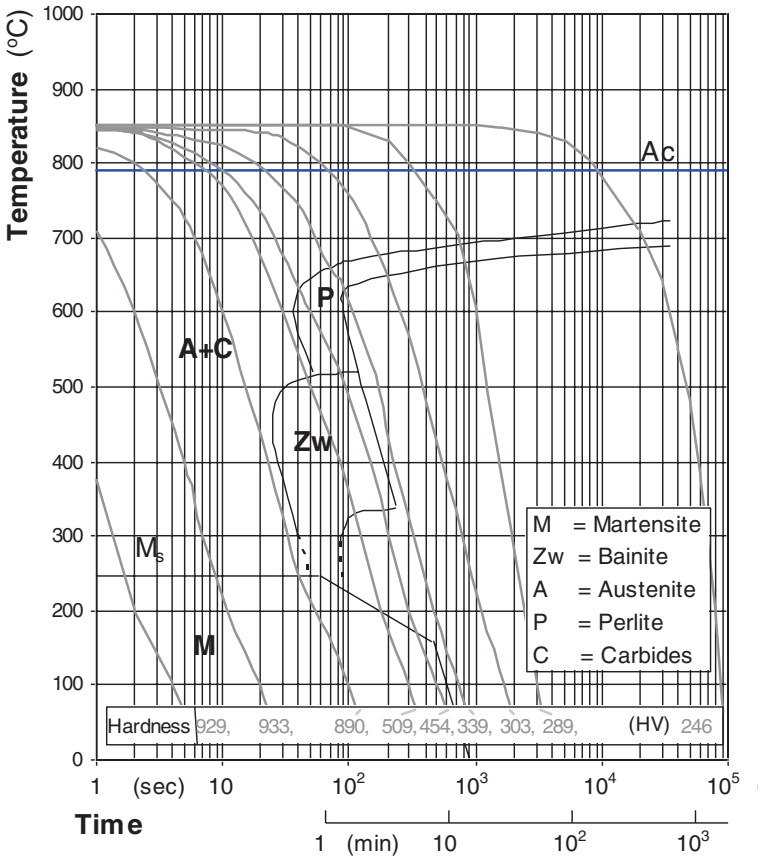

Fig. 3.27 CCT diagram for 100Cr6 steel for 860 °C austenitizing temperature

and is shown in Fig. 3.28. The heating rate achieved during grind hardening always exceeds 300 K/s [11, 12] and thus, based on Fig. 3.28, the austenitizing temperature is found to be 920 °C. Knowing the temperature field and the austenitizing temperature, we are led to the determination of the HPD.

3.6.3 Martensitization Temperature

The austenitization of the workpiece in elevated temperature, has another critical metallurgy effect that has to be taken into consideration as it reduces significantly the M_s temperature. In the case of 100Cr6, when the workpiece has been austenitized at 860 °C, the martensite transformation begins at 245 °C, but for an austenitization temperature of 1050 °C, the martensite transformation will not start until the temperature falls beneath 135 °C. Since in the grind-hardening process

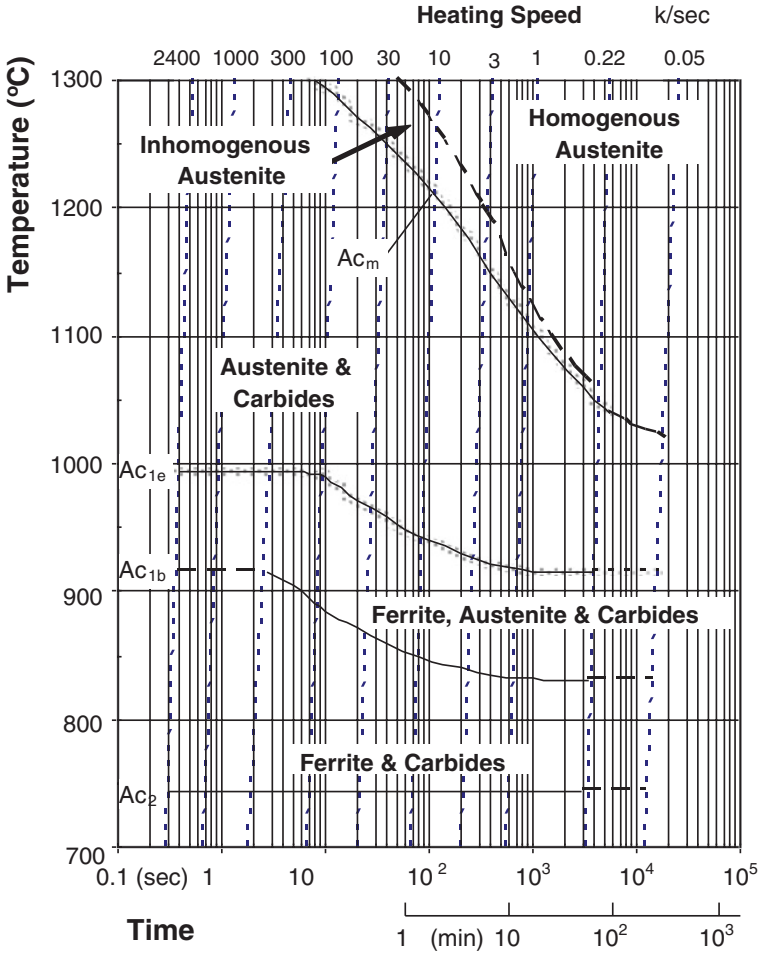

Fig. 3.28 Austenitization temperature as a function of heating rate for 100Cr6

the peak austenitizing temperature depends not only on the process parameters but also on the distance from the workpiece surface, the M_s line of the CCT diagram has to be determined for each point in the workpiece. For the determination of the relation between the M_s and the peak austenitizing temperatures, the experimental data stated in [44] were used and an exponential relation was assumed to relate these parameters (Fig. 3.29):

$$M_s = 2835.7e^{-0.0029T} \tag{3.60}$$

Based on the above considerations and using the temperature history calculated for each workpiece node with the FEA analysis, a modified CCT diagram, presenting different A_c and M_s temperatures, can be plotted for each node. Based

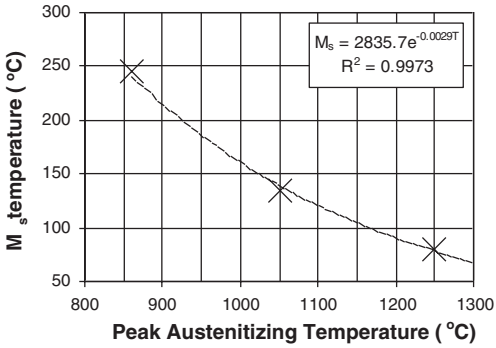

Fig. 3.29 M_S temperature dependence on peak austenitizing temperature for 100Cr6 (based on [44])

on these CCT diagrams, the microstructure and the micro-hardness HV_{CCT} on each workpiece node can be estimated. It should be noted however that the CCT diagram determined using this methodology, does not take into account the fact that during grind hardening, the workpiece undergoes high deformations at high strain rates which further alters the CCT diagram.

3.6.4 Retained Austenite

The micro-hardness calculated from the CCT diagram is based on the assumption that all austenite is transformed to martensite. However, the austenite transformation to martensite ends at a temperature, quite lower than that of the ambient. The extent of athermal transformation depends only on the degree of undercooling below the M_s temperature. The volume fraction of martensite transformation during undercooling, can be determined by using an experimental equation developed by Koistinen and Marburger [45] for Fe-C alloys containing between 0.37 and 1.1 % carbon:

$$f = 1 - e^{-1.10\times10^{-2}\Delta T} \tag{3.61}$$

where f is the volume fraction of martensite and ΔT is the undercooling below the M_s temperature.

3.6.5 Micro-Hardness

The hardness of the retained austenite is equal to that of the pre-treated material and therefore, the presence of retained austenite reduces the overall hardness of the workpiece. Considering that the overall hardness follows the inverse lever rule for a two-phase system, the overall hardness is given by the following equation:

$$HV = f \cdot HV_{\mathrm{CCT}} + (1 - f) \cdot HV_{\mathrm{Ret.Austenite}} \tag{3.62}$$

where HV is the overall hardness, HV_{CCT} is the hardness read from the CCT diagram for the specific cooling path and $HV_{Ret.Austenite}$ is the hardness of the retained austenite.

3.6.6 Hardness Penetration Depth

The hardness penetration depth (HPD) is a quantitative metric for characterizing the process outcome. It is also a design characteristic—specification of the component. From the process perspective, HPD is defined as the distance from the workpiece surface to its depth, where the hardness value is reduced to 80 % of the nominal value. There are a couple of different approaches in predicting the HPD theoretically. The HPD can be determined from the theoretically determined hardness profile as proposed by Salonitis and Chryssolouris [11] or can be approximated to be equal to the depth where the temperature exceeds that of austenitization as pointed out by Chryssolouris et al. [12]. It should be noted though, that the latter method can be used only when the critical quenching has been achieved, i.e. when bulky workpieces are hardened [12] and/or when coolant fluid is used for the grind hardening of small size workpieces [11]. The two methods were compared by Salonitis and Chryssolouris [11] and it was shown that the maximum error caused in the HPD estimation from the austenitization depth was ca. 8 %.

3.6.6.1 Maximum Achievable Hardness Penetration Depth

Both experimental and theoretical results indicate that HPD increases as the heat entering the workpiece material does. The heat entering the workpiece is a function of the process parameters. Increasing the depth of cut increases the material removal and thus the heat generation rates. On the other hand, the decrease in the workpiece speed allows for more heat to be dissipated within the workpiece material. However, higher values of heat entering the workpiece will result in a subsequent increase of the workpiece surface temperature. The workpiece temperature should not exceed the melting point of the material so as to avoid grain growth and increased retained austenite after quenching [42] that reduces the hardness of the treated layer [11]. Furthermore, the rapid melting and solidification that may occur in the heat affected zone during the surface hardening processes, results in coarsening and dissolution of the strengthening phases that degrade the strengthening of this area. The melting point depends on the workpiece material composition and can be calculated from its Fe-Fe_3C diagram [46]. In the case of 100Cr6, for example, this critical temperature is equal to 1315 °C. Therefore, the heat flux rate inducing the melting temperature at the workpiece surface is the maximum allowable rate to be generated during grind hardening for a specific set of depth of cut and workpiece speed. The HPD that will result from this heat flux rate will be the maximum to be achieved from this set of parameters.

3.6.7 Model Implementation and Validation

For the estimation of the metallurgical transformations, the hardness profile and the hardness penetration depth; the temperature field distribution and its evolution over time is required as input. The steps to be followed in order to fully characterize the process outcome are presented in Fig. 3.30, and can be considered as the continuation of Fig. 3.21.

3.6.7.1 CCT Diagram Modification

The available CCT diagrams are for conventional heat treatment processes where both heating and cooling takes place under controlled quasi-stationery rates. However, since in grind hardening both the heating and cooling rates are very rapid, the CCT diagram needs to be modified accordingly. Indicatively, the procedure for estimating the modified CCT diagram is presented hereafter. In Fig. 3.31, the temperature evolution for different depths below the workpiece surface is shown, as well as the various critical temperatures for the metallurgical changes.

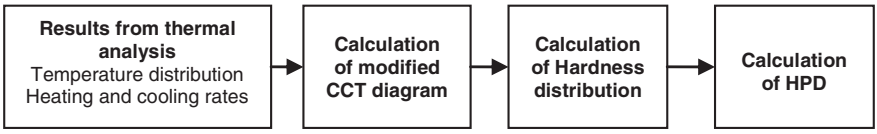

Fig. 3.30 Metallurgical changes modelling steps

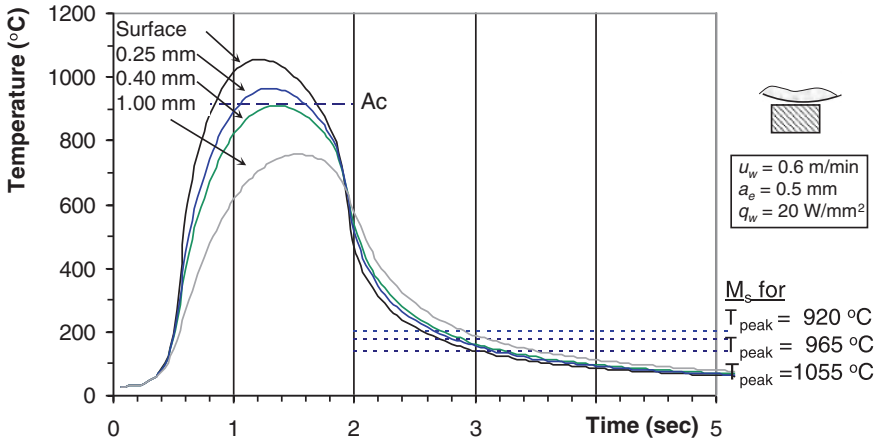

Fig. 3.31 Temperature distribution as a function of time and distance from the workpiece surface

The austenitization temperature in this case was estimated based on the method presented in Sect. 3.6.2, and is a function of the heating rate. For the process parameters presented in Fig. 3.31, the heating rate at the workpiece surface is close to 1,200 K/s, whereas in the depth where the temperature equals that of austenitization is about 700 K/s. Based on the data presented by Liedtke and Johnson [43] and Fig. 3.28, austenitzation temperature equals 920 °C for heating rates that exceed 300 K/s. On the other hand, the martzitization temperature can be calculated using Eq. (3.60), as a function of the peak temperature. Due to the fact that the peak temperature is different for every location on the workpiece, different martensitization temperatures are calculated (Fig. 3.31). Based on such calculations, the CCT diagram can be modified for every point in the workpiece. Indicatively, Fig. 3.32 presents the modified CCT diagram that was estimated for the temperature distribution shown in Fig. 3.31.

3.6.7.2 Hardness Distribution Estimation

The overall hardness will be different at each depth and can be calculated from the modified CCT diagram Eq. (3.62) as a function of the volumetric concentration of

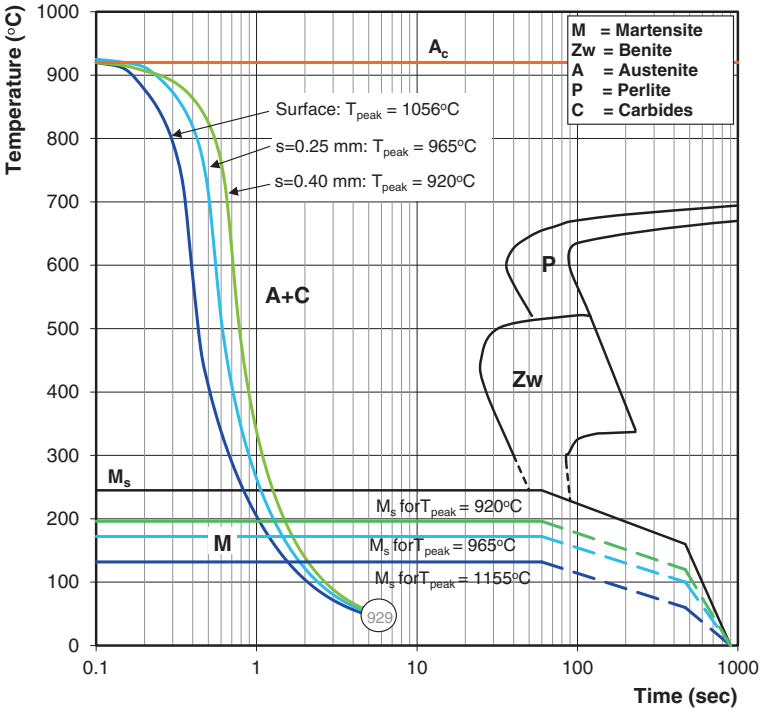

Fig. 3.32 Modified CCT diagram

Table 3.1 Hardness distribution calculation

	Distance from surface		
	0.00 mm	0.25 mm	0.40 mm
Heating rate (K/s)	1200	850	700
Austenitization temperature (°C)	920	920	920
Peak temperature (°C)	1056	965	920
Martensite temperature (Eq. 3.60 in °C)	133	173	197
Retained austenite (Eq. 3.61 in %)	41.3	36.5	35.5
CCT hardness (HV)	929	929	929
Calculated hardness (Eq. 3.62 HV)	**690**	**735**	**740**

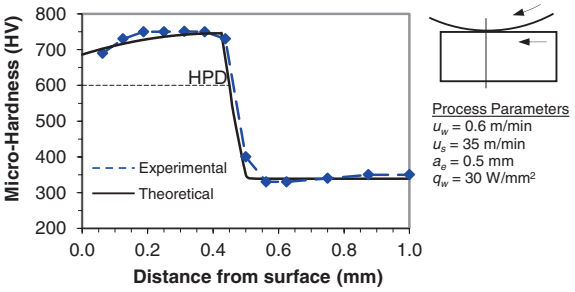

Fig. 3.33 Model verification for micro-hardness calculation

retained austenite. As it has been already noted, this is a function of the extent of undercooling below the martensitization temperature. As a result, the concentration of the retained austenite is maximum at the workpiece surface and decreases with the distance from the surface. Table 3.1 summarizes the calculated micro-hardness and Fig. 3.33 presents the experimental verification of the predictions.

3.6.7.3 Hardness Penetration Depth Estimation

It has been already stated that HPD is defined as the distance from the workpiece surface to its depth, where the hardness value is reduced to 80 % of the nominal value. Based on the calculated hardness distribution (Fig. 3.33), the HPD can be determined. Alternatively, it can be estimated from the depth where the temperature exceeds the austenitization temperature, as pointed out by Chryssolouris et al. [12]. They compared the two methods with experimental measurements and concluded that the calculation of the HPD using the hardness distribution provides better agreement with the experimental results. However, the effort needed for the determination of the hardness distribution is quite copious.

3.7 Modelling of Residual Stresses

The residual stresses are the result of inhomogeneous plastic deformations during quenching. The generation of the residual stresses is quite complex, with numerous affecting factors. The material type is one of the most important ones with heat transfer coefficient, thermophysical and mechanical properties, and phase composition influencing greatly the residual stresses. The higher the yield strength of the material the more elastic the thermal and transformation-induced macroscopic stresses will be generated in the part to be quenched. Thus, the residual stresses in general will be lowered with increasing yield strength of the material.

A typical residual stress profile generated is presented in Fig. 3.34. The most important factors are presented, being (a) the surface residual stress magnitude, (b) the maximum value measured and (c) the distance from the processed surface where the maximum value occurs and, finally (d) the beneficial depth.

Thermal surface treatments always result in residual stresses. The reasons for these stresses have been identified in a number of studies and can be summarized into (i) the thermal stresses due to thermal expansion or contraction during heating and cooling of the workpiece and (ii) the density changes due to the phase transformations in the workpiece material. In case of multiphase materials, residual stresses are also generated due to the different thermal expansion coefficients of the various phases and due to chemical reaction products formed on the surface of the workpiece material.

In general when heat treating workpieces, the cooling rate at the surface is higher than at the centre. The early thermal contraction at the surface is resisted by the incompressible core, resulting in tensile yielding at the surface. The continuous temperature reduction results in contraction of the workpieces core pulling the surface inwards. As a result of this inward pulling, compression stresses are generated near the surface. In materials with phase transformation, anisotropic volume change due to martensitic transformation adds to the complexity and magnitude

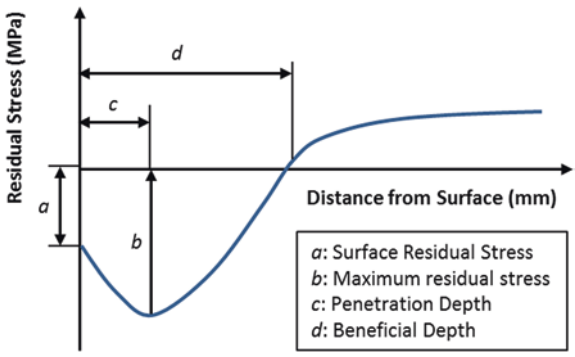

Fig. 3.34 Typical surface residual stress profile [47]

of the residual stress pattern. The residual stress system is self-equilibrating; if certain regions have compressive residual stresses, then somewhere else there must be offsetting tensile stresses.

For the case of grinding, surface residual stresses is a result of the thermal deformation due to heat dissipation in the grinding zone, the pressure between the grinding wheel and the workpiece, and the phase transformation of the material structure [48]. The balance between these three different mechanisms defines whether the final residual stresses are compressive or residual. It has been shown in past studies, focusing though on grinding and not grind hardening, that the pressure applied from the grinding wheel to the workpiece induces compressive residual stresses. On the other hand thermal deformation due to the heat dissipation results in tensile residual stresses [49]. The challenge is to incorporate the resulting residual stresses due to phase transformation. Phase change results in volume change; depending on whether the new structure occupies more space than the original phase the residual stresses can be either compressive or tensile. For the case of grind hardening we observe two subsequent phase transformations. From ferrite/perlite mixture before grinding to austenite (existing only when the workpiece material is above eutoctoid temperature) during the processing and finally to martensite due to quenching. Martensite presents body-centred tetragonal (BCT) crystal structure whereas ferrite presents body-centred cubic (BCC) crystal structure [42]. Since BCT occupies more space than BCC, martensitic phase transformation results into compressive residual stresses.

3.7.1 Modelling Using Finite Element Analysis

Similarly, for the case of residual stresses modelling, the thermal model developed is used as a basis. Thermal elements are replaced with elastic-plastic elements. The resulting model undergoes a non-linear elastic-plastic structural analysis using temperature-dependent material properties and a multi-linear isotropic hardening model. The non-linear mechanical analysis problem is described by the following general finite element equation:

$$[K(T)]\{u(t)\} + \{F(t)\} + \{F_{\text{th}}(t)\} = 0 \tag{3.63}$$

where $[K(T)]$ is the temperature-dependent stiffness matrix, $\{F(t)\}$ is the external load vector, $\{F_{\text{th}}(t)\}$ is the temperature load vector and $\{u(T)\}$ is the displacement vector.

For each load step, the nodal temperatures from the thermal analysis are read into the structural analysis. Nodal temperatures from thermal results are continued to be read into the structural analysis until the time when the model temperature has reached the environmental one. The structural boundary conditions set to workpiece are quite simple; all nodes at the bottom end of the workpiece are fixed to all directions. The structural loading includes the application of pressure

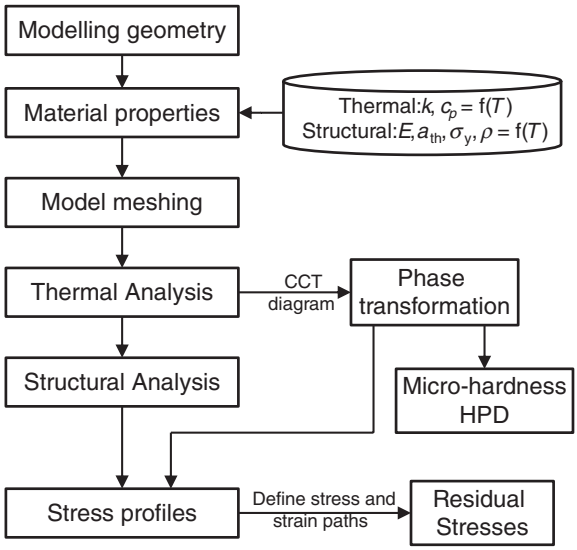

Fig. 3.35 Modelling approach for calculating residual stresses [50]

resulting from the grinding wheel–workpiece interaction at the elements that corresponds to the contact length for each load step. The non-linearity of material properties is taken into account through the von-Mises criterion, and plasticity is taken into consideration through kinematic strain-hardening law. The non-linear equation system solution is achieved through the Newton–Raphson algorithm, whereas Newmark integration scheme is applied for the numerical integration in the time domain. Salonitis [50] presented graphically the approach for predicting the residual stresses using FEA as shown in Fig. 3.35.

3.7.2 Model Implementation and Validation

Salonitis [50] validated this model for the case of grind hardening of AISI 1050 workpiece material both under wet and dry conditions. His analysis indicated that grind hardening without the application of coolant fluid result in tensile residual stresses across the whole depth of the heat treated layer (Fig. 3.36). The FEA model indicated that during dry grind hardening, the driving mechanism for the resulting residual stresses is the thermal deformation due to the high heat source generated in the grinding arc. Additionally, higher workpiece material results in lower martensite onset temperatures that leads to higher concentration of retained austenite. Austenite presents face-centred cubic (FCC) lattice structure with quite similar volume with original ferrite (BCC), thus the compressive stresses due to phase transformation are limited.

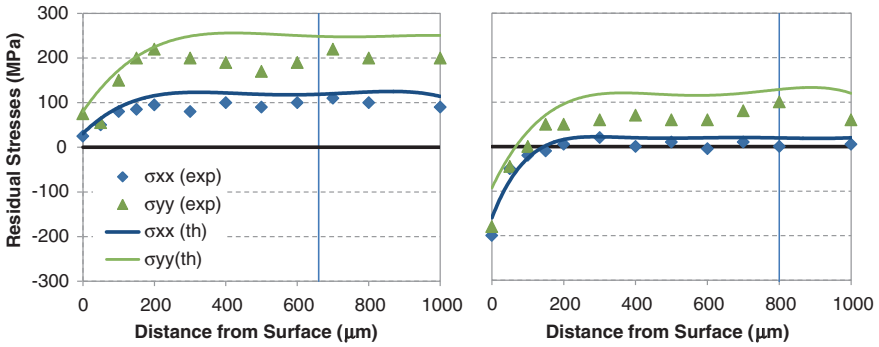

Fig. 3.36 Residual stresses after (*left*) dry and (*right*) wet grind hardening at the middle of the workpiece (*Vertical line* indicates the length of hardened layer) [50]

3.8 Integration of Models

Six models have been presented in the previous sections for simulating various aspects of the grind-hardening process. The models can be integrated all together for the holistic modelling of the grind-hardening process. In that case, we can identify five major phases that are sequentially connected for the estimation of the hardness profile, hardness penetration depth and residual stresses as a function of process parameters and the specification of the grind-hardening wheel (as can be seen in Fig. 3.37). During the first phase (phase A), the grinding forces as a function of process parameters and grinding wheel specification are determined. During the second phase (phase B), the heat generated within the grinding zone and its partition to the various heat sinks is estimated. In the subsequent phase (phase C), the temperature distribution along with the heating and cooling rates are estimated using finite element analysis. Phase D deals with the determination of the heat penetration depth and the micro-hardness distribution based on the estimated modified CCT diagrams. Finally, within the last phase (E) the residual stresses are estimated by solving the coupled thermal and structural finite element model.

Such an analysis can be used for developing process "maps" (a database) for the prediction of the process outcome as a function of process parameters. This database is based on diagrams linking, as an example, the hardness penetration depth with the heat flux entering the workpiece for a number of combinations of process parameters. Figure 3.38 presents an abstract of such a database developed by Salonitis [51] for the prediction of hardness penetration depth. Additionally, in Fig. 3.39, the database maximum hardness penetration depth diagram is presented.

3.8.1 Integrated Model and Database Validation

Salonitis et al. [52] used the database for estimating the process parameters to be used for achieving a specific hardness distribution and hardness penetration depth

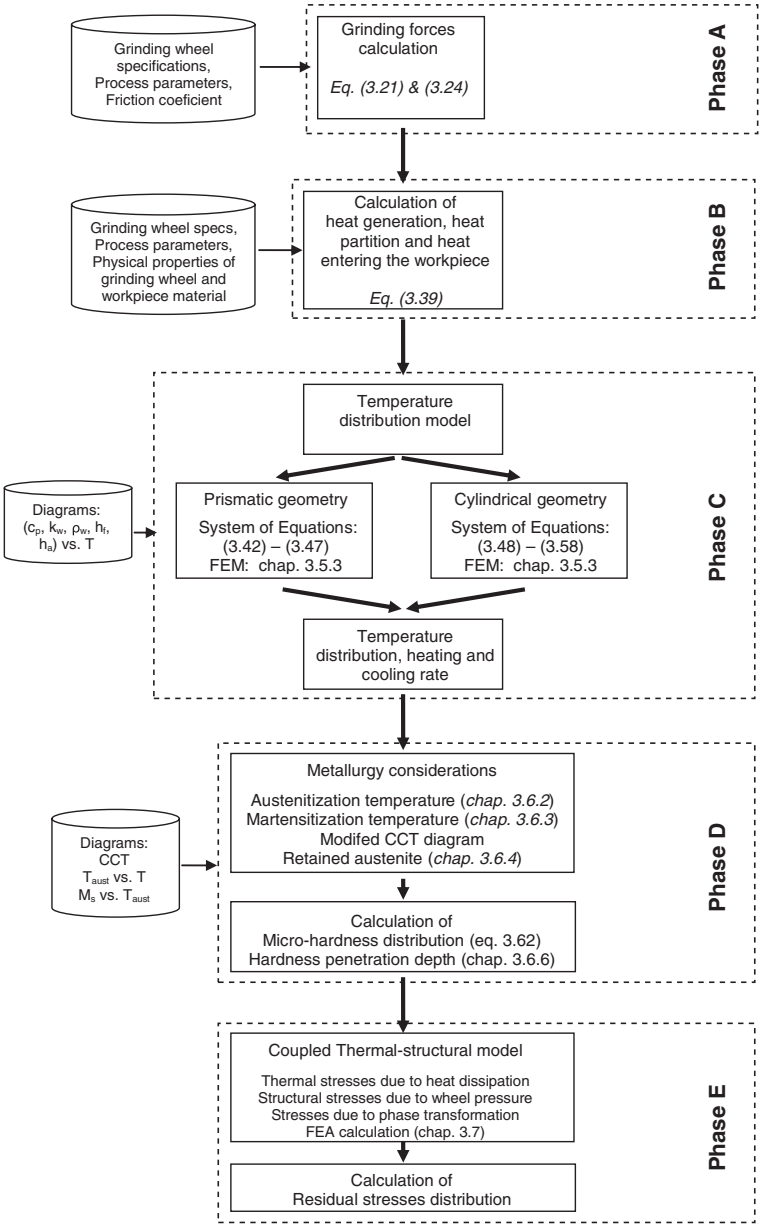

Fig. 3.37 Holistic model for grind-hardening simulation

to an actual industrial component (V-shaped guide). Having as a starting point the requirements and limitations, i.e. knowing the requested HPD and having a limitation on a specific process parameter (e.g. the feed speed), the heat flux can be determined for this set of variables, from the database of charts shown in Fig. 3.38.

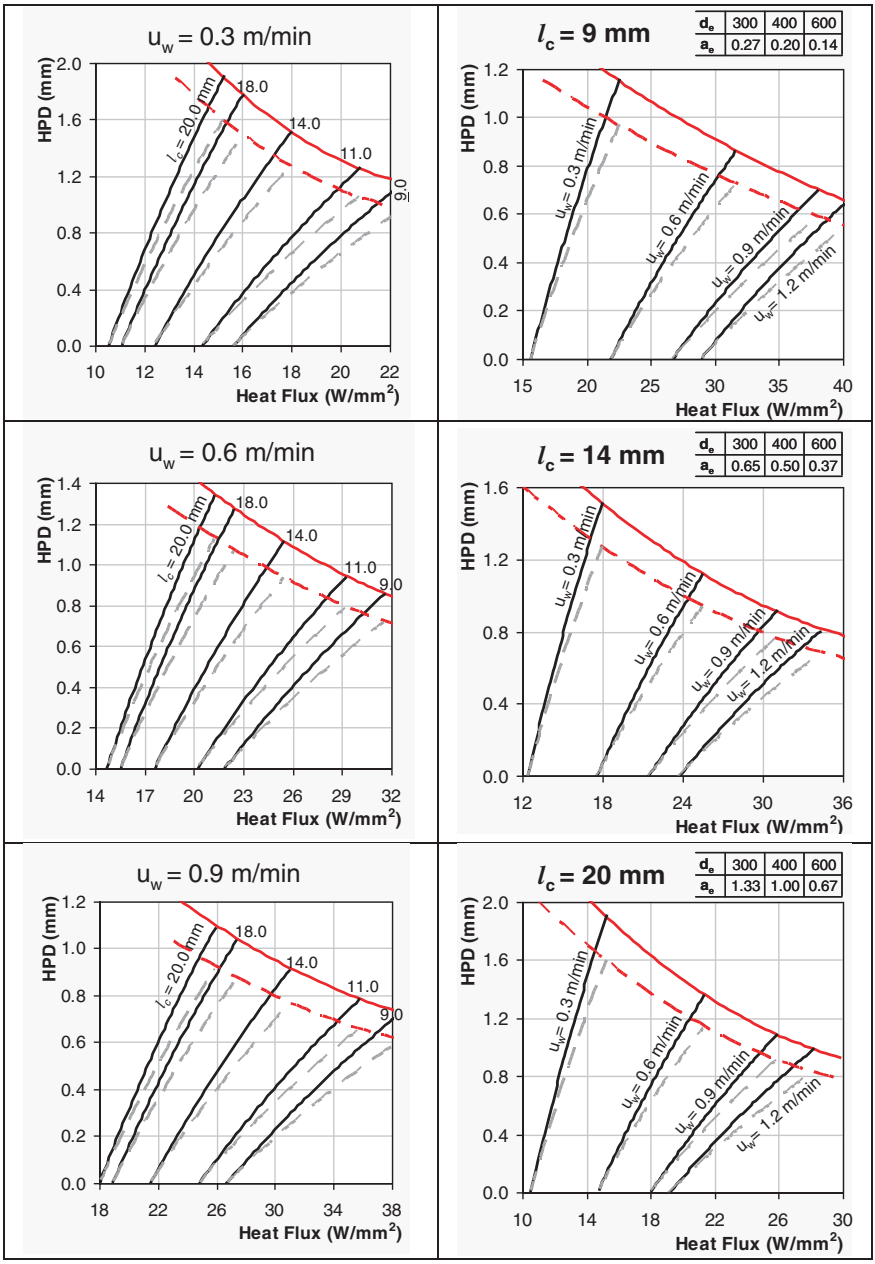

Fig. 3.38 Database diagrams for predicting the HPD as a function of process parameters (for AISI 52100—*dashed lines* are the experimentally tuned predictions) [51]

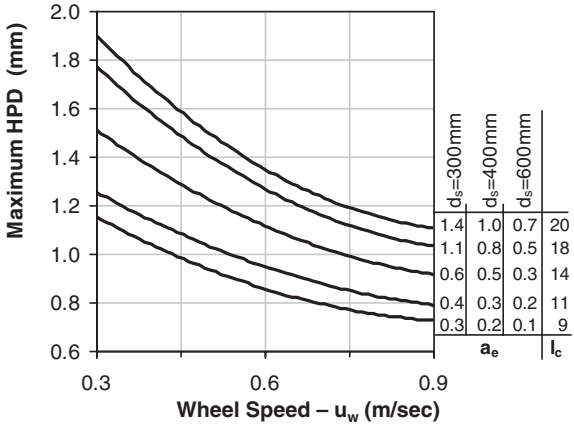

Fig. 3.39 Maximum hardness penetration depth predictions [51]

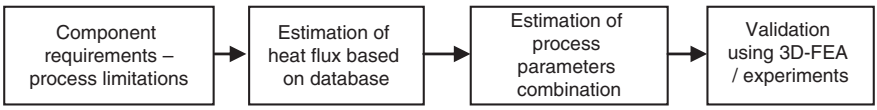

Fig. 3.40 Methodology for estimating the process parameters based on the product requirements and the process limitations

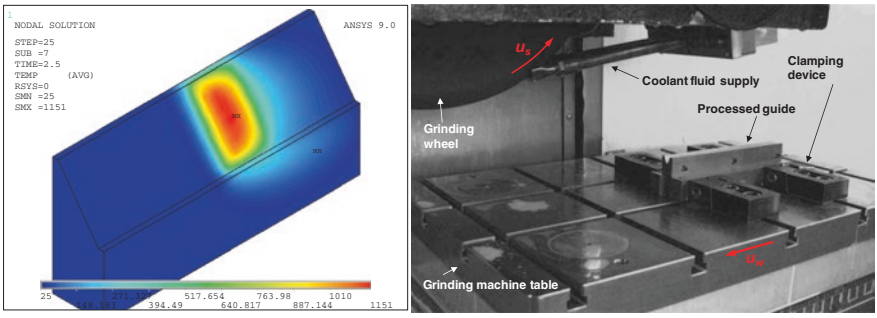

Fig. 3.41 *Left* Temperature field for $u_w = 0.6$ m/min, *Right* Experimental setup

In most cases, more than one combination of process parameters will give the requested result; the final selection lies in other issues, some of which are: the availability in grinding wheels, the grinding wheel wear, the grinding machine capabilities and the requested productivity. Figure 3.40 presents such an approach for estimating the process parameters graphically.

The V-shaped guide had to be hardened on the surface of both flanks, with a minimum surface hardness of 650 HV1 and a hardening depth of at least 0.3 mm. Using the database in Fig. 3.38, the requested HPD can be achieved with various combinations of process parameters. Some of the combinations can be rejected even before validation based on experience. For validation of the predictions, both a 3-D FEA model and experimental measurements were developed and used (Fig. 3.41).

References

1. Toenshoff HK, Peters J, Inasaki I, Paul T (1992) Modelling and simulation of grinding processes. CIRP Ann Manuf Technol 41(2):677–688
2. Salonitis K, Stavropoulos P, Kolios A (2014) External Grind Hardening Forces Modelling and Experimentation. Int J Adv Manuf Technol 70(1–4):523–530
3. Malkin S (1989) Grinding technology: theory and applications of machining with abrasives. Ellis Horwood, Chichester
4. Malkin S, Cook NH (1971) The wear of grinding wheels. Part 1. Attritious wear. ASME J Eng Ind 93:1120–1128
5. Hou ZB, Komanduri R (2003) On the mechanics of the grinding process—Part I. Stochastic nature of the grinding process. Int J Mach Tools Manuf 43:1579–1593
6. Kannapan S, Malkin S (1972) Effects of grain size and operating parameters on the mechanics of grinding. ASME J Eng Ind 94:833
7. Lichun L, Jizai F, Peklenik J (1980) A study of grinding force mathematical model. CIRP Ann Manuf Technol 29(1):245–249
8. Mishra VK, Salonitis K (2013) Empirical estimation of grinding specific forces and energy based on a modified werner grinding model. Procedia CIRP 8:287–292
9. Lavine AS (1991) Thermal aspects of grinding: the effect of heat generation at the shear planes. CIRP Ann Manuf Technol 40(1):343–345
10. Lavine AS (2000) An exact solution for surface temperature in down grinding. Int J Heat Mass Transf 43:4447–4456
11. Salonitis K, Chryssolouris G (2006) Cooling in grind hardening operations. Int J Adv Manuf Technol 33:285–297
12. Chryssolouris G, Tsirbas K, Salonitis K (2005) An analytical, numerical and experimental approach to grind hardening. SME J Manuf Process 7(1):1–9
13. Rowe WB, Morgan MN, Allanson DA (1991) An advance in the modelling of thermal effects in the grinding process. CIRP Ann Manuf Technol 40(1):339–342
14. Rowe WB, Morgan MN (1993) The effect of deformation on the contact area in grinding. CIRP Ann Manuf Technol 42(1):409–412
15. Zhou ZX, Van Lutterwelt CA (1992) The real contact length between grinding wheel and workpiece—a new concept and a new measuring method. CIRP Ann Manuf Technol 41(1):387–391
16. Lavine AS, Malkin S, Jen TC (1989) Thermal aspects of grinding with CBN wheels. CIRP Ann Manuf Technol 38(1):557–560
17. Rowe WB, Black SCE, Mills B, Qi HS, Morgan MN (1995) Experimental investigation of heat transfer in grinding. CIRP Ann Manuf Technol 44(1):329–332
18. Rowe WB, Morgan MN, Black SCE, Mills B (1996) A simplified approach to control of thermal damage in grinding. CIRP Ann Manuf Technol 45(1):299–302
19. Rowe WB, Black SCE, Mills B (1996) Temperature control in CBN grinding. Int J Adv Manuf Technol 12:387–392

20. Rowe WB, Morgan MN, Black SCE (1998) Validation of thermal properties in grinding. CIRP Ann Manuf Technol 47(1):275–279
21. Guo C, Malkin S (1992) Heat transfer in grinding. J Mater Process Manuf Sci 1:16–27
22. Guo C, Malkin S (1994) Analytical and experimental investigation of burnout in creep-feed grinding. CIRP Ann Manuf Technol 43(1):283–286
23. Guo C, Malkin S (1996) Effectiveness of cooling in grinding. Trans North Am Manuf Res Inst SME 1996 (NAMRI/SME) XXIV:111–116
24. Guo C, Malkin S (2000) Energy partition and cooling during grinding. SME J Manuf Process 2(3):151–157
25. Jin T, Cai GQ, Jeong HD, Kim NK (2001) Study on heat transfer in super-high-speed-grinding: energy partition to the workpiece in HEDG. J Mater Process Technol 111:261–264
26. Toenshoff HK, Brinksmeier E, Choi H-Z (1987) Abrasives and their influence on forces, temperatures, and surface. In: Proceedings of the 15th North American manufacturing research conference, pp 70–89
27. Rowe WB, Pettit JA, Boyle A, Moruzzi JL (1988) Avoidance of thermal damage in grinding and prediction of the damage threshold. CIRP Ann Manuf Technol 37(1):327–330
28. Salonitis K, Chryssolouris G (2007) Thermal analysis of grind-hardening process. Int J Manuf Technol Manage 12(1/2/3):72–92
29. Salonitis K, Chondros T, Chryssolouris G (2008) Grinding wheel effect in the grind-hardening process. Int J Adv Manuf Technol 38(1–2):48–58
30. Rowe WB (2001) Thermal analysis of high efficiency deep grinding. Int J Mach Tools Manuf 41:1–19
31. Rowe WB, Jin T (2001) Temperatures in high efficiency deep grinding (HEDG). CIRP Ann Manuf Technol 50(1):205–208
32. Hahn RS (1962) On the nature of the grinding process. In: Proceedings of the 3rd machine tool design and research conference, pp 129–154
33. Kim NK, Guo C, Malkin S (1997) Heat flux distribution and energy partition in creep-feed grinding. CIRP Ann Manuf Technol 46(1):227–232
34. Jin T, Stephenson DJ (2003) Investigation of the heat partitioning in high efficiency deep grinding. Int J Mach Tools Manuf 43:1129–1134
35. Chang CC, Szeri AZ (1998) A thermal analysis of grinding. Wear 216:77–86
36. Chiu N, Malkin S (1993) Computer simulation for cylindrical plunge grinding. CIRP Ann Manuf Technol 42(1):383–387
37. Eda H, Ohmura E, Yamauchi S (1993) Computer visual simulation on structural changes of steel in grinding process and experimental verification. CIRP Ann Manuf Technol 42(1):389–392
38. Lavine AS (1988) A simple model for convective cooling during the grinding process. J Eng Ind 110:1–6
39. Snoeys R, Maris M, Peters J (1978) Thermally induced damage in grinding. CIRP Ann Manuf Technol 27:571–579
40. Carslaw HS, Jaeger JC (1959) Conduction of heat in solids. Oxford University Press, London
41. Jin T, Cai GQ (2001) Analytical thermal models of oblique moving heat source for deep grinding and cutting. J Manuf Sci Eng 123:185–190
42. Krauss G (1993) Steels: heat treatment and processing principles, ASM International, Materials Park
43. Liedtke D, Jonsson R (1996) Warmebehandlung. Expert Verlag
44. Liedtke D, Jonsson R (1954) Atlas zur Waermebehandlung der Stahle, 1st edn. Verlag stahleisen mbH, Duesseldorf
45. Koistinen DP, Marburger RE (1959) A general equation prescribing the extent of the Austenite-Martensite transformation in Pure Iron-Carbon alloys and plain Carbon steels. Acta Metall 7:59–60
46. Pollack H (1988) Materials science and metallurgy, 4th edn. Prentice-Hall, Englewood Cliffs

47. Umbrello D, Ambrogio G, Filice L, Shivpuri G (2008) A hybrid finite element method–artificial neural network approach for predicting residual stresses and the optimal cutting conditions during hard turning of AISI 52100 bearing steel. Mater Des 29:873–883
48. Mahdi M, Zhang L (1999) Applied mechanics in grinding. Part 7: residual stresses induced by the full coupling of mechanical deformation, thermal deformation and phase transformation. Int J Mach Tools Manuf 39:1285–1298
49. Mahdi M, Zhang LC (1997) Applied mechanics in grinding-V. Thermal residual stresses. Int J Mach Tools Manuf 37:619–633
50. Salonitis K (2014) On surface grind hardening induced residual stresses. Procedia CIRP 13:264–269
51. Salonitis K (2006) A methodology for the prediction of the hardness distribution and the hardness penetration depth caused by grind-hardening process. Ph.D. dissertation, University of Patras, Patras, Greece
52. Salonitis K, Stavropoulos P, Stournaras A, Chryssolouris G (2007) Finite element modeling of grind hardening process. In: Proceedings of 10th CIRP International Workshop on Modeling of Machining Operations, pp 117–123

Chapter 4
Energy Efficiency and Environmental Impact Implications of Grind-Hardening Process

Abstract Energy efficiency is one of the key manufacturing challenges nowadays. The goal is to produce more with less energy. Utilization of a machine tool for performing simultaneously two processes can increase the energy efficiency of the machine tool used radically. At the same time, the environmental impact of the processing is critical as well. This environmental impact is a result of both the energy consumed and the side products of the process, emissions and so on. This chapter discusses the energy efficiency of the grind-hardening process and its environmental impact based on a life cycle assessment analysis.

4.1 Introduction

Manufacturing as one of the primary wealth-generating activities, can be defined as the transformation of materials and information into goods for the satisfaction of human needs. Turning raw materials though into consumer products is a major source of environmental pollution. This environmental pollution can be the direct outcome of the manufacturing process, or indirectly through the use of energy for running these processes. The availability and affordability of energy is becoming a critical parameter affecting the whole life cycle of the product, and subsequently the production phase as well. The large use of energy for industrial operations in Europe (32 % of the whole consumed energy) is responsible for significant CO_2 emissions and thus climate change [1].

Further to the energy efficiency issue, however, manufacturing waste involves a very diverse group of substances, and depends on the technology used, the nature of the raw material processed and the quantity that is discarded at the end of the chain.

The process of grind hardening can potentially increase the energy efficiency of the manufacturing and at the same time reduce the environmental burden. The process relies on controlling the generated heat for heating locally the processed workpiece in order to increase its surface hardness. The metallurgic change

K. Salonitis, *Grind Hardening Process*, SpringerBriefs in Manufacturing and Surface Engineering, DOI 10.1007/978-3-319-19372-4_4

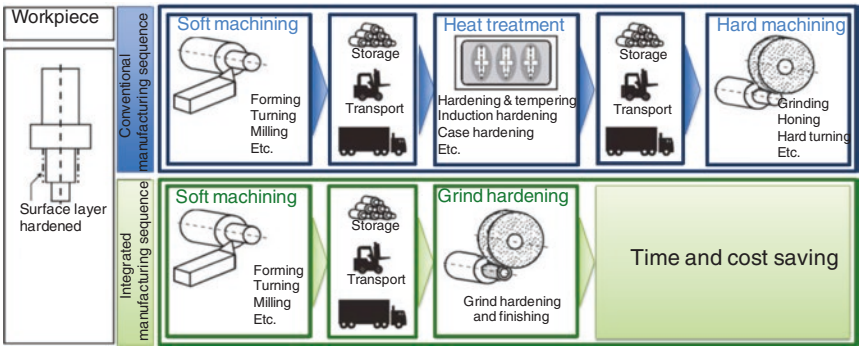

Fig. 4.1 Comparison of a conventional production chain and a production chain including grind hardening

required for the hardening is achieved by heating the surface above austenitization temperature and through the subsequent quenching martensitic transformation induced on the workpiece surface. The integration of the hardening process in the grinding can allow the elimination of the energy inefficient conventional hardening processes and at the same time eliminate the required transportation (Fig. 4.1). The impact on the energy efficiency and the environmental impact will be discussed in the following sections.

4.2 Energy Efficiency

Salonitis and Ball [2] discussed the importance of energy efficiency as one of the drivers for sustainability. They highlighted the need for including energy efficiency as one of the key metrics to be considered for decision-making in a manufacturing environment further to the conventional metrics of quality, time and flexibility. In general "energy efficiency" refers to technologies and standard operating procedures that reduce the volume of energy per unit of industrial production. IEA adopted definitions of energy efficiency are: "the goal of efforts to reduce the amount of energy required to provide products and services" and "achieving the same quality and level of some 'end use' of energy with a lower level of energy input".

A number of energy-related KPIs have been introduced and can be categorized into metrics focusing in the energy consumption (such as energy consumed per product, total on-site energy, total energy use, etc.), environmental impact (CO_2 emissions, greenhouse gas emissions, etc.), financial figures (e.g. energy cost), focusing on the process level, machine tool or production plant, etc.

Duflou et al. [3] indicated five different levels of energy efficiency analysis: device/process level, line/cell/multi-machine system, facility, multi-factory

system and enterprise/global supply chain. Each one of this analysis level relies on different assumptions, different input and provides different results. Salonitis and Ball [2] focused in two more generic levels: the machine tool level (that basically reflects the two first levels proposed by Duflou in a more holistic view) and the manufacturing system level (which can be linked to Duflou's subsequent two levels).

On a machine tool level, the analysis relies on the energy audit of the machine tool during the processing. During the last years, a number of studies have been presented dealing with the energy efficiency at this level, indicatively Kara and Li [4] presented the so called "unit process energy" method and Weinert et al. [5] developed the "energy blocks" method. It has been proven in the past that the energy consumed by machine tools during machining is significantly greater than the theoretical energy required in chip formation. Dahmus and Gutowski [6] showed, for instance, that the specific cutting energy accounts for less than 15 % of the total energy consumed by a modern automatic machine tool during machining. Salonitis [7] came to similar figures for the case of grinding.

It is essential to accurately measure the energy consumption during the process and cannot solely rely on the theoretical modelling of the process for the estimation of the energy consumption. For the determination of the energy consumption that is caused by various peripherals of the machine tools, the monitoring procedure has to be designed thoroughly in advance. Salonitis [8] developed a framework for determining the energy consumption of a machine tool. The main challenge when measuring machine tool consumption lies in the fact that machine tools are composed of a very large number of subsystems that are not possible to isolate and measure individually. Another challenge is the fact that different subsystems are included in each machine tool, so in order to come up with comparable results, the boundaries of the system under investigation have to be defined accurately. Salonitis' framework is composed of three major phases: the preparation phase, the measurement phase and the analysis phase. Within the preparation phase, the energy audit approach is structured and designed based on the characteristics of the machine tool to be analyzed. Within the second phase all the measurements are taking place. The final phase deals with the analysis of the results. The framework is schematically depicted in Fig. 4.2.

Salonitis [8] measured the energy consumption during grinding and grind-hardening process, following this approach in order to estimate the energy actually consumed for the processing itself and the energy consumed for the various peripherals. Figure 4.3 presents the effective power as measured during the grinding of a cylindrical component and the resulting conclusions of the analysis with regard to the energy demand per subsystem. It was thus revealed that near half of the energy consumed is for the coolant pump. Using the Pareto analysis the various subsystems are ranked with regard to the energy consumption, establishing in this way which subsystems are best to focus improvement efforts. Almost 80 % of the total effective power is drawn by only two subsystems, namely coolant pump and grinding wheel motor (spindle).

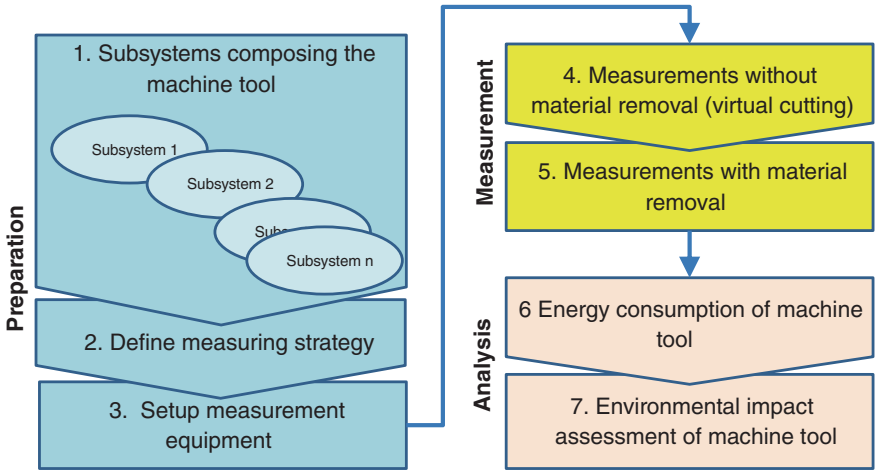

Fig. 4.2 Energy consumption measurement framework [8]

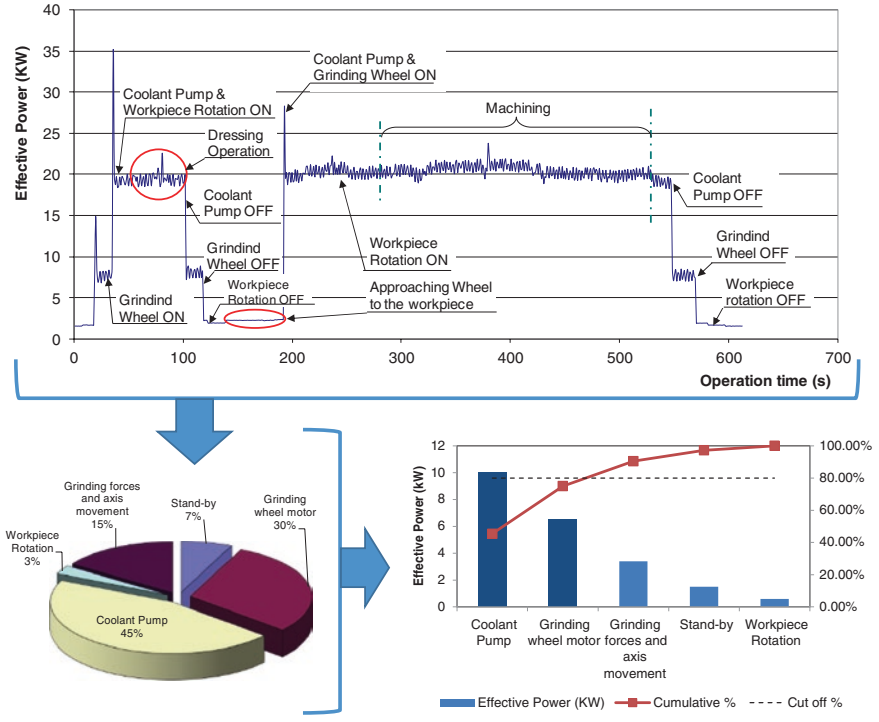

Fig. 4.3 Energy consumption analysis [2]

4.3 Environmental Impact Assessment

For assessing the environmental impact of the grind-hardening process, Life Cycle Assessment (LCA) methods can be used for comparing the environmental impact of the grind-hardening process versus the respective impact, caused by the utilization of conventional heat treatment methods for the production of the same part.

4.3.1 Introduction to Life Cycle Assessment

LCA models the complex interaction between a product and the environment. A more comprehensive definition for LCA is that of a methodology for assessing and evaluating the environmental, occupational health and resource consequences of a product through all phases of its life, i.e. extracting and processing raw materials, production, transportation and distribution, use, remanufacturing, recycling and final disposal [9].

The two major organizations that are involved in the definition of the LCA methods, setting up the rules for the utilization of such tools and furthermore dissemination of the LCA methodologies are the *Society for Environmental Toxicology and Chemistry* (SETAC) and the *International Organization for Standardization* (ISO).

The SETAC definition of LCA is [10]: "LCA is an objective process to evaluate the environmental burdens associated with a product, process, or activity by identifying and quantitatively describing the energy and materials used, and wastes released to the environment, and to assess the impacts of those energy and material uses and releases to the environment. The assessment includes the entire life cycle of the product or activity, encompassing extracting and processing raw materials; manufacturing; distribution; use; re-use; maintenance; recycling and final disposal; and all transportation involved. LCA addresses environmental impacts of the system under study in the areas of ecological systems, human health and resource depletion".

The ISO/FDIS standard in LCA [11] provides the following definition: "LCA is a technique for assessing the environmental aspects and potential impacts associated with product, by:

- Compiling an inventory of relevant inputs and outputs of a system
- Evaluating the potential environmental impacts associated with those inputs and outputs
- Interpreting the results of the inventory and impact phases in relation to the objectives of the study

LCA studies the environmental aspects and potential impacts throughout a product's life (i.e. cradle-to-grave) from raw material acquisition through production, use and disposal. The general categories of environmental impacts needing consideration include resource use, human health, and ecological consequences".

The scope thus of an LCA involves tracking all the materials and energy flows of a product from the retrieval of its raw materials out of the environment to the disposal of the product back into the environment. The objectives of the LCA can be summarized in the following bullets:

- the early definition of product life cycle and an estimation of expected resource consumption and environmental impacts across several phases of the product life cycle
- comparison of alternative product solutions or
- different process chains taking technological, economic and ecological aspects into consideration

The results of an LCA provide the basis for the development of environmental laws, taxes and regulations. In addition, industries use LCA to support product development in order to minimize the overall environmental impact of the product. Qualitative and quantitative characteristics of the product life cycle are taken into account by means of LCA during the conceptual design of each new product. This enables designers to estimate the costs and benefits associated with the design attributes of the product, energy consumption, materials requirement and afterlife choices of the product. Many companies make use of LCA to support their public claim of environmental responsibility.

4.3.2 Technical Framework of Life Cycle Assessment

The technical framework of LCA has been precisely defined by the SETAC and the ISO. In the present section the framework of LCA will be described in accordance to the guidelines that have been set by these two institutions.

In general, according to SETAC [12], LCA consists of the following four stages:

1. Goal Definition and Scoping
2. Life Cycle Inventory
3. Life Cycle Impact Analysis
4. Life Cycle Improvement Analysis

The LCA framework developed in ISO is slightly different:

1. Goal and Scope Definition
2. Inventory Analysis
3. Impact assessment
4. Interpretation

Apart from a small terminological point (the term Goal and Scope Definition) the major differences are the inclusion of “Interpretation” and the skipping of “Improvement Assessment”. The “Interpretation” is rather broad term and it includes sensitivity analyses and feedback on the “Goal and Scope Definition”.

Furthermore the "Valuation" is part of "Interpretation" instead of being a part of Impact Assessment [13].

Goal and scope definition
The first phase in LCA, establishes the purpose and scope of the study. These definitions are the most critical part of an LCA due to the strong influence on the results of the LCA. In LCA the minimum decisions and definitions that need to be made are the following:

- The purpose and the intended application
- The function of the studied systems and a defined functional unit
- The system boundaries applied
- The data quality needed
- The validation or critical review needed

Life Cycle Inventory (LCI)
LCI is an objective process of quantifying the inputs from the environment to the system and outputs from the system to the environment throughout the life cycle of a product, process or activity. This includes the production phase, the distribution, use and final disposal of the product. These inputs and outputs may include the use of resources and releases to air, water and land associated with the system.

The life cycle can be presented as a process tree where each box represents a process which forms part of the life cycle. Furthermore, every process has defined inputs and outputs. The main scope of this phase is to compose the LCI of all the environmental inputs and outputs associated with the product, known as table of impacts. Each impact is expressed as a particular quantity of substance.

LCI is iterative similarly to the definition of goal and scope. In the process of collecting data leading to better comprehending of the system, new data requirements may arise or limitation in the procedures followed for collecting data may appear and thus induce modifications in the data collection procedures as to meet the goals of the study. Furthermore, issues may be identified that require revisions to the goal or scope of the study.

Life Cycle Impact Analysis (LCIA)
LCIA [14] is a technical qualitative and/or quantitative process to characterize and assess the effects of the environmental loadings identified in the inventory component. A number of Life Cycle Impact Assessment methodologies have been presented:

- EPS (Environmental Priority Strategy). The complete chain of cause and effect from each impact on a human equivalent is calculated.
- Eco-points method was developed for the Swiss Government based on the distance-to-target principle. The distance between the current level of an impact and the target level is assumed to be representative of the seriousness of the emission.
- Eco-Indicator 99 and Eco-Indicator 95 developed by the Pre-Consultants [15].

4.3.3 Grind-Hardening LCA-Based Environmental Impact Assessment

Salonitis et al. [16] used LCA for comparing the environmental impact of the grind-hardening process versus the respective impact, caused by the utilization of conventional heat treatment methods in two different pilot cases: the production of raceways and tripod joints. The analysis indicated that the utilization of grind hardening decreases significantly the environmental impact on the production of steel parts. The process they followed for one of the cases (the raceway production) is presented hereafter, the reader can refer to their study for the second case as well.

The raceway is traditionally hardened using conventional heat treatment salt baths by an external wage hardener, outside the production facilities. When introducing grind hardening, four grinding cycles are requested and the conventional heat treatment is no longer required.

Life Cycle Inventory

The most intensive and demanding task in performing LCA is the LCI, since it includes all data collection. These data are required for the modelling of the system under consideration. The boundaries of the analysis were defined so as to provide a clear comparison of the environmental effect of the conventional and the modified process chains.

The next step was the collection of the required data for conducting the analysis. The energy consumption of every process step, the tool/grinding wheel wear, the debris from each process step and the fumes produced have been measured or estimated. For example, the distance from the production facility to the wage hardener's premises needs to be considered when estimating the embodied energy of the component. Based on either energy measurements or calculations the average energy consumption per part can be calculated.

Life Cycle Impact Assessment

Salonitis et al. [16] used three LCA methodologies for comparing the environmental impact of the process chain when substituting conventional hardening and rough grinding with grind hardening, namely: Eco-Indicator 99, Eco-Points 97 and EDIP/UMIP 96. Indicatively, Eco-Indicator 99 method expresses the emissions and resource extractions in 11 different impact categories (Carcinogenics, respiratory organics, respiratory inorganics, climate change, radiation, ozone layer, ecotoxicity, acidification/eutrophication, land use, minerals and fossil fuels) [16]. In Fig. 4.4 the comparison between these two different process chains is presented for all 11 impact categories. These rather abstract impact categories can be combined and grouped in three damage categories that present the different types of damage caused by them: the "Damage to human health", the "Damage to ecosystem quality" and the "Damage to resources". In Fig. 4.5, is shown the comparison of these production chains, as far as damage caused is concerned. The substitution of the conventional heat treatment with grind hardening results in 72 % reduction in the damage caused to the resources, 13 % reduction in the damage caused to the

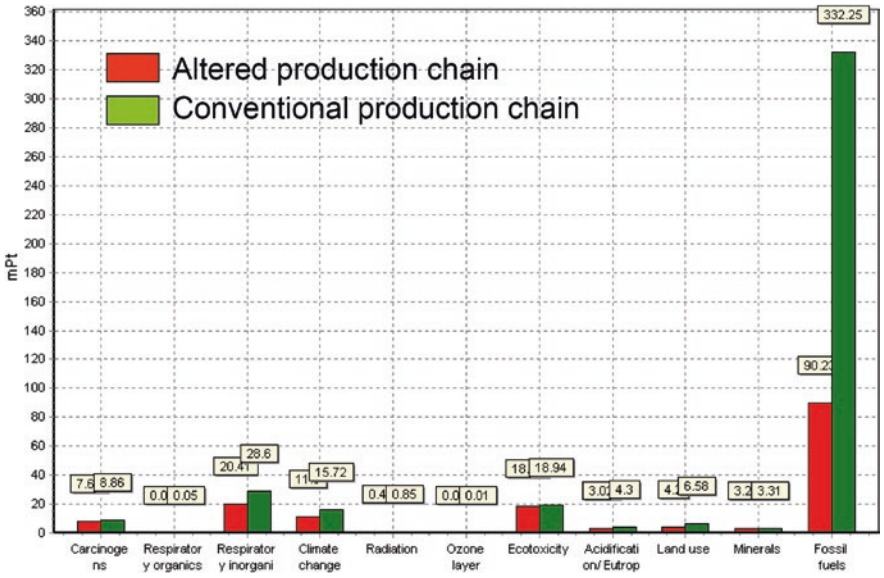

Fig. 4.4 Weighting comparison using Eco-Indicator 99 methodology [16]

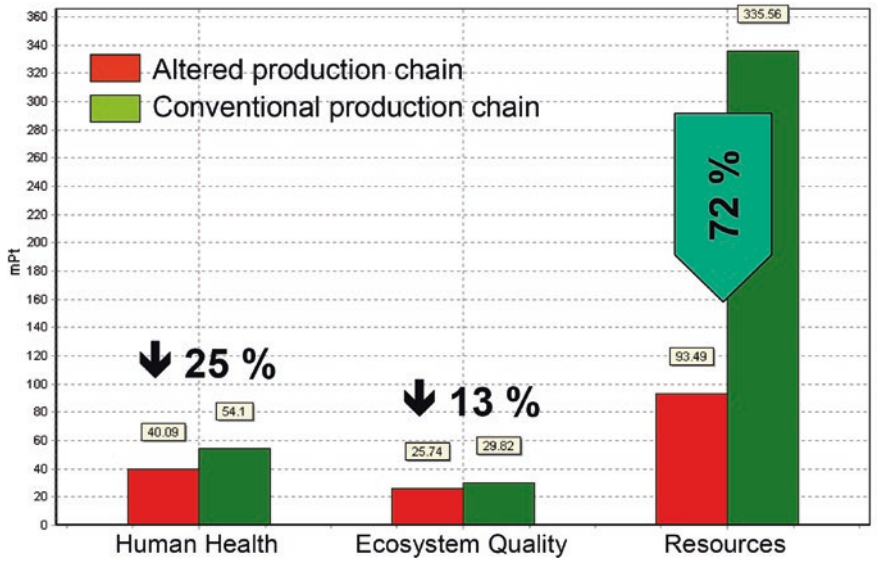

Fig. 4.5 Weighting comparison of damage categories using Eco-Indicator 99 methodology [16]

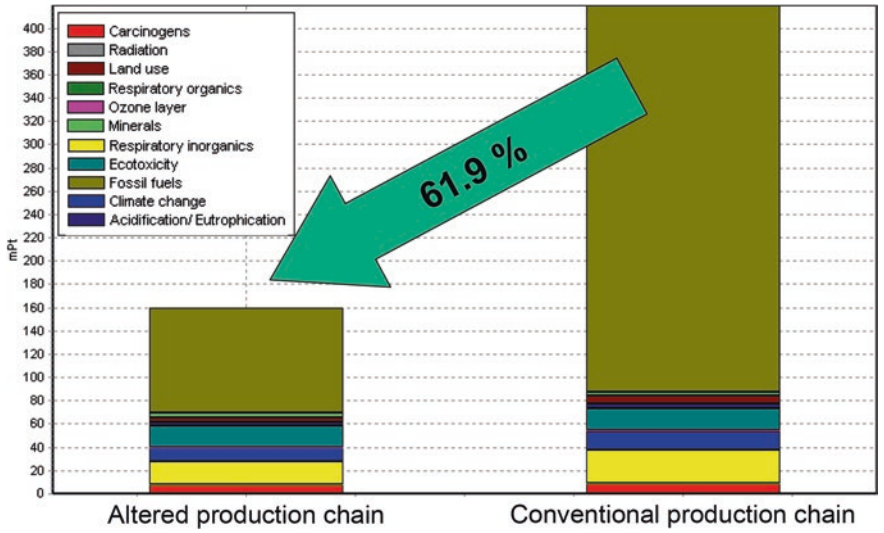

Fig. 4.6 Weighting comparison of damage categories using Eco-Indicator 99 methodology [16]

ecosystem quality and 25 % in the damage to resources. The relative seriousness of each damage category can be added for estimating the total (single) score that indicates the total environmental effect of each production chain (Fig. 4.6).

The LCA analysis of the raceway production chain and the comparison when substituting the conventional heat treatment and the rough grinding process with grind hardening has yielded an average reduction in the environmental damage by 45 %. Specifically, the Eco-Indicator method suggested a reduction in the overall environmental effect by 62 %. The Eco-points 97 method that uses target values rather than current ones (in comparison with the Eco-Indicator) and it is based on policy instead of sustainability levels suggested a reduction in the overall environmental effect by 28.1 %. Finally, EDIP/UMIP method resulted in a reduction in the overall environmental effect by 16 %.

References

1. IEA (2007) Tracking industrial energy efficiency and CO_2 emission
2. Salonitis K, Ball P (2013) Energy efficient manufacturing from machine tools to manufacturing systems. Procedia CIRP 7:634–639
3. Duflou JR, Sutherland JW, Dornfield S, Herrmann C, Jeswiet J, Kara S, Hauschild M, Kellens K (2012) Towards energy and resource efficient manufacturing: a processes and systems approach. CIRP Ann Manuf Technol 61(2):587–609
4. Kara S, Li W (2011) Unit process energy consumption models for material removal processes. CIRP Ann Manuf Technol 60(1):37–40
5. Weinert N, Chiotellis S, Seliger G (2011) Methodology for planning and operating energy-efficient production systems. CIRP Ann Manuf Technol 60(1):41–44

6. Dahmus J, Gutowski T (2004) An environmental analysis of machining. In: Proceedings of ASME International Mechanical Engineering Congress and R&D Exposition, pp 13–19
7. Salonitis K (2012) Efficient grinding processes: an energy efficiency point of view. In: Proceedings of the 10th international conference on manufacturing research (ICMR 2012), pp 541–546
8. Salonitis K (2015) Energy efficiency assessment of grinding strategy. Int J Energy Sect Manage 9(1):20–37
9. Alting L, Jorgnsen J (1993) The life cycle concept as a basis for sustainable industrial production. CIRP Ann Manuf Technol 42(1):163–167
10. Consoli F et al (1993) Guidelines for life cycle assessment: a code of practice. Society of environmental toxicology and chemistry (SETAC), SETAC Workshop, Sesimbra, Portugal
11. ISO 14040:1997 Environmental management—life cycle assessment—Principles and framework
12. SETAC (1993) Society of environmental toxicology and chemistry. A technical framework from life cycle assessment
13. Udo de Haes HA et al (1996) Definition document. LCANET Board
14. Udo de Haes HA et al (1996) Evaluation and development of the conceptual framework and methodology of life-cycle impact assessment. SETAC (North American & Europe) Workgroup on Life Cycle Assessment, Jan 1998
15. Pre-Consultants Ltd. http://www.pre.nl
16. Salonitis K, Tsoukantas G, Drakopoulos S, Stavropoulos P, Chryssolouris G (2006) Environmental impact assessment of grind-hardening process. In: Proceedings of the 13th CIRP International Conference on Life Cycle Engineering, pp 657–662

Chapter 5
Concluding Remarks and Outlook

Abstract The primary goal of this book is to review the state of the art of the grind-hardening process, the process modelling and the process impact in the environment in a comprehensive manner. Grind-hardening process is a novel hybrid process that can be considered as an alternative process for localized surface heat treatment. The physical process parameters affecting the process mainly include the feed speed, the cutting depth, the grinding wheel speed, the type of the grinding wheel and the use or not of coolant fluid. The key metrics that can be used for assessing the outcome of the process include the surface hardness, the hardness penetration depth and the residual stresses. The proper selection of the operating parameters offline can minimize the time required for setting up of the process and maximize the final quality of the component. In the present chapter, the brief description of the importance and findings of the grind-hardening process and resulting hardened components is presented.

5.1 Introduction

Grind hardening is a hybrid manufacturing process that can be used for the simultaneous surface hardening and grinding of metallic components. Due to the fact that both the grinding and grind-hardening processes are performed on the same machine tool with the same setup, there is no need for conventional heat treatment methods that are characterized by high energy consumption and the utilization of polluting treatment salts. Eliminating this processing stage reduces radically the need for other auxiliary processes such as cleaning and transportation to and forth to a wage hardener.

Grind hardening is based on controlling of the grinding process generated heat for heating locally the processed workpiece in order to increase its surface hardness. The metallurgic change required for the hardening is achieved by heating the surface above austenitization temperature and through the subsequent quenching martensitic transformation induced on the workpiece surface.

K. Salonitis, *Grind Hardening Process*, SpringerBriefs in Manufacturing and Surface Engineering, DOI 10.1007/978-3-319-19372-4_5

5.2 Summary

Chapter 1 briefly described the various processes and technologies that can be employed for the surface modification of a component. Grind hardening, being one of these processes, was also introduced and compared with other processes such as laser hardening, induction hardening and others. Within Chap. 2 the state of the art of grind-hardening process was presented. More than 120 papers were reviewed, covering the history of grind-hardening process from its introduction in the mid 1990s till today. The next chapter focused on the modelling of the grind-hardening process. Analytical and empirical formulas were developed for predicting the grinding wheel topography, the energy balance in the grinding wheel—workpiece interface, the resulting temperature distribution and the hardness distribution in the workpiece material. Finally, the residual stresses were modelled and predicted. For modelling the process, a number of different methods were used such as regression based on experimental results, analytical solution of the heat conduction problem, finite element analysis, etc. All sub-models were validated experimentally and finally they were integrated in an offline tool that can be used for the prediction of the optimum process parameters combination. Chapter 4 presented the environmental aspects of the process. The chapter is divided into two main themes, the first one being on the energy efficiency of the machine tool to be used for the grind-hardening process, the ways to capture the energy footprint and how to optimize it. The second theme focused on the environmental impact assessment though life cycle assessment. It was proven that grind hardening can potentially increase the energy efficiency of the manufacturing and at the same time reduce the environmental burden.

5.3 Outlook

Grind hardening has a short history; it was introduced by Brinksmeier and Brockhoff [1]. Initially, the research focus was on proving the feasibility of the process and certifying that the process outcome can be controlled in a repeatable way. A number of studies focused in checking whether the process can be used for a number of different materials. The research community, once convinced that the process has a future, invested effort in developing models for the better understanding of the process mechanisms and the prediction of the process parameters that can produce hardness profiles on the components that meet the design requirements [2–7].

However, as it has been identified at the outlook of Chap. 2, full industrial adoption of the grind-hardening process is restricted by a number of factors:

- Formation of overlapping areas. Overlapping areas are generated in cylindrical grinding when the grinding wheel approaches areas that have been already grind hardened. Particularly in cylindrical grind hardening, improper junction of

the hardened surface layer is generated in overlapping areas. In the overlapping area, the hardened surface layer material is annealed, resulting in reduced hardness and decreased hardness penetration depth. Thus grind-hardening technology today is limited to applications where overlapping areas are not generated like surface grinding applications or where the occurrence of overlapping areas can be accepted; for example in the area of bearing fits or runways for packing rings.

- The maximum achievable hardness penetration depth (HPD), is technologically restricted to about 2.5 mm due to high grinding forces and physical properties of the material.
- Grind-hardening technology is restricted by the wear of the grinding wheel resulting in relative low G-ratios (grinding ratio) and decreased cost savings.

On the other hand, the process can help improve the energy efficiency of the manufacturing significantly. The energy efficiency of the manufacturing processes [8] has evolved to be very important issue in the manufacturing sector and is not likely to lose its importance. The grind-hardening process, being a hybrid process combining two process steps into one, has high potentials in reducing the energy and carbon footprint of the manufacturing [9–11].

References

1. Brinksmeier E, Brockhoff T (1996) Utilization of grinding heat as a new heat treatment process. CIRP Ann Manuf Technol 45:283–286
2. Chryssolouris G, Tsirbas K, Salonitis K (2005) An analytical, numerical, and experimental approach to grind hardening. J Manuf Process 7(1):1–9
3. Salonitis K, Chryssolouris G (2007) Cooling in grind-hardening operations. Int J Adv Manuf Technol 33(3-4):285–297
4. Salonitis K, Chryssolouris G (2007) Thermal analysis of grind-hardening process. Int J Manuf Technol Manage 12(1/2/3):72–92
5. Salonitis K, Chondros T, Chryssolouris G (2008) Grinding wheel effect in the grind-hardening process. Int J Adv Manuf Technol 38:48–53
6. Salonitis K, Stavropoulos P, Kolios A (2014) External grind-hardening forces modelling and experimentation. Int J Adv Manuf Technol 70(1–4):523–530
7. Salonitis K, Kolios A (2015) Experimental and numerical study of grind hardening induced residual stresses on AISI 1045 Steel. Int J Adv Manuf Technol. doi:10.1007/s00170-015-6912-x
8. Salonitis K, Ball P (2013) Energy efficient manufacturing from machine tools to manufacturing systems. Procedia CIRP 7:634–639
9. Salonitis K (2012) Efficient grinding processes: an energy efficiency point of view.. In: Proceedings of the 10th international conference on manufacturing research (ICMR 2012), pp 541–546
10. Salonitis K (2015) Energy efficiency assessment of grinding strategy. Int J Energy Sect Manage 9(1):20–37
11. Salonitis K, Tsoukantas G, Drakopoulos S, Stavropoulos P, Chryssolouris G (2006) Environmental impact assessment of grind-hardening process. In: Proceedings of the 13th CIRP international conference on life cycle engineering, pp 657–662